UNIVERSITY OF CALIFORNIA, SAN DIEGO

Local Functional Input to Neurons in Deep Layers of Rat Visual Cortex

A dissertation submitted in partial satisfaction of the

Requirements for the degree of Doctor of Philosophy

in

Neurosciences

by

Amir Zarrinpar

Committee in charge:

Professor Edward M. Callaway, Chair
Professor Anirvan Ghosh, Co-Chair
Professor Daniel E. Feldman
Professor David H. Rapaport
Professor Massimo Scanziani

2006

The dissertation of Amir Zarrinpar is approved, and it is acceptable in quality and form for publication on microfilm.

_____

_____

_____

_____

_____
Chair

University of California, San Diego

2006

In the name of God, the Most Gracious, the Most Merciful

Dedicated to:

My family

Liza
Mom and Dad
Rose and Ali

Without whom this would have been impossible…

Also to the rats

Natura in minima maxima

TABLE OF CONTENTS

LIST OF FIGURES AND TABLES

ACKNOWLEDGEMENTS

I would like to acknowledge my thesis advisor, Ed Callaway, who taught me, and still teaches me, how to be a better investigator and scientist. I have always been in awe of his optimism, scientific knowledge and skill. I feel privileged to have been part of his lab. I would also like to thank my committee, Massimo Scanziani, David Rapaport, Dan Feldman, and Anirvan Ghosh. I am forever grateful for their exceptional advice, probing questions, and genuine concern.

I would also acknowledge the entire Callaway lab past and present for making this one of the best work environments I have experienced. Their friendship and camaraderie will be sorely missed. In particular I would like thank my fellow photostimulation experimenters, Tak Mori and Xiangmin Xu, without whom it would have taken an at least an extra year, if not longer, to finish this thesis. They always dropped whatever they were doing to help me with my experiments and analysis, whether it was to help write code or to figure out a problem with the electrophysiology rig. I am forever indebted to them.

I would also like specifically thank Dennis Barbour, Victor Borrell, Farran Briggs, Mauricio de la Parra, DeLaine Larsen, Tara Martinez, Keith Roby, Sandra Tye, Ian Wickersham, and Yumiko Yoshimura, all of whom have at one point or another taught me a technique that I have used and described in this thesis. Martha Bagnall and Aryn Gittis of the du Lac Lab have been especially generous with their time and with helping our lab get started with spike analysis. Their assistance in the interpretation of the spike analysis results was invaluable. August Tuan, of the Boynton lab, lent the usage of their superfast computers to analyze some of the larger files in my correlation

analysis. And finally, Rose Z. Zarrinpar helped analyze a large portion of the data for this thesis and without her assistance I certainly would not have been able to finish this thesis in time.

I would like to acknowledge several of my close friends for their support and advice during the entire research experience: Alexandra Nelson, August Tuan, Eric Frechette, and Will Go. They were always there to lend an ear, comfort fears, and give perspective. Graduate school would certainly not have been as much fun without them.

I would like to acknowledge my family who have been a pillar of support. Without them this would have been impossible. My parents, Azra and David, sacrificed so much for me to get to this point, and taught me the value of education and knowledge. My two best friends and confidants are my siblings, Ali and Rose.

Finally, I'd like to acknowledge Liza, my wife, who has been my partner throughout my entire graduate career. I could not have asked for a better companion to ride through the ups and downs of the last five years. She fills my life with happiness. I cannot even begin to imagine how much more difficult this would have been without her.

I have been supported by a Merck Fellowship, the Agnisky Endowment Fellowship, and by Medical Scientist Training Program Grant NIGMS07198.

The text of Chapter 2, in full, is a reprint of material published in Journal of Neurophysiology [Full citation: Zarrinpar A, Callaway EM (2006) Local connections to specific types of layer 6 neurons in the rat visual cortex. J Neurophysiol 95:1751-1761]. I was the primary investigator and first author of this manuscript and Edward M. Callaway directed and supervised the research. This study was funded by National Institutes of Health Grants EY-10742 and MH-63912. I would like to acknowledge DJ

Brasier for help in collecting a portion of the data that was ultimately used in the manuscript.

The text of Chapter 3, in full, is a reprint of material that is in preparation for submission as a manuscript. I was the primary investigator and will be the first author on the manuscript and Edward M. Callaway, the second-author, directed and supervised the research. This study was also funded by National Institute of Health Grants EY-10742 and MH-63912. I would like to acknowledge Takuma Mori for his generous help with writing some of the spike analysis programs, Martha Bagnall and Aryn Gittis whose discussions were extremely helpful in developing our spike analysis and interpreting the results, and Rose Z. Zarrinpar for her help in analyzing a significant portion of the data collected for this study.

The text of Chapter 4, in part, will be combined and published with those of chapter 3. I was the primary investigator and first author of this chapter and Edward M. Callaway, will be the second author for his role in directing and supervising this project, and for writing a portion of the introduction. The authors would like to acknowledge Rose Z. Zarrinpar for her help in analyzing a significant portion of the data collected for this study.

CURRICULUM VITA

1999	A.B. *Magna Cum Laude* in Psychology and Biology Harvard University, Cambridge, MA
1999-2008	Medical Scientist Training Program, University of California, San Diego
2006	Ph.D., University of California, San Diego

PUBLICATIONS

Zarrinpar, A. and Callaway, E.M. (in preparation) "Laminar sources of functional local input to layer 5 neurons of the rat visual cortex."

Zarrinpar, A., Deldin, P., and Kosslyn, S.M. (in press) "Effects of depression on central processing during visual mental imagery." *Cognition and Emotion*.

Zarrinpar, A. and Callaway, E.M. (2006) "Laminar sources of functional local input to layer 6 neurons of the rat visual cortex." *Journal of Neurophysiology*, 95: 1751-61.

Laeng, B., **Zarrinpar, A.,** and Kosslyn, S.M. (2003) "Do separate processes identify objects as exemplars versus members of basic-level categories? Evidence from hemispheric specialization." *Brain and Cognition*, 53: 15-27.

Zarrinpar, A. (2003) "Quarantine." *JAMA* 290: 2872.

Zarrinpar, A. (2003) "Roles for medical students in the political process." *JAMA* 290: 1774.

Zarrinpar, A. (2002) "Psychiatry and stigmatization." *JAMA* 287: 1856.

ABSTRACTS

Zarrinpar A., and Callaway, E.M. "Layer 6 cell types and their local functional input in the rat visual cortex." Abstract. Presented at the Society for Neuroscience, November, 2005.

Zarrinpar A., Brasier, D.J., and Callaway, E.M. "Laminar sources of functional local input to layer 6 pyramidal neurons of the rat visual cortex." Abstract. Presented at the Society for Neuroscience, November, 2003.

(continued)

Nguyen, A.H., Quinn, L.K., Merrill, D.A., **Zarrinpar, A.,** Tuszynski, M.H., and Chiba, A.A. "The Effects of BDNF Infusion into Entorhinal Cortex on Hippocampal Place-Fields in Aged Rats." Abstract. Presented at Stein Institute for Research on Aging Spring Conference, April 2002.

Zarrinpar, A., Deldin, P., and Kosslyn, S.M. "Mental Imagery in the Depressed: The role of prefrontal dorsolateral cortical hypoactivation." Abstract. Presented at the American Psychiatric Association Conference, May 2000.

ABSTRACT OF THE DISSERTATION

Local Functional Input to Neurons in Deep Layers of Rat Visual Cortex

by

Amir Zarrinpar

Doctor of Philosophy in Neurosciences

University of California, San Diego, 2006

Professor Edward M. Callaway, Chair

Unraveling the precise connectivity of underlying neural circuits will lead to a better understanding of how the cortex accomplishes even the most effortless task. It has been a fundamental goal of neurophysiology to identify individual cell types based on morphological and/or intrinsic physiological properties and to discover their respective role in the circuitry within which they are embedded. To understand visual cortical circuitry even better, this dissertation focuses on the deep layers (layers 5 and 6) of the rat visual system. These cells, which comprise more than half of the cortical depth in the rat, are in a unique position in the visual system circuitry. Compared to the superficial layers, the deep layers have a greater diversity of cell morphologies and probably play a more varied role in visual information processing.

We studied dendritic morphologies and local excitatory input to individual layer 6 and layer 5 neurons in rat visual cortex by combining intracellular labeling and recording with laser-scanning photostimulation. We found significant differences in the sources of local excitatory input to different cell types. In layer 6 we found six distinct cell subtypes which we characterized based on morphology and sublaminar organization. Most

notably, there were differences in local input to neurons that were likely to project only to the lateral geniculate nucleus versus those that were likely also to project to the lateral posterior nucleus. In layer 5 we distinguished three non-overlapping cell subtypes based on both their morphological and intrinsic physiological properties. Although all cell types received significant input from all layers. One subset of cells, presumed to be cortico-cortical projecting neurons, received stronger input from layer 4 and weaker input from layer 5 when compared to the others. We did not find any differences in input patterns between two subtypes that had similar morphology but different firing patterns. Using an analysis of synchronous activity, however, we showed that although the two cell types receive the same laminar input patterns, they receive input from different cell populations within those layers.

Chapter 1

General Introduction

> If you do not make headway into understanding a complex system, then study its structure and knowledge of its function will follow automatically.
>
> -Francis Crick (Ramachandran, 1985)

How can an organic cluster of intertwined cells give rise to staggering achievements of unfathomable complexity, such as the Sistine Chapel, or the 1812 Overture? It is difficult to answer this question when we barely understand how the brain accomplishes more basic tasks such seeing the Sistine Chapel, or hearing the 1812 Overture. Since the 1920s, science fiction novels and movies have been filled with robots that behave similar to human beings. In reality, however, these sophisticated machines do not yet exist. A better appreciation of the brain's complexity became apparent when computer engineers tried to create machines to mimic some of the most effortless tasks of the human brain (Pinker, 1997). Their failure has only intensified curiosity into the functioning of the cerebral cortex and how effortlessly and quickly the brain completes tasks that are still impossible to accomplish with robotics.

The cortex is comprised of trillions of cells, each connected to about tens of thousands of others, giving rise to one of the most complex biological systems. The brain requires precise connectivity of these underlying cells for information processing. Hence, understanding its function requires unraveling synaptic connectivity and creating

models and wiring diagrams of the cortex. This may seem like an insurmountable task, however, cortical circuitry models are based on certain principles. The evolution of such a system relies on both specific adaptation and developmental constraints (Gould, 1977). That is, specialization of brain regions is based on local adaptations to basic vertebrate neurogenesis and physiology. This suggests that there is a great deal of conservation of fundamental patterns in cortical cytoarchitecture. Across species there is strong evidence that specialization of a particular brain region is characterized by general organizational constraints as well as specific adaptations that allow a particular behavior (Finlay and Darlington, 1995). The study of brain structure and function must take advantage of these principles based on evolution.

Brodmann found perhaps one of the earliest evidence of this interplay of evolutionary constraints and adaptive specialization in his studies of the cytoarchitecture of the cortex of different kinds of mammals (Brodmann and Garey, 1999). He observed that cortex has a laminar organization, a general constraint on the adaptation of different brain regions. Specialized regions of the brain, such as the visual cortex, alter their laminar organization by adding cells and forming sublayers such as in layer 4 of visual cortex, working within the constraints set by the six layer organization.

This laminar organization is a feature of cortical evolution that has been an invaluable tool for studying function. Each layer is comprised of discrete excitatory cell types that share similar morphologies, play a particular role in the cortical circuit, project to different regions of the brain, and probably receive input from discrete regions or cell type populations. In this thesis I present three studies that show the cortical circuitry of two deep layers in the rat visual cortex. In order to understand these projects better, I

have provided some more information about key principles in cortical circuitry, the rat visual system, and the subcortical targets of the cells I have studied, as well as an introduction to functional connectivity.

1.1 Key Principles of Circuitry

Cajal was the first to notice that the cells could be categorized based on their cell features (Ramâon y Cajal et al., 1988). He was able to use cell morphology, such as structure of the somata, dendritic and axonal branching and projection patterns to create classes of neurons. For example, Cajal discovered one of the most fundamental divisions of cell types, spiny and aspiny neurons, though he may not at the time realized the physiological importance of this discovery: spiny neurons are excitatory, whereas aspiny neurons are inhibitory.

Since the time of Cajal, the morphology, connectivity, physiology, and even protein expression of many different neurons have been identified. An important assumption for those who study cortical circuitry is that each morphological cell type plays a unique role in the cortical circuitry, and that all cells of that same type play a similar role. This has been widely supported in study after study (Connors et al., 1982; Kawaguchi, 1993; Kawaguchi and Kubota, 1996, 1997; Dantzker and Callaway, 2000; Briggs and Callaway, 2001; Kawaguchi, 2001; Schubert et al., 2001; DeFelipe, 2002; Kawaguchi and Kondo, 2002; Chatterjee and Callaway, 2003; Schubert et al., 2003; Briggs and Callaway, 2005; Schubert et al., 2006; Zarrinpar and Callaway, 2006). One example is the parasol ganglion cell in the monkey retina, which has a distinct dendritic morphology in the monkey retina, receives input from all three cones via diffuse bipolar

cells and projects to the M layers of the dLGN. This cell population has a unique physiological property in that it is sensitive to lower contrasts, low spatial frequencies, and high temporal frequencies (Chatterjee and Callaway, 2002). Based on their physiological properties, we can deduce that these cells are involved in motion perception.

The principle that cell subtypes play a similar role in cortical circuitry, is buttressed by additional principles that help decipher cortical circuitry. Local networks are organized into vertical columns that encompass different cell types throughout all the layers (Peters and Kara, 1987; Jones, 2000). These cortical columns probably function as components or repeating motifs in a larger specialized network specific to a brain region. Hence the functioning of one such vertical component could reveal a great deal about the way that a particular region processes information. Cortical neurons also have a less predominant, but active horizontal network within each cortical layer (Gilbert, 1983). These connections probably function as communication between the components/units of vertical columns.

Others have adopted principles of cortical organization with which we disagree. One such assumption is that when axons project to a specific layer or area, they are only targeting cells with somata in that area and not the processes of neurons located in a different layer (Gilbert and Wiesel, 1983; Douglas and Martin, 2004). Their argument is that since the basal dendrites and soma comprise approximately 90% of the cell surface on which other cells can synapse, connections to apical dendrites of neurons can be ignored when making cortical circuitry models. This convenient simplification allows potential connections in the cortical circuitry to occur only in areas where axonal

branches overlap with cell somata. However, there is evidence that, in some cells, apical dendrites have specialized mechanisms in place to amplify connections to the most distal apical dendritic branches (Stuart and Sakmann, 1995; Stuart et al., 1997a; Stuart et al., 1997b; Larkum et al., 2001). Furthermore, studies using laser-scanning photostimulation, including those presented in this dissertation have shown that this rule simply does not hold for certain cell types (Briggs and Callaway, 2001).

Another point of debate is whether cortical connections are specific or promiscuous. That is, are cells picky about which cells they connect to? Or are cell connections made randomly? There is no simple answer to this question since cortical connections change over time during development (Larsen and Callaway, 2006) but also because of experience (Shepherd et al., 2003). However, there are two recent studies that demonstrate that the cortical circuit is highly specific. One study in layer 5 showed that bidirectional connections are more common than expected in a random network (Song et al., 2005). In layer 5 there is a high proportion of three-neuron connectivity patterns than would be expected by chance. In other words, if in layer 5 of the somatosensory cortex, if Cell A is connected to Cell B and to Cell C, there is a much greater than random chance that Cell B and C are connected to each other. Hence, connections tend to cluster and are not arranged randomly. Another recent study showed that there is fine scale specificity to the layer 2/3 of the rat visual cortex. Pairs of connected pyramidal neurons in layer 2/3 of the rat visual cortex have a high amount of synchronous input suggesting that they share input from the same presynaptic cells, whereas cells that were not connected do not (Yoshimura and Callaway, 2005).

In sum, cell types can be distinguished based on their morphological characteristics, physiological properties, and biochemical imprints. Each cell type probably plays a unique functional role in cortical circuitry. The cortical circuit is organized into vertical columns and these columns are repeated motifs in a specialized brain region. Finally, there is strong evidence that connections in the cortex are highly specific and cells do not connect to each other randomly. With these basic principles, we can start thinking about cortical organization of the visual cortex and how this may contribute to visual information processing. However, in order to understand cortical circuitry we must also understand how information enters the system.

1.2 The Rat Retino-geniculo-cortical (Visual) System

Rats have a functioning visual system, despite being nocturnal animals (Fig 1.1). Nearly all of the rat's photoreceptors are rods, with cones comprising less than one percent of photoreceptors in the retina (Szel and Rohlich, 1992). Eyes are located laterally and as a result provide a panoramic view, with some overlap of visual fields giving them binocular vision in the center 40-60° of the visual field. Nevertheless, there is some debate over the amount of ipsilateral projections from the retina. Early studies of the retinal projections of rats found that the only 5-10% of ganglionic axons projected ipsilaterally, while later studies have demonstrated that the acutal number is probably smaller (Lund, 1965; Jeffery, 1984).

There are four major nuclei that receive visual input from the retina: the dorsolateral geniculate nucleus, the ventrolateral geniculate nucleus, the superior colliculus, and the accessory optic system (Sefton et al., 2004). The dorsal lateral

geniculate nucleus (dLGN) in the thalamus is the primary processor of visual information. The ventral lateral geniculate nucleus (vLGN) is not as well studied, but may be responsible for phototic changes in circadian rhythms. The superior colliculus is responsible for saccadic eye movement and eye-head orientation. Finally, the accessory optic system is involved in vestibulo-ocular and opto-kinetic processing. It is important to note that there are perhaps more than a dozen retino-recepient nuclei in the rat visual system, however, these nuclei do not appear be involved in visual processing. Unlike the cat and monkey, only a minority of retinal ganglion cells project to the dorsolateral geniculate nucleus in the rat (Martin, 1986). In this thesis, only the dLGN will be considered further, though these nuclei may work in parallel and there is a some overlap in their circuitry.

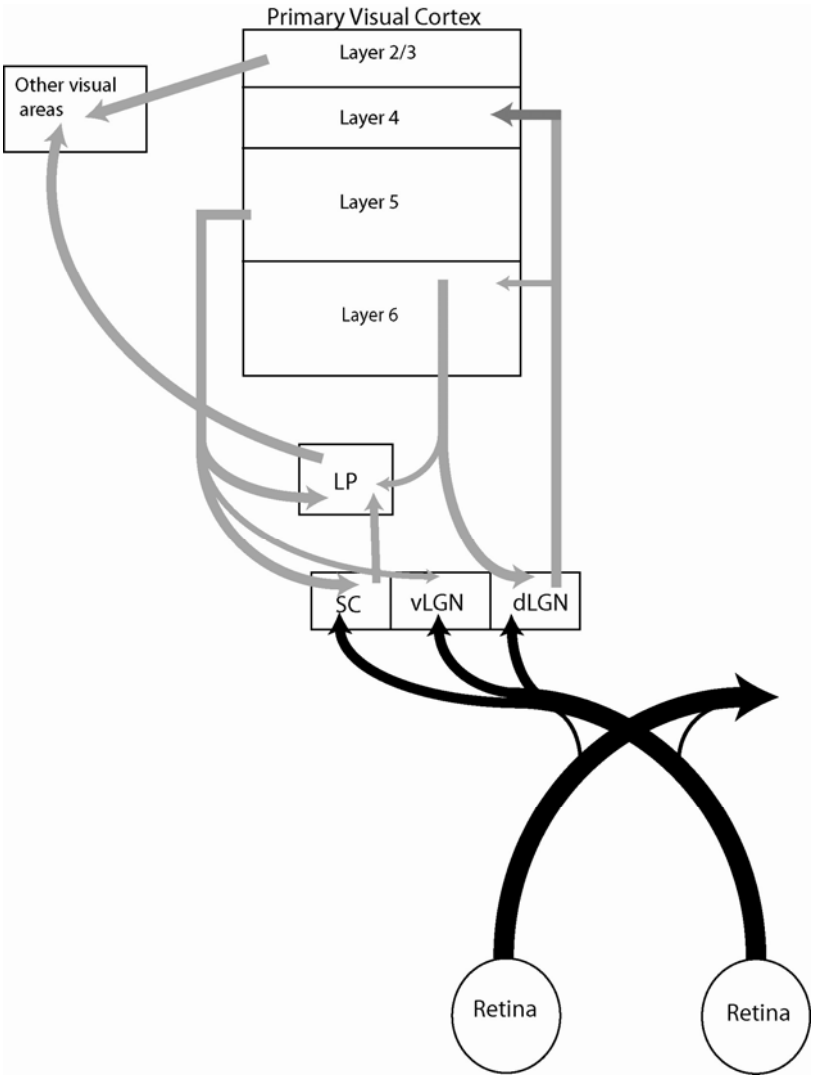

Figure 1.1: The Rat Visual System. The rat retinal ganglion cells provide visual information to the contralateral visual system, with only a small amount of ipsilateral projections (5-10%). The rat retina projects to the dorsal lateral geniculate nucleus (dLGN), the ventral lateral geniculate nucleus (vLGN) and the superior colliculus (SC), along with many other subcortical nuclei that are not shown above. The dLGN is the primary relay nucleus of the visual system and projects axons that terminate in layer 4 and the top half of layer 6 of the rat primary visual cortex. Cells in layer 2/3 of the rat visual cortex project to other cortical areas that are presumed to be involved in higher visual processing. Cells in the lower two layers project axons mainly to subcortical nuclei. They also project axons to other cortical areas and to the contralateral visual cortex via the corpus callosum. For example, cells in layer 6 provide feedback projections to the dLGN, to the contralateral visual cortex, as well as projections to the lateral posterior nucleus (LP), a higher order/secondary visual nucleus in the thalamus that projects to other cortical areas. Layer 5 cells also project to LP, as well as SC, vLGN, and other nuclei not shown above. It is important to note that one way deep layers can affect the processing of other cortical areas through nuclei like LP, which receive strong input from the infragranular layers as well as other subcortical visual areas (e.g. SC).

The dLGN is one of the primary recipients of retinal ganglionic axons and the first to process visual information that is ultimately relayed to the visual cortex. Although it is often described as the "primary relay center" to the visual cortex, it is clear that its function is more than just relaying visual information. The confluence of efferent processes, not only from the retina, but also from the visual cortex, the reticular system, and other thalamic nuclei suggests that there is some level of processing that occurs before visual information is relayed to the visual cortex (Sherman and Guillery, 2002).

Structurally, the dLGN of the rat is different from other mammals used in vision research (i.e. monkey and cat). These latter animals display a clearly laminated dLGN, with each lamina containing cells that are morphologically and/or physiologically distinct. However, the rat dLGN has no obvious lamination and appears to be homogenous, which could give an impression that the rat dLGN is undifferentiated and lacks the sophisticated organizational features of other mammals. However, the rat dLGN has some basic level of functional organization (Reese, 1988). For example, there is a topographic distribution of the retinal projections to the dLGN, retinal ganglion cells that project to different areas of the dLGN have different morphologies and appear to be different cell types (Martin, 1986), and there is a crescent-shaped region of binocularity adjacent to the optic disc (Reese and Jeffery, 1983). Cells in the dLGN mostly project to the ipsilateral visual cortex. Axons terminate in layer 4 and upper layer six, and to a smaller extent layer 1.

The rat primary visual cortex (V1) has been identified on the basis of three criteria: (1) electrophysiology (Adams and Forrester, 1968), (2) cytoarchitectual (Reid

and Juraska, 1991) and (3) connection to dLGN (Ribak and Peters, 1975). V1 can be distinguished from other "higher" order visual through a Nissl or cytochrome oxidase stain. V1 appears to be striated at layer 4, where there is a higher density of cells that appear darker in appearance. Because of this appearance layer 4 is considered the granular layer, making the layers above (i.e. layer 2/3) the supragranular layer, and the ones below (layers 5 and 6) the infragranular layers. The visual cortex can be split into two regions based on whether the region receives binocular or monocular input. However, these regions are difficult to distinguish based on Nissl stain or cytochrome oxidase stains.

Peters and collaborators did a series of experiments that provide a great deal of detail on the cortical inputs and synaptic connectivity of V1. Most people have interpreted the termination of dLGN thalamocortical neurons in V1 to mean that they selective connect only to layer 4 pyramidal and stellate neurons. However, Peters and collaborators have shown that the axons synapse on all neuron elements in layer 4. For example 83% of synapses of the dLGN axons projecting to V1 synapse onto the spines of dendrites of layer 4 stellate cells, dendrites of layer 4 pyramidal cells, apical dendrites of layer 5 and layer 6 neurons, and basal dendrites of layer 3 cells. About 15% of synapses are on the shafts of apical dendrites of layer 5 pyramids and on aspiny neurons (Peters et al., 1976; Peters and Feldman, 1976; Peters and Saldanha, 1976; Peters and Feldman, 1977; Peters et al., 1979; Peters and Kara, 1985a, 1985b; Peters et al., 1985; Peters and Kara, 1987). Further analysis of the geniculocortical axons show that the axons projecting to layer 6 are collateral branches of same axons that project to layer 4 (Bode-Greuel et al., 1987).

V1 has many similarities with the visual system of other mammals. Retinal cells project to a primary sensory nucleus (considered a relay center) where one level of processing can occur. Visual information is then relayed to the visual cortex with major axon ending occurring in layer 4 and upper layer 6. However, in the rat subcortical structures make up a much larger percentage of the brain than other "higher" mammals (e.g. cat and monkey). V1 probably has fewer cortico-cortical connections and less cortical processing of visual information than say the monkey. Visual driven behavior in the rat is probably dominated by subcortical computations. It is therefore not surprising that, in the rat, layer 2/3, the main cortical projecting layer of V1, is considerably small, especially when compared to layer 5 and 6. The latter two layers, which mainly project to subcortical nuclei, compose greater than half of the cortical depth.

Furthermore, there is a great deal of similarity between V1 and other sensory areas of the rat, such as the somatosensory cortex, which is far better studied. The somatosensory cortex also has a granular layer that is characteristic of most sensory systems. Comparing and contrast two different sensory systems could reveal other functional and/or organizational constraints to cortical specialization.

1.3 Connections within Visual Cortex

Callaway (1998) and Gilbert (1983) proposed slightly different models of cortical circuitry based on anatomical observation in the macaque and the cat visual cortices, respectively (Figure 1.2). The models differ greatly on the role that the deep layers play in local cortical circuitry. It is unclear whether these differences are due to some fundamental species differences or from different methodologies used to develop the

circuits. Here we present some basic connections that exist in local cortical circuits that are incorporated into both circuits, as well as discuss some differences that exist between the two circuits.

As mentioned above, cells in layer 4 are probably the major recipients of excitatory input from the dLGN. Although the synapses from dLGN are strong driving synapses, they constitute only a small proportion of synapses to layer 4 spiny neurons (Sherman, 2001; Sherman and Guillery, 2002). The majority of excitatory synapses originate in layer 6 and from other layer 4 neurons.

Layer 4 cells have axon terminals that form a strong connection to layer 2/3 (Dantzker and Callaway, 2000). Anatomical studies show narrow vertically oriented projections to layers 5 and 6 (Burkhalter, 1989). Cells in layer 2/3 make widespread connections within the same layer and project strongly to layer 5 (Burkhalter, 1989) as well as making cortico-cortical projections to other visually activated cortical areas. Although axonal projections does not imply connection, there is physiological evidence that some neurons in layer 5 receive monosynaptic excitatory input from layer 2/3 as well as from layer 6 (Kenan-Vaknin et al., 1992; Thomson and Bannister, 1998; Reyes and Sakmann, 1999). Layer 2/3 provides other cortical areas with the outcome of information processed in the visual cortex. Layer 5, on the other hand, is the major output layer to the subcortical regions.

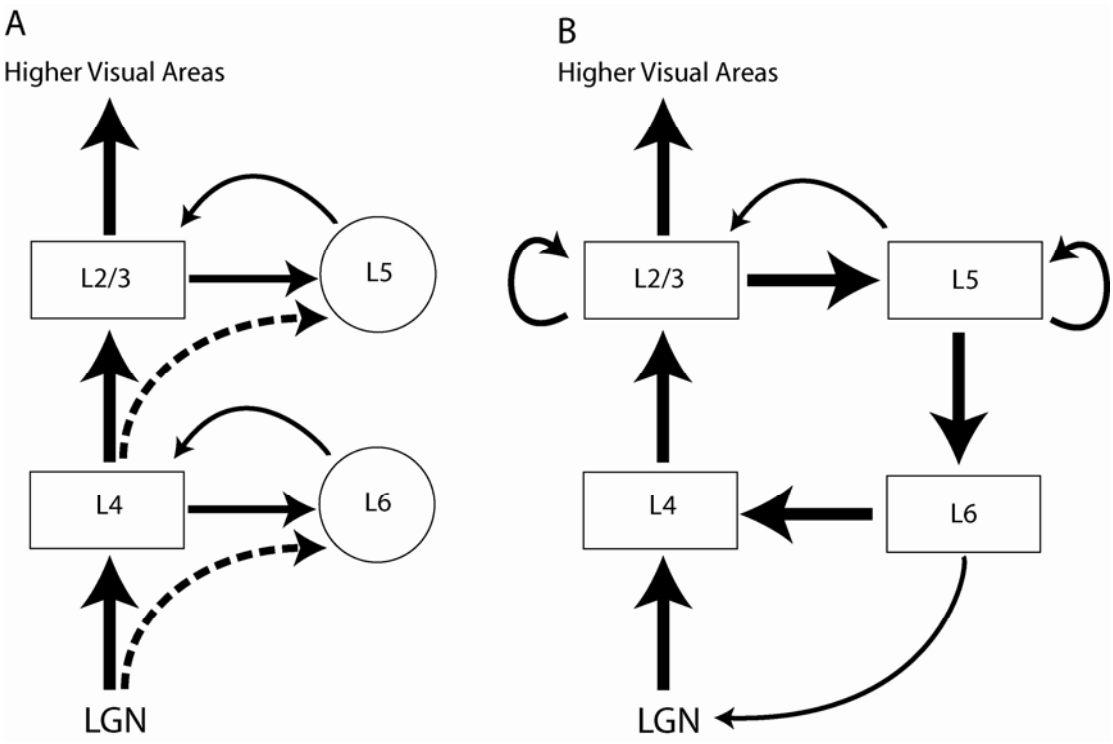

Figure 1.2: Two Examples of Cortical Circuitry Models. (A) A two-level model of local cortical circuitry proposed by Callaway (1998). Each level of processing includes a feedforward component (left rectangles) and a feedback component (right circles). Sizes of arrows reflect relative strength of excitatory input. For the feedforward components, each level gets strong excitatory input from the level underneath it, and in the same vein provides a strong output to the level above it. Feedback components receive weaker input from the level below and the components on the same level. Feedback components also provide strong feedback connections to the components on the same level. Hence, feedforward components send information directly to the next level, whereas feedback components process both the input and output of the components on the same level and play a modulatory role in the progression of information through the levels. (adapted from Callaway, 1998). (B) Illustration of dominant connections in the circuitry model proposed by Gilbert and Wiesel (1983). This model proposes a more recurrent processing of information by the two deep layers. Like the model proposed in (A), excitatory input from LGN goes through two levels before going on to higher visual areas. However, the output to higher visual areas is also sent to layer 5 which serves a modulatory role of layer 2/3 output. Layer 5 also relays excitatory input to layer 6 which can modulate both layer 4 and LGN. (adapted from Douglas & Martin, 2004).

The two models predict different roles for deep layers of the cortex. In the Callaway model, layer 5 should receive strong input from both layer 4 and layer 2/3, whereas in the Gilbert and Wiesel model, layer 5 cells would receive their strongest input from layer 2/3 and weaker input from layer 4. Along the same vein, in the Callaway model of cortical circuitry, layer 6 cells should receive strong input from layer 4, but weaker input from layer 2/3 and 5. However, Gilbert and Wiesel predict a strong input from layer 5 and weaker input from the superficial layers. These models are perhaps complicated by the fact that both layer 5 and 6 have a diverse population of cells that seem to serve different functional roles.

It is unclear what role the cells in the deep layers play in cortical circuitry and, as illustrated, there is some disagreement about their potential inputs. The great diversity of excitatory cell types in the deep layers suggests that these layers play roles in multiple aspects of visual processing. Further evidence of their multifaceted role becomes evident when one assesses the multiple areas of subcortical and cortical projections.

1.4 Subcortical Projections from the Deep Layers

The main targets of excitatory cells in the deep layers of V1 are a wide array of subcortical nuclei and to contralateral and probably ipsilateral regions (as opposed to layer 2/3 which does not project to subcortical regions) (Koester and O'Leary, 1992; Kasper et al., 1994). Although the role of these subcortical projections is not completely understood, they appear to be involved in not only feedback circuitry but also feedforward information processing. For example, deep layers can affect cortical processing of visual information by projecting to subcortical nuclei that have efferents

terminating in other cortical areas. In this section a description of some of the subcortical projections of the deep layers of V1 will be provided. More detailed description of cell morphologies and their specific projections are discussed in greater detail within each individual chapter.

Although the retina provides the main input to the dLGN, based on synaptic strength, numerically the largest input to dLGN comes from the visual cortex (Garey et al., 1991). Axons from cells located in layer 6 of the visual cortex synapse onto geniculate cells in the retinotopically related part of the ipsilateral dLGN (Jacobson and Trojanowski, 1975).

Inactivation of the visual cortex either by cryoblockade, or with KCl cotton wick, affected the physiological and receptive field responses of the cells in the dLGN. Physiologically, after cortical inactivation, cells in the reticular formation (a primary target of cortico-thalamic cells; Bourassa and Deschenes, 1995) were significantly depressed. However, few cells in the dLGN were affected, with only a minority being inhibited (Kayama et al., 1984). Although the activity of cells seems to be unaffected, the receptive field properties change with cortical inactivation. After cryogenic block, the center excitation of the on-center and off-center geniculate cells remained unchanged or in some cases increased suggesting a decrease in surround inhibition. More remarkably, however, they found that half of the on-center surround and nearly all of the off-center surround excitatory responses were either reduced or absent. This study shows that corticothalamic cells can both excite and inhibit cells in the dLGN. Since corticothalamic cells are excitatory it appears that they mediate their inhibitory effects through inhibitory interneurons in the dLGN or in the reticular system.

Deep layers of V1 project extensively to the lateral posterior nucleus (LP; Mason and Groos, 1981). LP, which is in the latero-dorsal thalamus lies medio-caudally from the dLGN and is considered the homologue of the primate pulvinar (Harting et al., 1972). LP is considered a "higher-order" nucleus (since it's main input is not directly from the retina like the dLGN) that interconnects many cortical areas (Guillery, 1995). Because it is the recipient of powerful synapses from layer 5 and since it projects to layer 4 of higher order cortical areas, some believe that the LP plays a significant and important role in visual processing (Guillery and Sherman, 2002). LP also provides feedback to V1 with axons that terminate in layer 5A and layer 1 (Herkenham, 1980).

The large driving synapses to LP from V1 are from cells in layer 5 that also project to the pontine nuclei and the superior colliculus (Mason and Groos, 1981; Bourassa and Deschenes, 1995), as well as cells located in the lower part of layer 6 which have smaller axons with synaptic bouton en passant (Bourassa and Deschenes, 1995; Zhang and Deschenes, 1998). LP also receives significant projections from sectors of the reticular formation and the superior colliculus, another projection target of layer 5 pyramidal cells (Koester and O'Leary, 1992; Kasper et al., 1994; Pinault and Deschenes, 1998).

In sum, the subcortical projections of the cells in the deep layer are quite extensive and can affect visual processing in profound ways. For example, layer 6 cells can alter the response dLGN cells by affecting their receptive field properties. In the rat, the deep layers comprise more than half of the cortical length, while in other mammals (such as the cat and monkey) they comprise a smaller proportion. This suggests that in

the rat the subcortical projections of the rat visual cortex play a more important role in visual processing than do the cortico-cortical projecting neurons.

1.5 Functional Connectivity

Most of the connections discussed in the previous sections are deduced from overlap of dendrites and axons or in some cases electron microscopy. Although these techniques provide information about whether a connection can exist, or if a synapse is present between two different cell types based on a few cells, they reveal little about the functionality of the connection. For example, it's unclear how strong these synapses are, or if potentials from distal synapses can be detected at the soma. In the experiments presented in this dissertation, we combine information about the cells morphological and/or physiological characteristics with functional connectivity to cells in the vertical column.

We detect functional connectivity with a technique called laser-scanning photostimulation (Callaway and Katz, 1993). Photostimulation involves targeted photolysis of molecularly caged glutamate within a brain slice preparation while simultaneously recording intracellularly from an individual neuron. Focal, light-induced uncaging of glutamate causes an action potential in neurons with somata located within a small distance of the stimulation site. Connectivity between the presynaptic neurons firing action potentials and postsynaptic recorded cell is measured as excitatory post synaptic currents. Functional connectivity is assessed after hundreds of stimulation sites within a brain slice. During the experiment, the cell is filled with a dye so that the cell's morphology can be appreciated and analyzed following the recording. Using the

postsynaptic recordings made from the discrete stimulation sites, we can generate a map with the laminar sources of functional excitatory input onto a single, anatomically defined neuron. The power of this preparation is that it can detect functional connections where anatomical observation of axonal projections predicted weak or no connectivity.

This method has been an invaluable tool in analyzing functional cortical circuits, linking cell morphology to physiological characteristics and connection patterns. In my thesis I present three studies that took advantage of this powerful assay to distinguish between different cell types in the deep layers of the rat visual cortex. Understanding the functional role of these cell types will bring us one step closer to unraveling the precise connectivity of neural circuits and, with it, how the cortex can accomplish complex tasks, like vision, so effortlessly.

1.6 References

Adams AD, Forrester JM (1968) The projection of the rat's visual field on the cerebral cortex. Q J Exp Physiol Cogn Med Sci 53:327-336.

Bode-Greuel KM, Singer W, Aldenhoff JB (1987) A current source density analysis of field potentials evoked in slices of visual cortex. Exp Brain Res 69:213-219.

Bourassa J, Deschenes M (1995) Corticothalamic projections from the primary visual cortex in rats: a single fiber study using biocytin as an anterograde tracer. Neuroscience 66:253-263.

Briggs F, Callaway EM (2001) Layer-specific input to distinct cell types in layer 6 of monkey primary visual cortex. J Neurosci 21:3600-3608.

Briggs F, Callaway EM (2005) Laminar patterns of local excitatory input to layer 5 neurons in macaque primary visual cortex. Cereb Cortex 15:479-488.

Brodmann K, Garey L (1999) Brodmann's Localisation in the cerebral cortex. In. River Edge, NJ: Imperial College Press.

Burkhalter A (1989) Intrinsic connections of rat primary visual cortex: laminar organization of axonal projections. J Comp Neurol 279:171-186.

Callaway EM, Katz LC (1993) Photostimulation using caged glutamate reveals functional circuitry in living brain slices. Proc Natl Acad Sci U S A 90:7661-7665.

Chatterjee S, Callaway EM (2002) S cone contributions to the magnocellular visual pathway in macaque monkey. Neuron 35:1135-1146.

Chatterjee S, Callaway EM (2003) Parallel colour-opponent pathways to primary visual cortex. Nature 426:668-671.

Connors BW, Gutnick MJ, Prince DA (1982) Electrophysiological properties of neocortical neurons in vitro. J Neurophysiol 48:1302-1320.

Dantzker JL, Callaway EM (2000) Laminar sources of synaptic input to cortical inhibitory interneurons and pyramidal neurons. Nat Neurosci 3:701-707.

DeFelipe J (2002) Cortical interneurons: from Cajal to 2001. Prog Brain Res 136:215-238.

Douglas RJ, Martin KA (2004) Neuronal circuits of the neocortex. Annu Rev Neurosci 27:419-451.

Finlay BL, Darlington RB (1995) Linked regularities in the development and evolution of mammalian brains. Science 268:1578-1584.

Garey LJ, Dreher B, Robinson SR (1991) The organization of the bisual thalamus. In: Neuroanatomy of the Visual Pathways and Their Development (Dreher B, Robinson SR, eds), pp 176-234. London, UK: Macmillan Press.

Gilbert CD (1983) Microcircuitry of the visual cortex. Annu Rev Neurosci 6:217-247.

Gilbert CD, Wiesel TN (1983) Functional organization of the visual cortex. Prog Brain Res 58:209-218.

Gould SJ (1977) Ontogeny and phylogeny. Cambridge, Mass.: Belknap Press of Harvard University Press.

Guillery RW (1995) Anatomical evidence concerning the role of the thalamus in corticocortical communication: a brief review. J Anat 187 (Pt 3):583-592.

Guillery RW, Sherman SM (2002) Thalamic relay functions and their role in corticocortical communication: generalizations from the visual system. Neuron 33:163-175.

Harting JK, Hall WC, Diamond IT (1972) Evolution of the pulvinar. Brain Behav Evol 6:424-452.

Herkenham M (1980) Laminar organization of thalamic projections to the rat neocortex. Science 207:532-535.

Jacobson S, Trojanowski JQ (1975) Corticothalamic neurons and thalamocortical terminal fields: an investigation in rat using horseradish peroxidase and autoradiography. Brain Res 85:385-401.

Jeffery G (1984) Transneuronal effects of early eye removal on geniculo-cortical projection cells. Brain Res 315:257-263.

Jones EG (2000) Microcolumns in the cerebral cortex. Proc Natl Acad Sci U S A 97:5019-5021.

Kasper EM, Larkman AU, Lubke J, Blakemore C (1994) Pyramidal neurons in layer 5 of the rat visual cortex. I. Correlation among cell morphology, intrinsic electrophysiological properties, and axon targets. J Comp Neurol 339:459-474.

Kawaguchi Y (1993) Groupings of nonpyramidal and pyramidal cells with specific physiological and morphological characteristics in rat frontal cortex. J Neurophysiol 69:416-431.

Kawaguchi Y (2001) Distinct firing patterns of neuronal subtypes in cortical synchronized activities. J Neurosci 21:7261-7272.

Kawaguchi Y, Kubota Y (1996) Physiological and morphological identification of somatostatin- or vasoactive intestinal polypeptide-containing cells among GABAergic cell subtypes in rat frontal cortex. J Neurosci 16:2701-2715.

Kawaguchi Y, Kubota Y (1997) GABAergic cell subtypes and their synaptic connections in rat frontal cortex. Cereb Cortex 7:476-486.

Kawaguchi Y, Kondo S (2002) Parvalbumin, somatostatin and cholecystokinin as chemical markers for specific GABAergic interneuron types in the rat frontal cortex. J Neurocytol 31:277-287.

Kayama Y, Shosaku A, Doty RW (1984) Cryogenic blockade of the visual cortico-thalamic projection in the rat. Exp Brain Res 54:157-165.

Kenan-Vaknin G, Malach R, Segal M (1992) Excitatory inputs to layer V pyramidal cells of rat primary visual cortex revealed by acetylcholine activation. Brain Res 574:147-156.

Koester SE, O'Leary DD (1992) Functional classes of cortical projection neurons develop dendritic distinctions by class-specific sculpting of an early common pattern. J Neurosci 12:1382-1393.

Larkum ME, Zhu JJ, Sakmann B (2001) Dendritic mechanisms underlying the coupling of the dendritic with the axonal action potential initiation zone of adult rat layer 5 pyramidal neurons. J Physiol 533:447-466.

Larsen DD, Callaway EM (2006) Development of layer-specific axonal arborizations in mouse primary somatosensory cortex. J Comp Neurol 494:398-414.

Lund RD (1965) Uncrossed visual pathways of hooded and albino rats. Science 149:1506-1507.

Martin PR (1986) The projection of different retinal ganglion cell classes to the dorsal lateral geniculate nucleus in the hooded rat. Exp Brain Res 62:77-88.

Mason R, Groos GA (1981) Cortico-recipient and tecto-recipient visual zones in the rat's lateral posterior (pulvinar) nucleus: an anatomical study. Neurosci Lett 25:107-112.

Peters A, Feldman ML (1976) The projection of the lateral geniculate nucleus to area 17 of the rat cerebral cortex. I. General description. J Neurocytol 5:63-84.

Peters A, Saldanha J (1976) The projection of the lateral geniculate nucleus to area 17 of the rat cerebral cortex. III. layer VI. Brain Res 105:533-537.

Peters A, Feldman ML (1977) The projection of the lateral geniculate nucleus to area 17 of the rat cerebral cortex. IV. Terminations upon spiny dendrites. J Neurocytol 6:669-689.

Peters A, Kara DA (1985a) The neuronal composition of area 17 of rat visual cortex. II. The nonpyramidal cells. J Comp Neurol 234:242-263.

Peters A, Kara DA (1985b) The neuronal composition of area 17 of rat visual cortex. I. The pyramidal cells. J Comp Neurol 234:218-241.

Peters A, Kara DA (1987) The neuronal composition of area 17 of rat visual cortex. IV. The organization of pyramidal cells. J Comp Neurol 260:573-590.

Peters A, Feldman M, Saldanha J (1976) The projection of the lateral geniculate nucleus to area 17 of the rat cerebral cortex. II. Terminations upon neuronal perikarya and dendritic shafts. J Neurocytol 5:85-107.

Peters A, Kara DA, Harriman KM (1985) The neuronal composition of area 17 of rat visual cortex. III. Numerical considerations. J Comp Neurol 238:263-274.

Peters A, Proskauer CC, Feldman ML, Kimerer L (1979) The projection of the lateral geniculate nucleus to area 17 of the rat cerebral cortex. V. Degenerating axon terminals synapsing with Golgi impregnated neurons. J Neurocytol 8:331-357.

Pinault D, Deschenes M (1998) Projection and innervation patterns of individual thalamic reticular axons in the thalamus of the adult rat: a three-dimensional, graphic, and morphometric analysis. J Comp Neurol 391:180-203.

Pinker S (1997) How the mind works, 1st Edition. New York: Norton.

Ramachandran VS (1985) The neurobiology of perception. Perception 14:97-103.

Ramâon y Cajal S, DeFelipe J, Jones EG (1988) Cajal on the cerebral cortex: an annotated translation of the complete writings. New York: Oxford University Press.

Reese BE (1988) 'Hidden lamination' in the dorsal lateral geniculate nucleus: the functional organization of this thalamic region in the rat. Brain Res 472:119-137.

Reese BE, Jeffery G (1983) Crossed and uncrossed visual topography in dorsal lateral geniculate nucleus of the pigmented rat. J Neurophysiol 49:877-885.

Reid SN, Juraska JM (1991) The cytoarchitectonic boundaries of the monocular and binocular areas of the rat primary visual cortex. Brain Res 563:293-296.

Reyes A, Sakmann B (1999) Developmental switch in the short-term modification of unitary EPSPs evoked in layer 2/3 and layer 5 pyramidal neurons of rat neocortex. J Neurosci 19:3827-3835.

Ribak CE, Peters A (1975) An autoradiographic study of the projections from the lateral geniculate body of the rat. Brain Res 92:341-368.

Schubert D, Kotter R, Luhmann HJ, Staiger JF (2006) Morphology, electrophysiology and functional input connectivity of pyramidal neurons characterizes a genuine layer va in the primary somatosensory cortex. Cereb Cortex 16:223-236.

Schubert D, Kotter R, Zilles K, Luhmann HJ, Staiger JF (2003) Cell type-specific circuits of cortical layer IV spiny neurons. J Neurosci 23:2961-2970.

Schubert D, Staiger JF, Cho N, Kotter R, Zilles K, Luhmann HJ (2001) Layer-specific intracolumnar and transcolumnar functional connectivity of layer V pyramidal cells in rat barrel cortex. J Neurosci 21:3580-3592.

Sefton AJ, Dreher B, Harvey A (2004) Visual System. In: The Rat Nervous System, 3rd Edition Edition (Paxinos G, ed), pp 1083-1165. St. Louis, MO: Elsevier.

Shepherd GM, Pologruto TA, Svoboda K (2003) Circuit analysis of experience-dependent plasticity in the developing rat barrel cortex. Neuron 38:277-289.

Sherman SM (2001) Tonic and burst firing: dual modes of thalamocortical relay. Trends Neurosci 24:122-126.

Sherman SM, Guillery RW (2002) The role of the thalamus in the flow of information to the cortex. Philos Trans R Soc Lond B Biol Sci 357:1695-1708.

Song S, Sjostrom PJ, Reigl M, Nelson S, Chklovskii DB (2005) Highly nonrandom features of synaptic connectivity in local cortical circuits. PLoS Biol 3:e68.

Stuart G, Sakmann B (1995) Amplification of EPSPs by axosomatic sodium channels in neocortical pyramidal neurons. Neuron 15:1065-1076.

Stuart G, Schiller J, Sakmann B (1997a) Action potential initiation and propagation in rat neocortical pyramidal neurons. J Physiol 505 (Pt 3):617-632.

Stuart G, Spruston N, Sakmann B, Hausser M (1997b) Action potential initiation and backpropagation in neurons of the mammalian CNS. Trends Neurosci 20:125-131.

Szel A, Rohlich P (1992) Two cone types of rat retina detected by anti-visual pigment antibodies. Exp Eye Res 55:47-52.

Thomson AM, Bannister AP (1998) Postsynaptic pyramidal target selection by descending layer III pyramidal axons: dual intracellular recordings and biocytin filling in slices of rat neocortex. Neuroscience 84:669-683.

Yoshimura Y, Callaway EM (2005) Fine-scale specificity of cortical networks depends on inhibitory cell type and connectivity. Nat Neurosci 8:1552-1559.

Zarrinpar A, Callaway EM (2006) Local connections to specific types of layer 6 neurons in the rat visual cortex. J Neurophysiol 95:1751-1761.

Zhang ZW, Deschenes M (1998) Projections to layer VI of the posteromedial barrel field in the rat: a reappraisal of the role of corticothalamic pathways. Cereb Cortex 8:428-436.

Chapter 2

Local Connections to Specific Types of Layer 6 Neurons in the Rat Visual Cortex

2.1 Abstract

Because layer 6 of the cerebral cortex receives direct thalamic input and provides projections back to the thalamus, it is in a unique position to influence thalamocortical interactions. Different types of layer 6 pyramidal neurons provide output to different thalamic nuclei, and it is therefore of interest to understand the sources of functional input to these neurons. We studied the morphologies and local excitatory input to individual layer 6 neurons in rat visual cortex by combining intracellular labeling and recording with laser-scanning photostimulation. As in previous photostimulation studies, we found significant differences in the sources of local excitatory input to different cell types. Most notably, there were differences in local input to neurons that, based on analogy to barrel cortex, are likely to project only to the lateral geniculate nucleus of the thalamus versus those that are likely to also project to the lateral posterior nucleus. The more striking finding, however, was the paucity of superficial layer input to layer 6 neurons in the rat visual cortex, contrasting sharply with layer 6 neurons in the primate visual cortex. These observations provide insight into differences in function between cortical projections to first order versus higher-order thalamic nuclei and also show that these circuits can be organized differently in different species.

2.2 Introduction

Layer 6 of the cerebral cortex contains a diverse population of neuron types. Understanding the functional connectivity of each cell type is important for revealing their roles in cortical processing. Pyramidal neurons in layer 6 of primary sensory cortices are the source of corticothalamic input to the primary thalamic relay nuclei. These cells are thought to be involved in feedback circuitry (Bourassa and Deschenes, 1995; Zhang and Deschenes, 1997, 1998). A subset of these corticothalamic layer 6 cells also targets the higher-order thalamic nuclei. Although the function of the higher-order thalamic nuclei is not well understood, one theory is that they mediate cortico-cortical interactions (Guillery and Sherman, 2002).

Corticothalamic neurons of layer 6 have a sublaminar organization. In the rat cortex, cells in the upper half of layer 6 in the somatosensory and visual cortices project to their respective primary relay nuclei, the ventroposterior medial nucleus (VPm) and the lateral geniculate nucleus (LGN; Bourassa and Deschenes, 1995; Zhang and Deschenes, 1997). Cells in the lower half of layer 6 of the somatosensory and visual cortex, project both to their respective higher-order thalamic nuclei [the posterior thalamic nucleus (Po) and the lateral posterior nucleus (LP), respectively] and to their primary nuclei (Bourassa and Deschenes, 1995; Zhang and Deschenes, 1997). The sublaminar organization of these cells suggests that they could have distinct morphologies and intracortical connectivity.

Although in the rat visual cortex retrograde labeling has identified the sublaminar organization of corticothalamic projection neurons, there have been few studies that have analyzed the detailed morphologies of these cells, particularly comparing the cells in the

upper and lower sublayers to find quantifiable differences. As a result, the intracortical circuitry of the layer 6 pyramidal cells is poorly understood, and the role that these cells may play in the visual cortical circuitry is still incomplete. One model of cortical circuitry (Gilbert, 1983; Gilbert and Wiesel, 1983), based primarily on anatomical studies of the cat visual cortex, proposed that the main cortical input to layer 6 is from layer 5 with little input from superficial layers. However, more recent laser-scanning photostimulation studies of input to layer 6 pyramids in macaque visual cortex found that some types of layer 6 pyramidal cells receive strong superficial layer input (Briggs and Callaway, 2001). These results bolstered cortical circuitry models that suggested deep layer neurons are important for providing feedback to superficial layers (Callaway, 1998). It is unclear whether these different hypothesized circuits might reflect methodological differences, differences between species, or cell-type dependent diversity within each species.

This study has two objectives: (1) to characterize the morphological diversity of neurons in layer 6 of the rat visual cortex and to distinguish quantitatively between cell subtypes and (2) to characterize the laminar organization of functional excitatory inputs to these subtypes. By comparing our results to those found in other cortical regions, and other species, the role of layer 6 in visual cortical circuitry can be better understood.

2.3 Materials and Methods

2.3.1 Slice preparation

Vibratome-cut coronal slices (400 μm) were prepared from the primary visual cortex of P25-P30 Long-Evans rats. Slices were cut in ice cold oxygenated (95% O_2/5%

CO_2) artificial cerebral spinal fluid (aCSF, 125 mM NaCl, 5 mM KCl, 26 mM $NaHCO_3$, 1.25 mM KH_2PO_4, 1.33 mM $MgSO_4$, 10 mM d-(+)-glucose, 3.15 mM $CaCl_2$, 1 mM kynurenic acid) and then maintained submerged in the same aCSF solution heated to 35-37˚C.

2.3.2 Photostimulation and Input Maps

We used an infrared Olympus DIC microscope with a 40x, 0.8 NA water immersion lens to visualize and target layer 6 neurons for whole-cell recordings in living brain slices. Glass microelectrodes (6-10 MΩ resistance) filled with a potassium-gluconate-based intracellular solution (130 mM K-gluconate, 10 mM HEPES, 2 mM $MgCl_2$, 10 mM EGTA, 0.5 mM $CaCl_2$, 2.54 mM Na_2ATP) contained 0.5-1% biocytin for cell labeling.

Local stimulation of presynaptic input neurons by light-evoked conversion of 'caged' glutamate to glutamate ("photostimulation") was used to map laminar sources of functional connections onto individual recorded neurons (Callaway and Katz, 1993; Katz and Dalva, 1994; Sawatari and Callaway, 1996, 2000; Briggs and Callaway, 2001, 2005; Yoshimura et al., 2005). Brain slices were bathed in oxygentated aCSF (without kynurenic acid) containing 100-125 μM 'caged' glutamate [γ-(α-carboxy-2-nitrobenzyl) ester, trifluoroacetate, L-glutamic acid – 'CNB-glutamate'; Molecular Probes, Eugene, OR] at room temperature. Ultraviolet light (10-ms flash from an argon-ion laser) was focused to photostimulate a small discrete spot in the plane of the brain slice through the 40x microscope objective positioned above the slice. Whole-cell voltage-clamp recordings (-65 mV) were made from a single layer 6 postsynaptic neuron, and inward

excitatory postsynaptic currents (EPSCs) resulting from photostimulation of presynaptic neurons were measured.

To map the locations of input to a single cell, up to 500 sites were stimulated sequentially in a pseudo-random pattern that covered all cortical layers. Stimulation sites were located throughout a rectangular area surrounding the recorded neuron, typically extending ~200 μm laterally on either side of the cell and vertically from the white matter to layer 1. After each photostimulation event, voltage clamp records were made for each stimulation trial to detect EPSCs. In addition, photostimulation trials were interleaved with control trials (no stimulation) to obtain spontaneous EPSCs (sEPSCs). After completion of photostimulation and recordings from a cell, the laser was used to burn alignment sites (< 10 μm) into the slice so that x-y photostimulation coordinates could be assigned to their corresponding positions in the tissue. Laminar borders were determined using both cytochrome oxidase stain and thionin/Nissl stain.

The spatial resolution of this technique allows mapping of laminar-specific excitatory input in rat visual cortex. We supplemented previously published measures (Dantzker and Callaway, 2000; Yoshimura et al., 2005) with a series of experiments to assess the spatial resolution of the laser-scanning photostimulation with our given parameters. This was also to ensure that the spatial resolution of cells did not differ between layers. Loose-patch extracellular recordings were made of cells throughout the cortical column (~3-5 cells in each layer). We recorded the frequency of action potentials after a photostimulation event and found that our results matched previously published experiments; cells fired action potentials when focal uncaging occurred within ~50 μm from cell soma (see Dantzker and Callaway, 2000; Yoshimura et al., 2005).

2.3.3 Morphological Analysis

After photostimulation, slices were fixed with 4% paraformaldehyde in 0.1 M PBS for at least 12-24 hours, then submerged in 30% sucrose in PBS. Then the slices were resectioned at 80 μm, and stained for cytochrome oxidase and biocytin to reveal alignment sites, laminar borders, and neuronal morphology using methods previously described (Fig. 2.1A, see Yabuta and Callaway, 1998a, 1998b). Nissl stain of the visual cortex revealed that layer 6 can be divided into two parts. The upper part (usually called layer 6 or layer 6A) which is approximately 350 μm thick is separated from the white matter by a narrow, light band of oval shaped cells (usually called layer 6B), that is no thicker than 100 μm. Furthermore layer 6A could be easily separated from layer 5B with a combination of cytochrome oxidase and Nissl stains. Layer 6A was darker than layer 5B in cytochrome oxidase and more densely populated than layer 5B with Nissl stain. We will only discuss cells located in layer 6A in this study and will refer to it as layer 6. Because the thickness of layer 6A varies from slice to slice and animal to animal, we normalized the depths of the cells within this layer by dividing the distance of the soma from the layer 6A/6B border to entire length of layer 6A.

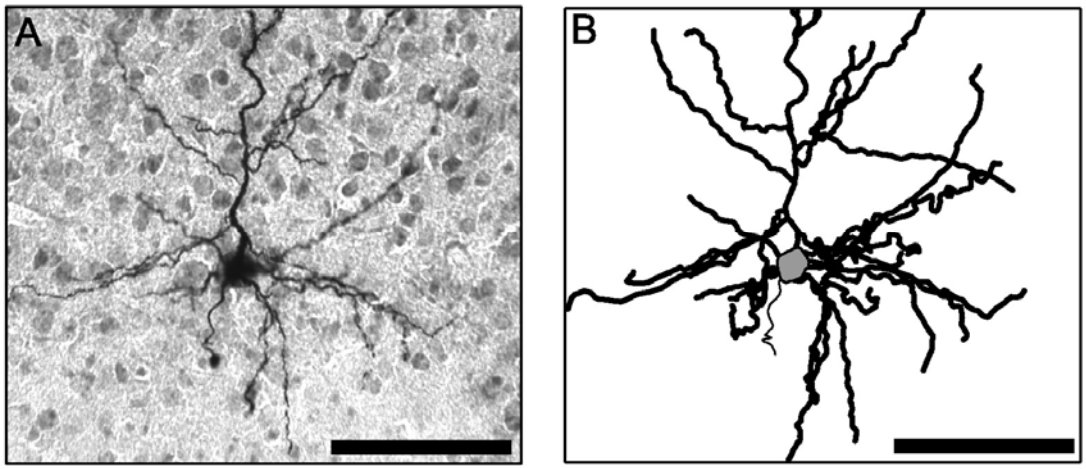

Figure 2.1: Neurolucida Reconstruction of Cells. (A) Cytochrome oxidase and thionin stained section containing a biocytin-labeled layer 6 pyramidal neuron. (B) Neurolucida reconstruction of cell in (A). Dendrites are in dark black lines, soma is gray, and axon is thin line. Scale bars are 200 microns.

After staining, labeled dendritic processes were reconstructed using a 40x objective (oil immersion, 1.30 NA) and Neurolucida, a computerized system (MicroBrightField, Inc., Williston, VT; see Figs. 2.1B, 2.3). After neuronal reconstructions were completed, sections were counterstained for thionin to visualize borders not well delineated with cytochrome oxidase stain alone. Each neuronal reconstruction, showing the morphology of the cell, the laminar borders, and the alignment sites, were aligned with the coordinate map of stimulation sites using Adobe Illustrator (Adobe Systems, San Jose, CA). Using custom software made with Matlab (The MathWorks, Inc., Natick, MA) we measured the length of basal and apical dendrites, as well as the numbers of their respective branches and terminations within each layer. Cells with poor biocytin labeling, such that their anatomical type could not be determined, were excluded from the study. Some cells were well-labeled without collecting of photostimulation data, and are included only for the anatomical studies. For nine of the cells, the soma was lost during resectioning. For these cells the depth of the soma within layer 6 was incalculable, but, since the cut occurred near the base of apical dendrite, enough of the apical dendrite structure remained to classify the cells based on their morphology.

Because we were concerned that cortical columns may be askew to the plane of the slice and hence may affect the number of evoked EPSCs from superficial layers, we took certain precautions to insure that the circuitry to the apical dendrite was intact. First, we blocked the tissue during slicing to minimize the skewing of the apical dendrite and neuron column to the plane of the slice. Second, we eliminated any cells that had apical dendrites that were angled more than 30° from the plane of the slice. Finally we did five

control experiments, where we obtained simultaneous recordings from layer 5 and layer 6 pyramidal cells. Previous photostimulation experiments in layer 5 (Schubert et al., 2001) show that layer 5 pyramidal cells receive strong input from superficial layers, regardless of cell subtype. Likewise, in our control experiments we found that layer 5 pyramidal cells received strong superficial input whereas concurrent measurements from layer 6 pyramidal cells within the same slice showed an absence or weakness of input from these layers (see Figure 2.2 and Results). Finally, our data shows that there is no relationship between a cell's input and/or strength of input from superficial layers and its apical dendrite angle (in relation to the plane of slice; data not shown). Hence, it is unlikely that the angle of slice cutting prevented detection of connections from the superficial layers.

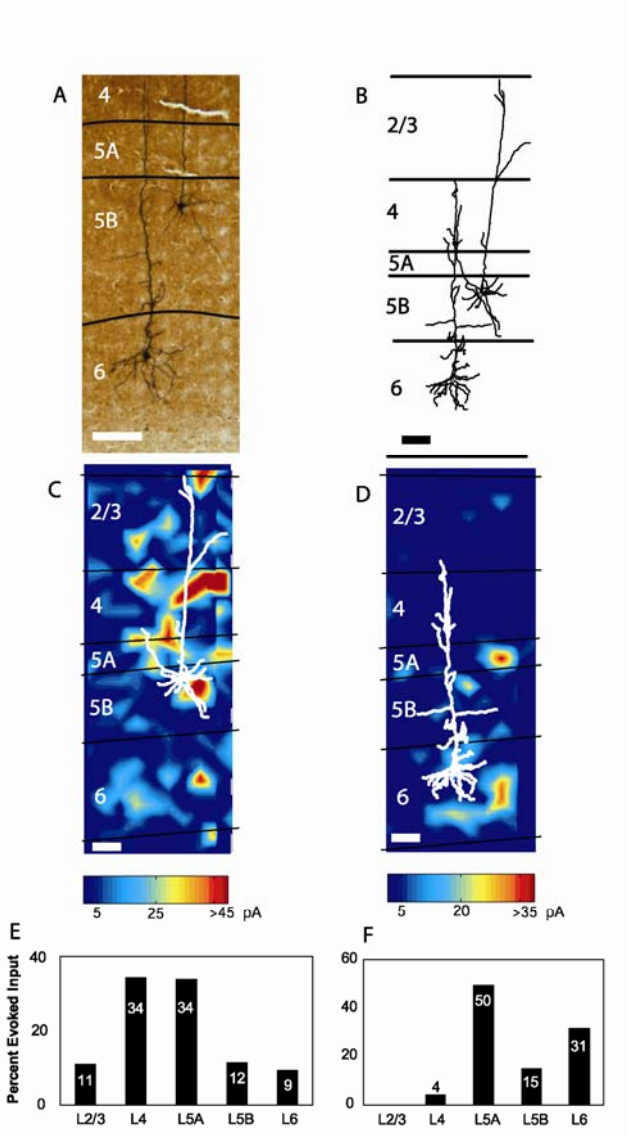

Figure 2.2: Simultaneous Recording from Layer 5 and Layer 6 cells. Input maps to a layer 5 pyramid and a layer 6 pyramid recorded simultaneously. These results are typical of all five dual recording experiments. (A) Cytochrome oxidase and thionin stained section containing a biocytin-labeled layer 5 and a layer 6 (Type II tufted) pyramidal neurons. (B) Neurolucida reconstruction of dendritic arbors of cells in (A). Dendrites are in dark black lines, soma is gray. (C, D) Laminar excitatory input to the two cells depicted in (A) and (B). Pseudo-colored input maps demonstrate patterns of excitatory input. These input maps are linear interpolations of the sum of EPSC amplitude values (minus spontaneous EPSCs) Colored horizontal scale bars indicate the corresponding sum of EPSC amplitude values for input maps Camera lucida drawings of dendrites (*white lines*) and soma (*white*) are overlaid onto plots. Laminar borders are represented by horizontal black lines and labeled on the left. (C) Layer 5 pyramidal neuron that received significant input from all layers. (D) Layer 6 (Type II tufted) pyramidal cell (corresponding to cell D0408C1 in Table 2.3), that received significant input from Layer 4, 5A, 5B, and 6. (E) Bar graph representing the percent of total evoked input from each layer for cell in (C). (F) Bar graph representing the percent of total evoked input from each layer for cell in (D). White bars in (A, C, D) and black bar in (B) represent 100 microns.

2.3.4 Analysis of EPSCs

We analyzed EPSCs that occurred during the first 150 ms following photostimulation. This window was chosen because presynaptic neurons fired most of their APs during this time (see Dantzker and Callaway, 2000; Yoshimura et al., 2005), indicating that shorter analysis windows would exclude photostimulation-evoked EPSCs. We distinguished direct effects of focal uncaging of glutamate on the recorded cell, which had a distinct shape (longer rise-time) and occurred immediately after glutamate uncaging (shorter latency; see, for example, Fig. 2.5A trace 3) from EPSCs, and included only EPSCs in our analysis. Following photostimulation, within ~50 μm of the recorded cell, direct currents sometimes exceeded 100 pA and decayed over 100 ms, preventing EPSCs from being separately identified at these locations and thus, these sites were excluded from analysis. The amplitudes and numbers of EPSCs were measured for every stimulation site and for the no-stimulation controls using peak analysis software from Synaptosoft (Leonia, New Jersey) and other custom software. Each trial was assigned a value in pA, equal to the sum of the peak amplitudes of all detectable EPSCs. Stimulation sites were then assigned to their correct cortical layer, and EPSC amplitudes for all stimulation sites within a layer were pooled together using custom Matlab programs. Laminar groupings of EPSC sum of amplitudes were then compared with spontaneous EPSCs to identify statistically significant differences in EPSCs from a particular layer using Mann Whitney U tests. We also calculated the mean value of summed EPSC amplitudes for that layer as well as for control trials, measuring spontaneous EPSCs. To quantify the evoked input (EI) from a particular layer, the mean

sum of amplitudes of spontaneous events was subtracted from the mean sum of amplitudes for each layer. The relative strength of excitatory input from each layer was calculated by dividing the EI for that layer by the sum of the EIs from all layers for that same cell. Cells were then grouped based on their morphological characteristics. In addition, if a cell did not receive significant input from a layer, the EI for that layer was set to 0 in order to avoid negative EI and EI percentages. Significant differences in layer-specific EI percentages between cell types were determined using Mann Whitney U Test.

To illustrate input patterns for individual cells, smoothed graphs of excitatory input were generated using custom Matlab programs (see Fig. 2.5 and Fig. 2.7). Values of the sum of amplitudes for each individual stimulation site were used to create these smoothed plots using linear interpolation. These plots illustrate estimated evoked activity measured in a given cell (mean sum of EPSC amplitudes for simulated trials minus mean sum of EPSC amplitudes for spontaneous trials) after stimulation at various locations. These plots are purely for illustration of the source of input; no part of the quantitative analyses was based on these linear interpolations.

2.4 Results

2.4.1 Morphological Results

We intracellularly labeled and reconstructed the morphologies of eighty-nine layer 6 neurons in rat visual cortex. All cells were categorized into six different subtypes based on their dendritic morphology. Most of these subtypes have been described in Zhang and Deschenes (1997) single-cell labeling study of layer 6 in the rat

somatosensory cortex, and we found that all our visual cortical cells had homologous morphologies to cells in somatosensory cortex.

Thirteen cells had aspiny dendrites, local pervasive axonal projections, and non-pyramidal somata (Fig. 2.3A) and were classified as inhibitory interneurons (13/89, 14.6%). These cells were found in the upper two-thirds of layer 6 (Fig. 2.4A, Table 2.1). The lack of these cells in the lower third is nearly significant ($p = 0.06$, Fisher Exact Test).

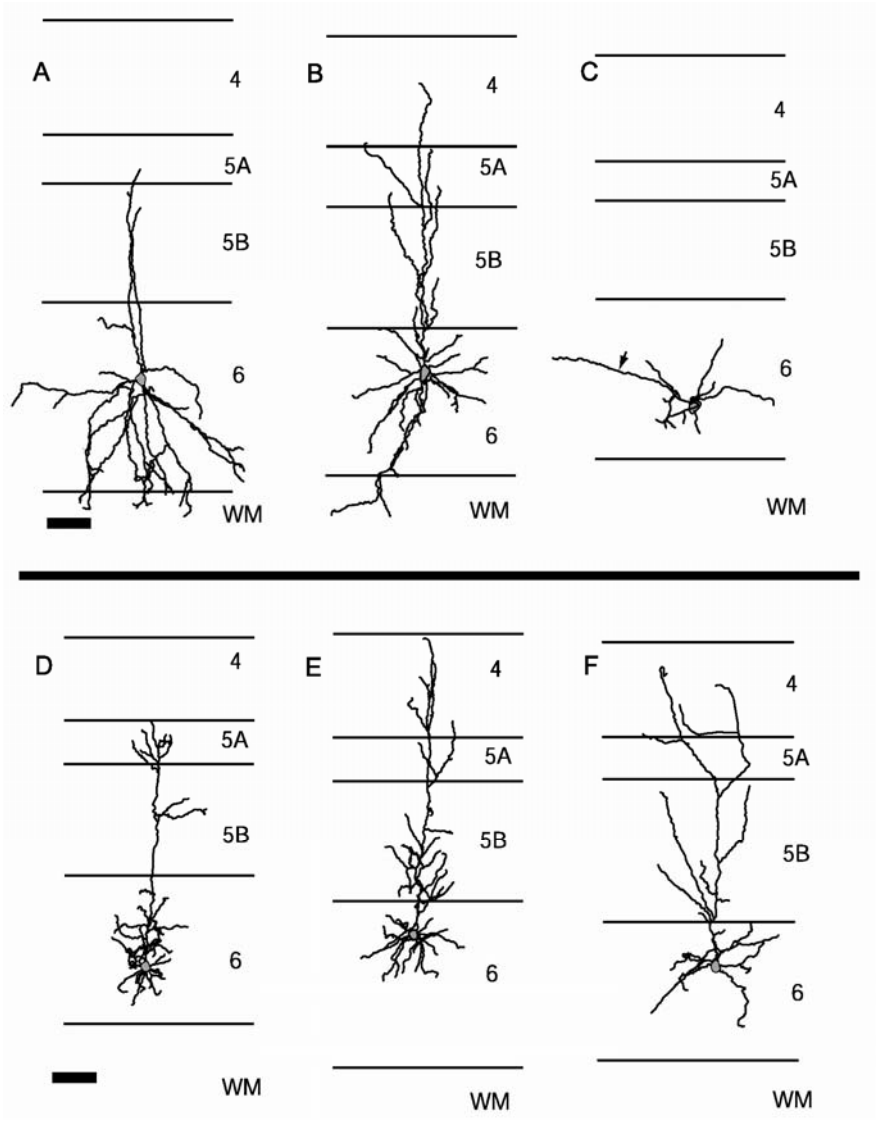

Figure 2.3: Six Main Subtypes of Neurons in Layer 6. Here we show Neurolucida drawing of 6 different neuron subtypes differentiated by dendritic morphology in layer 6 of rat visual cortex. Dark lines represent dendrites and gray represents somata. Axons have been excluded from the drawings. (A) Inhibitory interneuron, identified by smooth, aspiny dendrites and non-pyramidal soma. (B) Bipolar excitatory cell, characterized by two large-diameter, vertically oriented spiny dendrites. One large-diameter dendrite projects toward the pia, while the other projects into the white matter. (C) Inverted pyramidal cells, characterized by pyramidal soma but a thick large-diameter dendrite (*arrow*) that did not project from the pial side of the soma. In this case, the thick large-diameter dendrite ran parallel to the pia. (D) Type I tufted pyramidal cell, characterized by an apical dendrite that had many perpendicular branches in layer 6, sparse perpendicular branches in layer 5B, and a tuft of dendritic branches in layer 5A, with none of the dendrites projecting into layer 4. Basal dendrites are contained within layer 6. (E) Type II tufted pyramidal cell, characterized by an apical dendrite with perpendicular branches in layer 5B and with one dendritic tuft that extends through two layers (layer 5A and layer 4). (F) Non-tufted pyramidal cell, characterized by long angular branches from the apical dendrite, especially at the layer 5B/6 border. Apical dendrite does not end in a tuft. Both scale bars represent 200 microns.

The remaining neurons all had spiny dendrites suggesting that they were excitatory neurons. Most had a typical pyramidal morphology (see below). However, nine cells had modified pyramidal morphologies described previously as bipolar excitatory (4/89 cells, 4.5%) or inverted pyramidal cells (5/89 cell, 5.6%; Zhang and Deschenes, 1997). Bipolar excitatory cells (Fig. 2.3B) were characterized by two large-diameter, vertically-oriented, spiny dendrites. One of these dendrites projected toward the pial surface while the other projected into the white matter. The large diameter basal dendrite in all cases was much thicker and longer than other basal dendrites, making these cells quite distinct from other pyramidal cells. Bipolar excitatory cells were found throughout the layer (Fig. 2.4A), and their counterparts in the rat somatosensory cortex had cortico-cortical projecting axons (Zhang and Deschenes, 1997).

Inverted pyramidal cells (Fig. 2.3C) had a pyramidal shaped soma but the thick, large-diameter dendrite (the "apical" dendrite) did not project from the pial side of the soma. In fact these cells were essentially pyramidal cells that were rotated so that their "apical" dendrite ran, in most cases, parallel to the pia, or more rarely, into the white matter. The axons of these cells projected from the side of the soma opposite the "apical" dendrite. These cells were also found throughout the depth of layer 6 (Fig. 2.4A), and their counterparts in the rat somatosensory cortex had cortico-cortical projecting axons (Zhang and Deschenes, 1997).

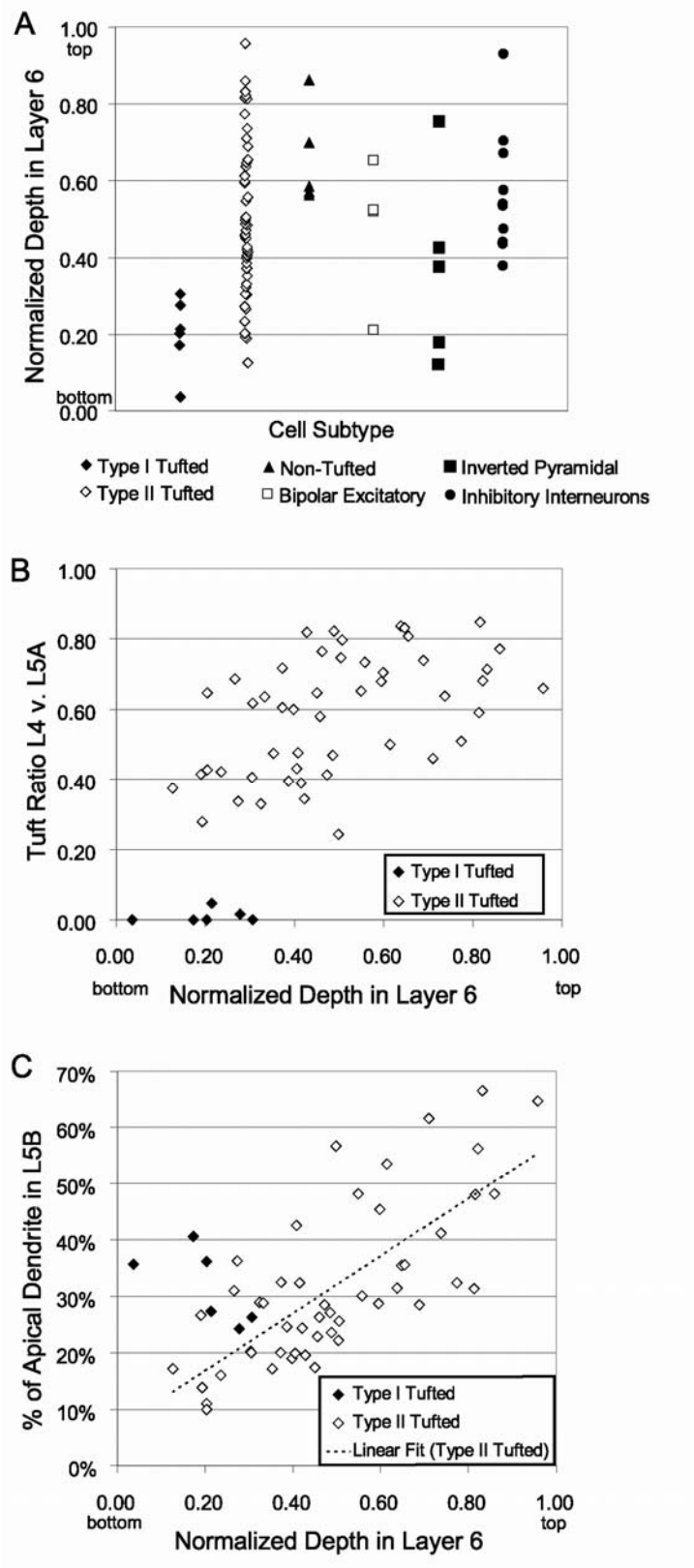

Figure 2.4: Sublaminar Organization of Cell Subtypes. (A) Distribution of cell subtypes within layer 6. The normalized depth within layer 6 is defined by the distance of the center of soma from the layer 6A/6B border divided by total length of layer 6A. Type I tufted pyramidal cells are located in the lower third of layer 6A whereas Type II tufted pyramidal cells are found throughout the entire layer (see also Table 1). Non-Tufted cells are found in the upper half of layer 6. All other types of cells are found throughout the layer. (B) The relationship of normalized cell depth and tuft ratio. The tuft ratio is calculated by dividing the length of apical dendrite in layer 4 by the sum of the lengths in layer 4 and layer 5A. Type I and Type II tufted pyramidal cells are clearly separated and not part of a continuum. (C) The relationship of normalized cell depth to the percentage of apical dendrite in layer 5B. Percentage of apical dendrite in layer 5B is determined by dividing the length of apical dendrite in layer 5B by total apical dendritic length. Dotted line is only fitted to Type II tufted pyramidal neurons ($p < 0.001$). Type I tufted pyramidal neurons do not follow the same trend (see text).

The great majority of cells (62/89, 69.7%), were “tufted” pyramidal cells (Figs. 2.3D, E). These cells had a characteristic apical dendrite that had many near-perpendicular branches in layer 6, usually sparse perpendicular branches in layer 5B, and a tuft of dendritic branches that initiated in layer 5A and sometimes continued through layer 4. Their basal dendrites radiated in all directions but remained confined to layer 6. Among this group of cells we found two morphologically distinct groups of cells, Type I (which has a tuft in one layer, 5A) and Type II (which has a tuft in two layers, 5A and 4).

Type I tufted neurons (Fig. 2.3D; 8/89, 9.0% of all cells) were found only in the lower third of layer 6 (Fig. 2.4A) and nearly the entire apical dendritic tuft was contained within layer 5A, with no dendrites in layer 4. These cells were similar in both morphology and laminar depth to rat somatosensory cortex layer 6 cells that projected to both VPm and Po (Zhang and Deschenes, 1997). Type II tufted neurons (Fig. 2.3E, 54/89, 60.7% of all cells) were found throughout layer 6 (Fig. 2.4A). They had a series of dendritic branches in layer 5A which continued into and branched in layer 4. Hence, a larger proportion of their apical dendritic tufts was in layer 4 compared to Type I tufted cells. These cells were similar to rat somatosensory cortex layer 6 cells that projected only to VPm and not to Po (Zhang and Deschenes, 1997). Our quantitative criterion for separating tufted cells into these two groups was the apical dendrite length in layer 4 divided by the sum of apical dendrite length in layer 4 plus layer 5A (“apical tuft ratio”). If this proportion was approximately zero, then the cell was classified as a Type I tufted cell, whereas cells classified as Type II tufted cells had a proportion greater than 0.2. In accordance to this classification system, the average tuft proportion of Type I tufted cells

(range: 0.00 to 0.05, mean = 0.008) was significantly different ($p < 0.0001$) from Type II Tufted cells (range: 0.24 to 0.85, mean = 0.579; Fig. 2.4B).

We found a significant difference between Type I and Type II tufted cells in the depth of their somata within layer 6. We determined a normalized depth for each cell by dividing the distance from the cell body to the layer 6A/6B border by the thickness of layer 6A (0.0 = bottom of layer 6; 1.0 = top of layer 6). The average depths for Type I and Type II neurons were 0.20 (range = 0.036 to 0.306) and 0.49 (range = 0.126 to 0.958), respectively. This difference was significant (Mann Whitney U Test, $p < 0.0005$). Since our sample was not uniformly distributed within the depth of layer 6, we split layer 6 into three subregions based on depth to compare the proportion of Type I and Type II tufted cells in each portion (see Table 2.1). In the top and middle thirds of layer 6 the proportions of Type II tufted cells did not differ (as a proportion of all layer 6 cells; 10/16, 62.5% in top third; 27/43, 62.8% in middle third). However, in the lower third of layer 6, the proportion of Type II tufted cells was slightly lower to 57.1% (12/21). Type I tufted cells only resided in the lower third of the layer 6 and comprised more than a quarter of the population of cells from that portion of the layer (6/21, 28.6%). This non-uniform distribution explains why we sampled a relatively small number of Type I tufted cells, however, even within the bottom third of layer 6, Type II cells were twice as common as Type I cells.

We were concerned that Type I tufted and Type II tufted cells could be part of the same continuum of cells. However, two pieces of evidence suggest that they are two distinct populations. When we plotted the depth ratio for the each cell against its respective apical tuft ratio, the cells fell into two separate groups suggesting that they are

distinct (Fig. 2.4B). In addition, there was a difference between these two populations in the relationship between the cell depth and percentage of dendritic length in layer 5B (Fig. 2.4C). Type II cells showed a positive significant trend in this relationship such that as these cells got closer to layer 5B the percentage of their apical dendrite in layer 5B increased ($R^2 = 0.54$, $p < 0.0001$). Type I cells had the opposite trend; as cells got closer to layer 5B the percentage of their apical dendrite in layer 5B decreased ($R^2 = 0.44$). For cells in the bottom 31% of layer 6 (which contains all the Type I tufted cells) there was a significant difference in the percentage of the apical dendrite in layer 5B between Type I tufted cells (31.7%, range = 24.3% to 40.6%) and Type II tufted cells (20.2%, range = 10.0% to 36.2%, Mann Whitney U Test, $p < 0.05$).

Previous studies have shown that cells in the rat somatosensory cortex have similar morphologies to what we have found in the rat visual cortex (Zhang and Deschenes, 1997). More specifically, in the somatosensory cortex, cells in the lower half which project to VPm and Po also have an apical dendrite that has sparse branching in layer 5B and an apical tuft in layer 5A. Somatosensory cells in the upper half which project to VPm but not Po have an apical dendrite that tufts in layer 4. Based on these homologous relationships and earlier studies showing the sublaminar projections of the rat visual cortex (Bourassa and Deschenes, 1995), we suspect that the Type I tufted cells are projecting to LGN and LP, whereas Type II tufted cells are only projecting to LGN.

A small group of layer 6 pyramidal cells ("Non-Tufted" cells, 5/89, 5.6%) were characterized by their long angular branches from the apical dendrite, especially at the layer 5B/6 border (Fig. 2.3F). Their apical dendrite did not end in a tuft, and these cells had homologous morphology to cortico-cortical projecting "short pyramidal" cells in rat

somatosensory cortex. In addition, non-tufted pyramidal cells were sampled only in the top half of layer 6 and with an average depth of 0.66 (range = 0.563 to 0.862), which was significantly different from Type I tufted cells (Mann Whitney U Test, $p < 0.005$) and nearly significantly different from Type II tufted cells (Mann Whitney U Test, $p = 0.05$).

2.4.2 Photostimulation Results

We used laser-scanning photostimulation to map the local sources of excitatory input to fifty-nine layer 6 cells. A complete table of the photostimulation results for all of our cells is provided in Table 2.2 and Table 2.3 with sample local excitatory input patterns for each cell type provided in Figures 2.5 and 2.7.

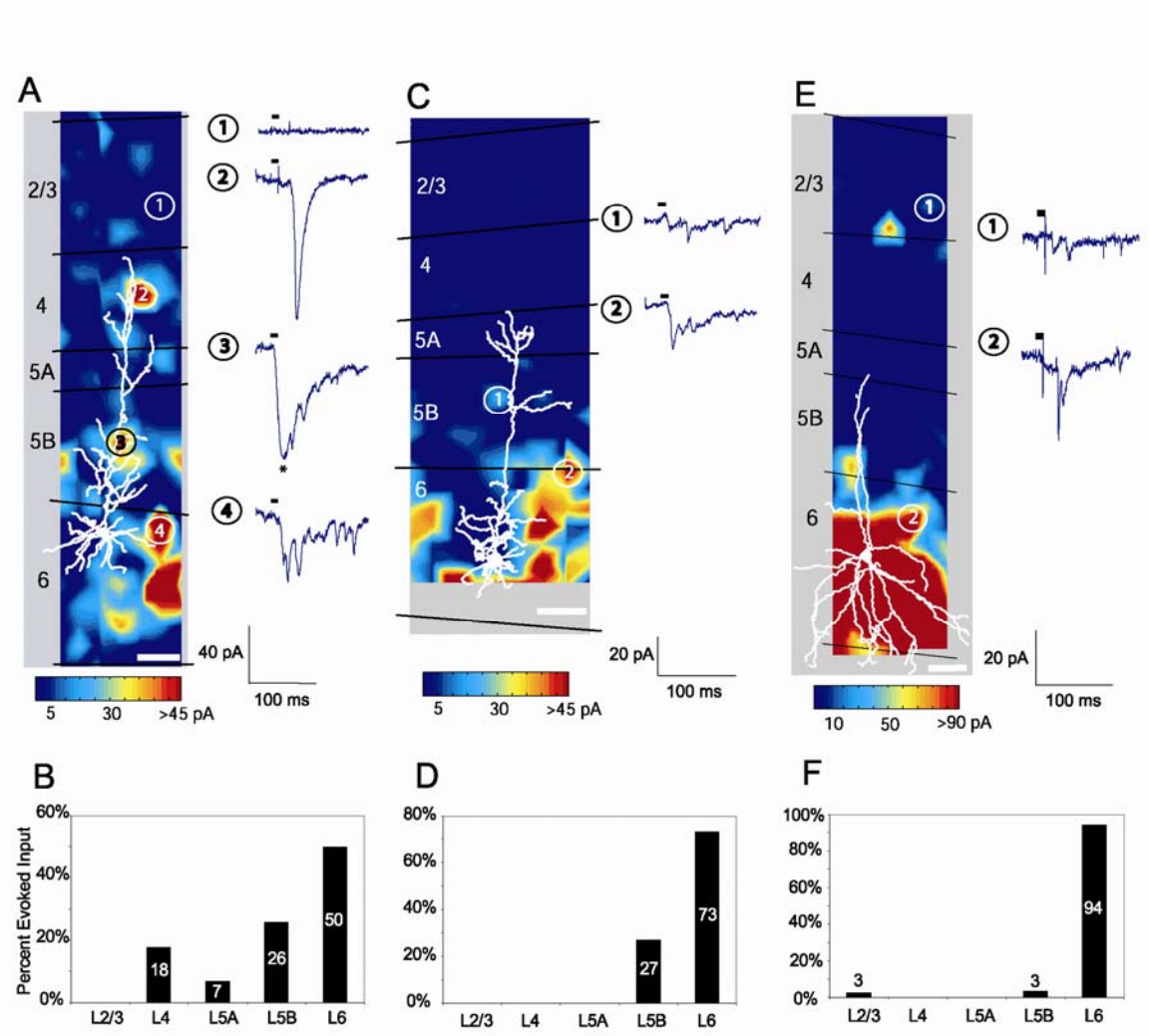

Figure 2.5: Examples of Laminar Excitatory Input to Three Layer 6 Cells. Pseudo-colored input maps demonstrate representative patterns of excitatory input to three individual neurons (see Fig. 2.3). To the right of each input map are example voltage-clamp recordings (-65 mV holding potential) made while stimulating presynaptic regions signified by the corresponding circled numbers. Short dashes above each trace show the duration of photostimulation and onset of glutamate activation. The currents marked with an asterisk (*) are direct responses to glutamate uncaging and are omitted from analysis. Percentage of evoked excitatory input (EI, see text) from each layer is illustrated in the bar graphs below each plot. (A) Type II tufted pyramidal neuron (cell number Z1204e – see Table 2.3; Figure 2.3D) that received significant input from layers 4, 5A, 5B, and 6, but not from layer 2/3. (B) Bar graph representing the percent of total EI from each layer for cell in (A). (C) Type I tufted pyramidal neuron (cell number Z0423d – see Table 2.2; Figure 2.3E) that received significant input from layers 5B and 6, with no significant input from layers 2/3, 4, or 5A. (D) Bar graph representing the percent of total EI from each layer for cell in (C). (E) Inhibitory interneuron (cell number Z0826e – See Table 2.2; Figure 2.3A) that received significant input from layers 2/3, 5B, and 6, but no significant input from layers 4 or 5A. (F) Bar graph representing the percent of total EI from each layer for cell in (E). A brief electrical noise corresponding with shutter closure occurred in a few of these traces (i.e., trace 2 in A, trace 1 and 2 in E). White scale bars represent 200 microns.

Type I and Type II tufted cells had significant differences in their local laminar input (Figs. 2.3A-B, 2.6A). We collected photostimulation data for seven Type I tufted and thirty-eight Type II tufted pyramidal cells. Sample input patterns for Type II and Type I tufted pyramidal cells are shown in Figures 2.5A and 2.5B. All Type I tufted and Type II tufted cells received significant input from layer 6. Significant input from layer 5B was somewhat less common for Type I tufted cells (5/7, 71.4%) than Type II tufted cells (37/38, 97.4%; see Fig. 2.6A). This difference was nearly significant (Fisher's Exact Test, $p = 0.06$). Significant input from layer 5A was significantly less common for Type I tufted cells (1/7, 14.3%) than Type II tufted cells (23/38, 60.5%; Fisher's Exact Test, $p < 0.05$; Fig. 2.6A). Type I and Type II tufted cells differed most significantly in their input from layer 4. Fifty-eight percent (22/38) of Type II tufted cells received significant input from layer 4, whereas no Type I tufted cell received significant input from layer 4 (Fisher's Exact Test, $p < 0.01$; Fig. 2.6A). Neither cell type received much input from layer 2/3. Only two (2/38, 5.3%) Type II tufted cells and no Type I tufted cell received significant input from layer 2/3 (not significant; Fig. 2.6A).

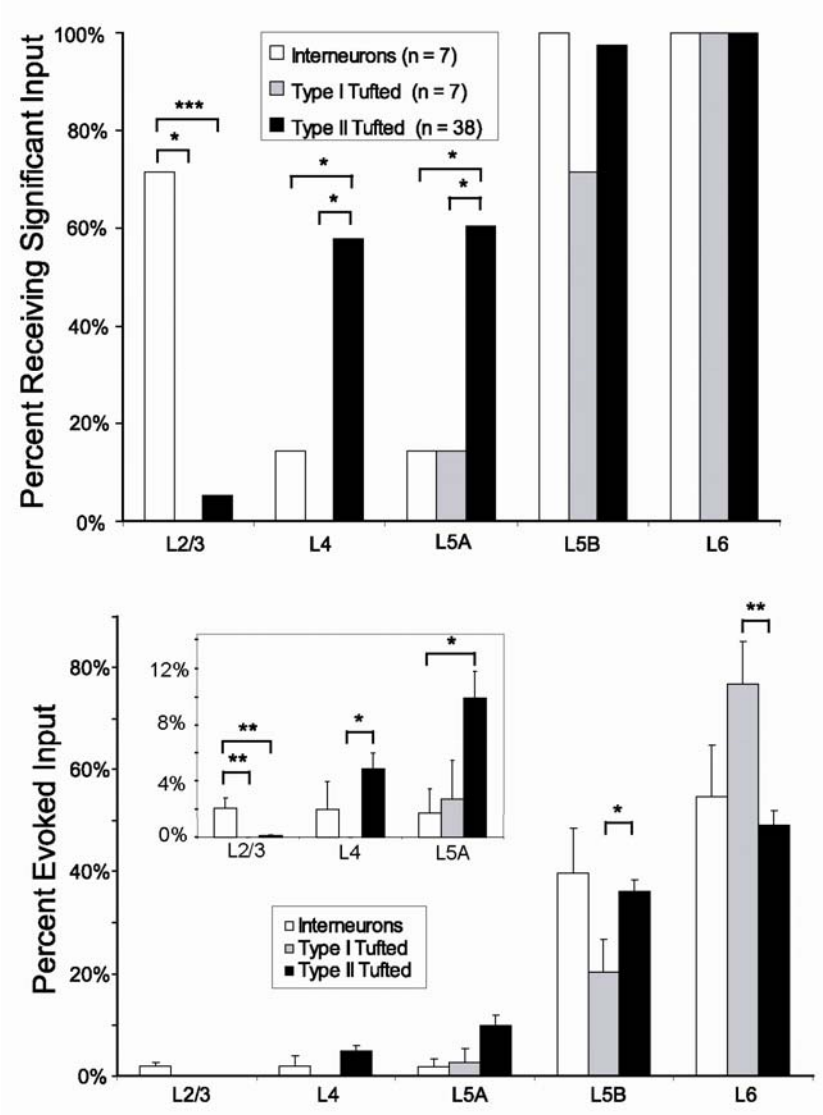

Figure 2.6: Laminar Input to the Three Main Subtypes of Layer 6 Neurons. (A) Percentages of neurons of each type receiving significant input compared with spontaneous trials for each cortical layer. Interneurons as a group were more likely to receive significant input from layer 2/3 than other cell types (Fisher Exact Test, Type I, $p < 0.05$, Type II, $p < 0.0005$). Type II cells as a group received significantly more input from layer 4 (Type I, $p < 0.01$, Interneurons, $p < 0.05$) and layer 5A (Type I, $p < 0.05$, Interneurons, $p < 0.05$). Almost all cells received significant input from layer 5B. All cells, without exception received significant input from layer 6. (B) Mean ± SEM percent of total evoked input for each layer for the three main subtypes of cells. Inset graph is an enlargement of the input from the three superficial layers. Interneurons received a larger percentage of evoked input from layer 2/3 than other cell types (Mann Whitney U test, Type I, $p < 0.005$, Type II $p < 0.005$). Type II tufted cells received a larger percentage of their evoked input from layer 4 than did type I cells ($p < 0.05$) and from layer 5A than did interneurons ($p < 0.05$). Type II tufted cells also received a larger percentage of their evoked input from layer 5B compared to Type I tufted cells ($p < 0.05$). Conversely, Type I tufted cells received a larger percentage of their evoked input from layer 6 compared to Type II tufted cells ($p < 0.005$). * denotes a significance of $p < 0.05$; ** denotes a significance of $p < 0.005$; *** denotes a significance of $p < 0.0005$.

We also analyzed the relative strength of excitatory input from each layer to the Type I and Type II tufted cells. Although these cells received differential inputs from superficial layers, the strongest inputs to both cell types came from layer 6 (Fig. 2.6B). Nevertheless, relative strength of input from the deeper layers differed between Type I and Type II tufted cells. Type I tufted cells received a greater percentage of their evoked excitatory input from layer 6 (76.8 ± 8.2%; mean ± SEM) than did Type II tufted cells (49.0 ± 3.0%, Mann Whitney U test $p < 0.005$, Fig. 2.6B). Conversely, Type II tufted cells received a larger percentage of their excitatory input from layer 5B (36.1 ± 2.4%) than did Type I tufted cells (20.4 ± 6.4%, Mann Whitney U test $p < 0.05$, Fig. 2.6B).

As expected from the proportions of cells receiving significant layer 4 input, the relative strength of evoked input from layer 4 for Type II tufted cells was significantly greater than for Type I tufted cells (4.9 ± 1.1%, versus 0.0%, respectively, Mann Whitney U Test, $p < 0.05$, Fig. 2.6B). The relative strength of evoked input from layer 5A for Type II tufted cells was greater than for Type I Tufted cells (9.9 ± 1.9%, versus 2.7 ± 2.7%, respectively) but the difference was not significant (Mann Whitney U Test, $p = 0.08$, Fig. 2.6B).

Interneurons comprised seven cells out of the population characterized with photostimulation. A typical excitatory input pattern to an interneuron is illustrated in Fig. 2.5E. All interneurons received significant input from both layers 5B and 6 (Fig. 2.6A). Only one inhibitory cell received significant input from layer 4 and layer 5A (1/7, 14.3%). However, five cells (5/7, 71.4%) received significant input from layer 2/3. The proportion of cells receiving input from layer 2/3 was significantly greater than for each

of the tufted pyramidal cell subtypes (Fisher Exact Test, Type I, $p < 0.05$, Type II, $p < 0.0005$, Fig. 2.6A). Nevertheless, the strongest excitatory input to layer 6 inhibitory cells was from the deeper layers, with 54.6 ± 10.1% of their input coming from layer 6 and 39.6 ± 8.9% of their input from layer 5B. Despite the prevalence of significant input from layer 2/3 it was quite weak; only 2.1 ± 0.7% of the excitatory input to interneurons came from layer 2/3. Nevertheless, the strength of input form layer 2/3 to interneurons was significantly more than for other cell types (Mann Whitney U test, $p < 0.005$). Also the strength of input from layer 5A was significantly less for interneurons than for Type II tufted cells (Mann Whitney U Test, $p < 0.05$).

Our photostimulation results for the other three cell types were limited. We only had photostimulation results for two non-tufted cells, three bipolar excitatory cells, and three inverted pyramidal cells (see Table 2.2), which was not enough to draw a conclusion about possible differences between cell types. Sample input patterns for these three more rare subtypes are provided in Figure 2.7. However, we did find that there was some internal consistency in these groups of cells. For example, both non-tufted pyramidal cells received significant excitatory input from all the layers. Both bipolar excitatory cells received some significant superficial layer input and received stronger input from layer 5B than layer 6. All three inverted pyramidal cells received no significant superficial input and received their largest input from layer 6. Like other cell types, these cells all received the great majority of their excitatory inputs from layers 5B and 6 and not from more superficial layers.

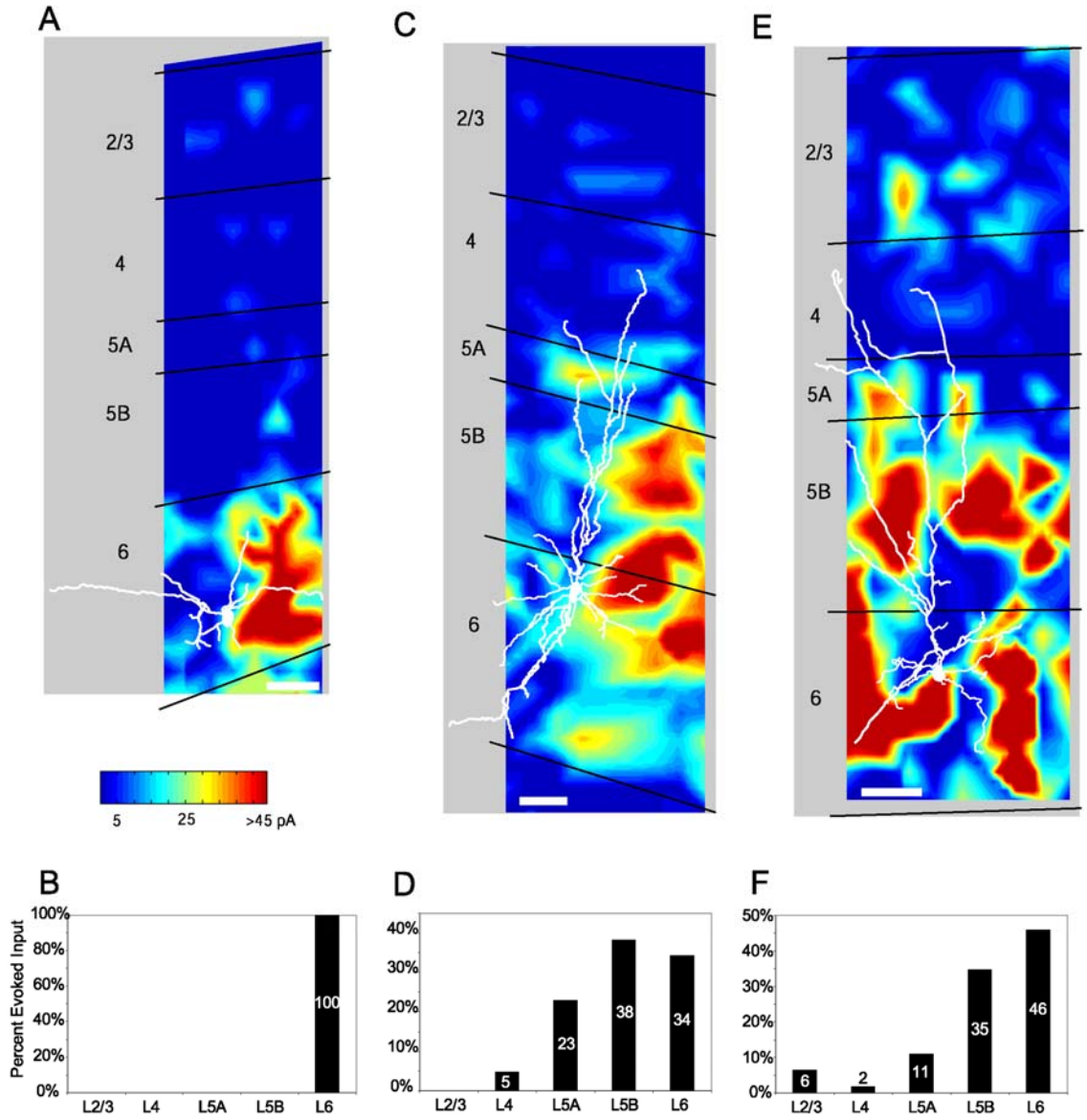

Figure 2.7: Examples of Laminar Excitatory Input to Three Relatively Rare Layer 6 Pyramidal Cells. Pseudo-colored input maps are similar to those described in Figure 2.5. Colored horizontal scale bar in (A) applies to all three maps. White scale bars represent 200 microns. (A) Inverted pyramidal neuron (cell number Z0203a – see Table 2.2; Figure 2.3C) that received significant input only from layer 6. (B) Bar graph representing the percent of total evoked input from each layer for cell in (A). In this case the only significant input came from layer 6. (C) Bipolar excitatory pyramidal neuron (cell number Z0421z – see Table 2.2; Figure 2.3B) that received significant input from layers 4, 5A, 5B, and 6, but not from layer 2/3. (D) Bar graph representing the percent of total evoked input from each layer for cell in (C). In this case the strongest input came from layer 5B followed closely by layer 6. The weakest significant input came from layer 4. (E) Non-tufted pyramidal neuron (cell number Z0331a1 – see Table 2.2; Figure 2.3F) that received significant input from all the layers. (F) Bar graph representing the percent of total evoked input from each layer for cell in (E). In this case the strongest input came from layer 6 followed by layer 5B. The weakest significant input came from layer 4.

In summary, our photostimulation results indicate that cells with different morphologies receive different patterns of laminar input. The most striking differences are between the two tufted pyramidal cell subtypes. Type I tufted cells have no detectable superficial excitatory input but receive strong excitatory input from the deeper layers, especially layer 6. Type II tufted cells also receive their strongest excitatory input from layer 6, but proportionally less than Type I tufted cells. On the other hand they receive stronger excitatory input form layers 4, 5A, and 5B. Finally, inhibitory interneurons and non-tufted pyramids, which also receive their strongest excitatory input from layer 6, were the only cell subtypes that received significant excitatory input from layer 2/3.

2.5 Discussion

2.5.1 Overview

Primary sensory cortices have many common organizational features across cortical areas and across species. For example, input from primary thalamic nuclei targets cortical layers 4 and 6, and corticothalamic feedback originates from layer 6 pyramidal neurons. Furthermore, the cortical layers containing neurons that project axons to layer 6 are also conserved across areas and species. These similarities suggest the layer 6 neurons might be connected similarly across cortical areas and play similar functional roles. Our findings, however, demonstrate that the sources of local excitatory input to layer 6 pyramidal neurons in the rat visual cortex are strikingly different from those in the monkey visual cortex. Monkey layer 6 pyramids can receive very strong input from superficial cortical layers often exceeding the strength of deep layer input to the same cell

(Briggs and Callaway, 2001). In contrast, rat layer 6 neurons invariably received the great majority of their excitatory input from deep layers.

Previous anatomical studies of rat layer 6 cortical neurons identified a large diversity of morphological subtypes (van Brederode and Snyder, 1992; Zhang and Deschenes, 1997). Our study is no exception. In the rat visual cortex, we found six subtypes of neurons based on their dendritic morphology. Consistent with a different functional role for each layer 6 cell type, we also identify systematic differences in the laminar sources of local excitatory input to each cell type.

2.5.2 Cell Type Specific Circuits

The most common types of pyramidal cells encountered in our studies of the rat visual cortex are remarkably similar in their morphology to layer 6 pyramidal neurons in rat somatosensory cortex. Zhang and Deschenes (1997), who classified their cells based not only on dendritic morphology but also based on their axonal projections, found six subtypes of neurons, suggesting that these cells are common to sensory cortices and may play analogous functional roles. We have adopted the same names for our cell types when the homology was clear (i.e. excitatory bipolar cells, inverted pyramidal cells). One major change in terminology is our Type I and Type II tufted pyramidal cells, which we distinguished by dendritic morphology whereas Zhang and Deschenes classified based on axonal projections. We find that the dendritic arbors of Type I tufted cells are indistinguishable from the tufted cells in the somatosensory cortex that project to VPm and Po, while Type II tufted cells are similar to those in the somatosensory cortex that project to VPm (Zhang and Deschenes, 1997).

Furthermore, some subtypes of layer 6 cells have a sublaminar organization. Earlier studies of rat visual cortex found that cells in the upper and lower half had different thalamic projections (Bourassa and Deschenes, 1995), a characteristic that is also shared with the somatosensory cortex (Zhang and Deschenes, 1997). Three main differences exist in the sublaminar organization of our cells and that of Zhang and Deschenes. First, they found cells homologous to our Type II tufted cells in only the upper half of somatosensory cortex layer 6, whereas we found Type II tufted cells throughout the layer. This discrepancy may be the result of a difference in classification criteria. Although Zhang and Deschenes found tufted pyramidal cells throughout the entire layer, they did not classify many of their cells since they could not identify their axonal projections. Hence it is unclear whether these cells would have met our criteria for Type II tufted cells. Second, Zhang & Deschenes found a much larger number of cells homologous to our non-tufted pyramidal cells (23/84 versus our 5/89) and did not find a sublaminar organization to these cells. This suggests that short pyramidal/non-tufted cells may play a more common role in the rat somatosensory cortex than in visual cortex. Zhang and Deschenes found that some of the short pyramidal cells projected across the corpus callosum. In the visual cortex, cells projecting across the callosum are found close to the vertical meridian (Lund and Lund, 1970) and are restricted to the top of layer 6 (as well as other layers, Olavarria and Van Sluyters, 1983). This difference could explain the small number and sublaminar organization of our non-tufted cells. Finally, Zhang and Deschenes found a much larger number of cells homologous to our Type I tufted cells, which they found in the lower half instead of lower third of layer 6.

In addition to our anatomical findings, we identified the laminar sources of functional excitatory input to individual neurons (see Figure 2.8 for summary). Type I tufted cells received input mainly from layer 6 and layer 5B with none of the cells receiving significant input from the superficial layers. Type II tufted cells received input mainly from layer 6 and layer 5B but also, to a lesser extent, from layers 5A and 4. Furthermore, the proportion of layer 5B to layer 6 input was greater for Type II tufted cells compared to Type I tufted cells. Interneurons as a class received more input from layer 2/3 than any of the tufted groups. They also received significant input from layer 5B, but their strongest input was from layer 6.

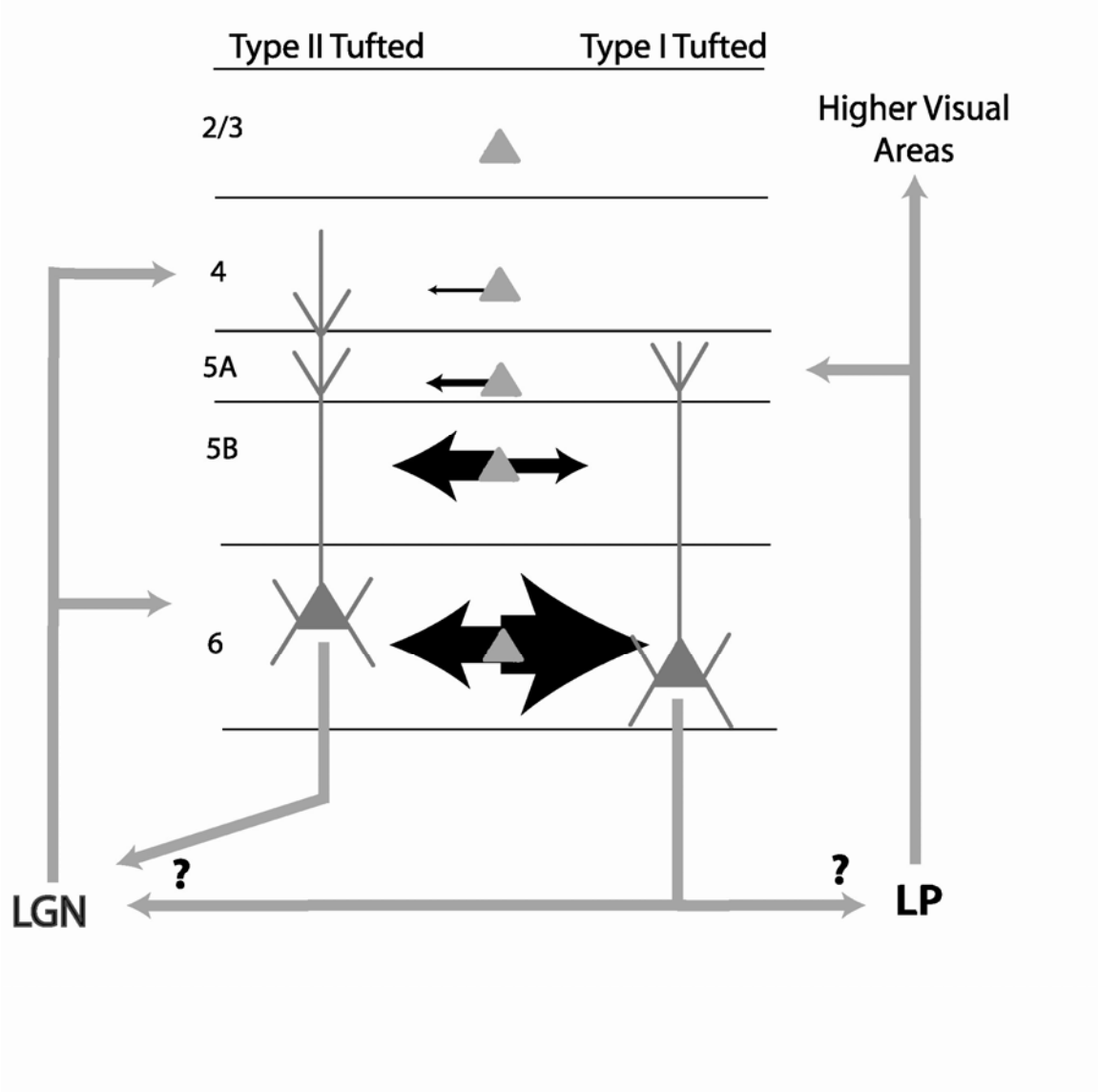

Figure 2.8: Schematic Diagram of Functional Input to Two Tufted Subypes. Thickness of black arrows represents the strength and directionality of the source of local excitatory input to the two different cell subtypes. Type II tufted cells receive significant local input from layers 4, 5A, 5B, and 6. The inputs from layers 4 and 5A are weak, whereas the inputs from layers 5B and 6 are strong and nearly equal to each other. Type I tufted cells only received significant local input from layer 5B and layer 6. The input from layer 6 is much larger than that from layer 5B. Based on previous work in the rat visual cortex and homology of these cells to those of the rat somatosensory cortex, Type II tufted cells probably project to LGN, while Type I tufted cells project to both LGN and LP (*middle grey arrows*). Possible input to the layer 5A tufts of both cell types are projections from LP to layer 5A of rat visual cortex (*grey arrows at right*). Also, a possible input to the layer 4 tuft of Type II tufted cells is thalamocortical axons from the LGN that terminate in layer 4 (*grey arrows at left*). Thalamocortical axons from the LGN also terminate in upper layer 6, likely connecting to both cell types. This data suggests that both cell types play a role in thalamocortical feedback loops, one involving LP and LGN (Type I tufted cells), while the other is more close related to the LGN (Type II tufted cells).

Since the dendrites of layer 6 cells overlap with axonal projections of cells in all other layers, layer 6 cells potentially could have received input from any of the layers. The actual patterns of functional laminar input that we measured could not have been predicted from previous anatomical studies. It is clear from our study that cells in superficial layers connect to layer 6 cells with a high level of specificity. Several observations make this point. Although one might have predicted that Type II tufted cells would receive more input from layer 4 than Type I tufted cells, because of their dendritic branches within that layer, one would not have predicted that the input from that layer would be so weak compared to the deeper layers. Based on morphology alone, one might predict that Type I tufted cells would receive significant input from layer 5A, and that the strength of this input would be greater than that for Type II tufted cells. This is, of course, not the case since, as a class, Type I tufted cells do not receive significant input from layer 5A and Type II tufted cells receive stronger input from layer 5A than other cell types. Furthermore, since tufted cells have only short perpendicular dendritic branches in layer 5B, one might have predicted they would not get strong input from layer 5B. However, again, this was not the case; almost all the cells received significant strong input from layer 5B. From anatomical studies alone, it would not have been possible to predict that layer 2/3 connects preferentially with inhibitory interneurons, nor would it have been possible to predict that the strongest input to layer 6 cells is from other layer 6 cells.

Recent studies of paired recordings in layer 6 have suggested that cells that are morphologically similar to the Zhang and Deschenes cortico-cortical cells provide more of the excitatory input to layer 6 pyramidal cells (Mercer et al., 2005), while those similar

to corticothalamic cells provide excitatory input to interneurons (West et al., 2005). However, these studies used layer 6 cells from the cat visual cortex, the rat somatosensory cortex, and the rat visual cortex. It is unclear how many of the layer 6 pairs were specifically from rat visual cortex, nor do they analyze the frequency of connections between cells of the same type (e.g. corticothalamic cells to corticothalamic cells). Hence, further work is necessary to test for the possibility of cell-type specific connectivity within layer 6.

2.5.3 Species Differences

Despite similarities in the basic organization and structure of cortex across areas and species, the rich overlap of axonal and dendritic arbors across all cortical layers provides for the possibility of connectional diversity embedded within this common structure. Anatomical studies of cat visual cortex suggested that layer 5 was the main source of excitatory input to layer 6 and that the superficial layers did not provide strong input to this layer (see Gilbert, 1983; Gilbert and Wiesel, 1983). Because layer 5 does not receive direct geniculocortical input and the geniculocortical collaterals to layer 6 were sparser than those to layer 4, it was presumed that several stages of information processing preceded the flow of information to layer 6. In this model the thalamus drives layer 4, which in turn projects to layer 2/3, layer 2/3 to layer 5, and finally layer 6 is driven by layer 5. However, laser-scanning photostimulation studies in macaque primary visual cortex found that many layer 6 pyramidal neurons received strong functional input from more superficial layers, including layer 2/3 and layer 4, which could exceed the strength of input from layer 5 (Briggs and Callaway, 2001). These findings supported a

cortical circuitry model in which layer 6 plays an earlier and more integrative role in visual processing (Callaway, 1998). It was unclear whether the differences in these two models reflected different methodology or if there were species differences.

In the present study we used the same methods as (Briggs and Callaway, 2001) and find that in the rat, connections to layer 6 pyramidal neurons in visual cortex are strikingly different from those of monkeys. The connections in rat are, however, similar to those proposed for cat visual cortex (Gilbert, 1983); local excitatory input arises predominantly from layers 5B and 6, with very little or no input from more superficial layers. These findings demonstrate major species differences between monkeys and rats in the connectivity of layer 6 pyramidal neurons in the visual cortex.

Monkey and rat visual cortices also differ in the relationships between layer 6 and higher-order thalamic nuclei. Layer 6 pyramids in macaque V1 do not project axons to the pulvinar (the higher-order thalamic nucleus homologous to LP; Lund et al., 1975) and afferent axons from the pulvinar terminate in layer 2/3 of V1 rather than layer 5A (Ogren and Hendrickson, 1977; Rezak and Benevento, 1979), hence overlapping with only a small subset of layer 6 cells that project their apical dendrites to that layer. In contrast, layer 6 tufted pyramids in the rat visual cortex seem to play an important role in two corticothalamic systems. Type I tufted cells, which probably project to both LP and LGN, receive input only from layer 6 and layer 5B, the same two layers containing neurons that project to LP (Bourassa and Deschenes, 1995). Furthermore, these cells have large elaborate dendritic tufts in layer 5A, where they probably receive synaptic input from afferent axonal arbors of LP neurons (Herkenham, 1980). Type II tufted cells, which probably project only to LGN, have dendritic tufts in layer 4 and a soma and basal

dendrites in layer 6, the two layers that receive afferent axonal arbors from the LGN. Furthermore, they receive input from layer 4 and layer 6 cells which are post-synaptic to geniculocortical pathway. In addition these cells also have dendritic tufts in layer 5A where they probably receive input from LP, and they receive strong input from layer 5B cells which project to LP. Hence, Type II tufted cells probably provide the LGN with feedback reflecting activity in both corticothalamic systems. In the monkey, interactions with the pulvinar nucleus of the thalamus, instead involves only a population of layer 5 neurons that do not provide input to the LGN. Thus, the two corticothalamic systems appear to operate more independently in the monkey visual system than in the rat.

These basic species differences in the circuitry of layer 6 cortical neurons might reflect more fundamental differences in the organization of the rodent versus the primate brain. One of the hallmarks of primate evolution is the remarkable enlargement of the cerebral cortex relative to subcortical brain structures (Finlay and Darlington, 1995; Clark et al., 2001). These evolutionary changes are paralleled by similar increases in primates in the numbers of visual cortical areas and the numbers of neurons making direct cortico-cortical connections. Thus, there has been a clear evolutionary trend for an increasing role of cortical relative to subcortical structures. Since connections from primary visual cortex to higher cortical areas originate from superficial cortical layers, the connection from superficial layers to layer 6 neurons in primate V1 may reflect the need to integrate this information with subcortical computations. In contrast, visually driven behaviors in rats are likely dominated by subcortical computations and therefore require less direct integration with superficial cortical layers. Alternatively, future studies investigating local input to layer 6 pyramidal neurons in the rat barrel cortex, could reveal that

superficial input is more closely related to the relative dominance of cortical versus subcortical processing systems in different sensory modalities rather than evolutionary trends.

2.6 Acknowledgements

The text of Chapter 2, in full, is a reprint of material published in Journal of Neurophysiology [Full citation: Zarrinpar A, Callaway EM (2006) Local connections to specific types of layer 6 neurons in the rat visual cortex. J Neurophysiol 95:1751-1761]. I was the primary investigator and first author of this manuscript and Edward M. Callaway, the second author, directed and supervised the research. This study was funded by National Institutes of Health Grants EY-10742 and MH-63912. I would like to acknowledge DJ Brasier for help in collecting a portion of the data that was ultimately used in the manuscript.

Table 2.1: Distribution of Cell Somata Within the Depth of Layer 6
Layer 6 was split into three equal depths. The number of each cell type sampled within the depth is indicated. Percentages (in parentheses) show the proportion of each cell type relative to all cells at the same depth.

	Lower Third	Middle Third	Upper Third	Total
Inhibitory Interneurons	0 (0.00%)	8 (18.6%)	3 (18.8%)	11
Bipolar Excitatory	1 (4.8%)	3 (7.0%)	0 (0.00%)	4
Inverted Pyramidal	2 (9.5%)	2 (4.6%)	1 (6.2%)	5
Non-Tufted	0 (0.00%)	3 (7.0%)	2 (12.5%)	5
Type I Tufted	6 (28.6%)	0 (0.00%)	0 (0.00%)	6
Type II Tufted	12 (57.1%)	27 (62.8%)	10 (62.5%)	49
Total	21 (100%)	43 (100%)	16 (100%)	80

Table 2.2: Laminar Sources of Evoked Excitatory Input for Nontufted Cells, Inverted Pyramidal Cells, Inhibitory Interneurons, and Type I Tufted Cells.
Cells are sorted by anatomical subtype. Layers with significant input to the cell show a percentage signifying the proportion of total evoked excitatory input that originated from that layer. Layers that provided non-significant input are denoted by *n.s.* Values emboldened in the table correspond to cells shown in Figures 2.3, 2.5, and 2.7.

Cell Type	Cell Number	L2/3 Input	L4 Input	L5A Input	L5B Input	L6 Input
Non-Tuft	Z0416z	7.98%	7.86%	10.35%	22.55%	51.26%
Non-Tuft	**Z0331a1**	**6.44%**	**1.83%**	**11.10%**	**34.68%**	**45.95%**
BIP	Z0124a	3.08%	*n.s.*	11.83%	55.34%	29.75%
BIP	**Z0421z**	***n.s.***	**4.84%**	**22.85%**	**38.16%**	**34.15%**
INV	Z0208a	*n.s.*	*n.s.*	6.54%	25.62%	67.84%
INV	Z0902a	*n.s.*	*n.s.*	*n.s.*	17.52%	82.48%
INV	**Z0203a**	***n.s.***	***n.s.***	***n.s.***	***n.s.***	**100.00%**
INT	Z1204c	3.51%	13.88%	12.10%	43.90%	26.61%
INT	Z0903e1	5.17%	*n.s.*	*n.s.*	62.86%	31.96%
INT	Z0903b	2.54%	*n.s.*	*n.s.*	26.05%	71.41%
INT	**Z0826e**	**2.51%**	***n.s.***	***n.s.***	**3.37%**	**94.11%**
INT	Z0819a1	0.62%	*n.s.*	*n.s.*	48.05%	51.33%
INT	Z0203c	*n.s.*	*n.s.*	*n.s.*	22.95%	77.05%
INT	Z1204d	*n.s.*	*n.s.*	*n.s.*	70.07%	29.93%
Type I	Z0414d	*n.s.*	*n.s.*	19.16%	42.16%	38.68%
Type I	Z0416c	*n.s.*	*n.s.*	*n.s.*	33.11%	66.89%
Type I	Z0417a	*n.s.*	*n.s.*	*n.s.*	30.34%	69.66%
Type I	Z0820a	*n.s.*	*n.s.*	*n.s.*	26.82%	73.18%
Type I	**Z0423d**	***n.s.***	***n.s.***	***n.s.***	**10.53%**	**89.47%**
Type I	Z0414a	*n.s.*	*n.s.*	*n.s.*	*n.s.*	100.00%
Type I	Z0210b	*n.s.*	*n.s.*	*n.s.*	*n.s.*	100.00%

Table 2.3: Laminar Sources of Evoked Excitatory Input for Type II Tufted Cells.
Layers with significant input to the cell show a percentage signifying the proportion of total evoked excitatory input that originated from that layer. Layers that provided non-significant input are denoted by *n.s.* Values emboldened in the table correspond to cells shown in Figures 2.3 and 2.5.

Type II	Z1208c	2.28%	1.11%	9.20%	18.77%	68.64%
Type II	Z0423a1	1.60%	5.39%	10.67%	59.61%	22.74%
Type II	**Z1204e**	***n.s.***	**17.62%**	**6.89%**	**25.78%**	**49.72%**
Type II	Z0414f	*n.s.*	15.03%	2.34%	42.39%	40.24%
Type II	Z0210a1	*n.s.*	12.69%	31.58%	13.61%	42.12%
Type II	Z0407a1	*n.s.*	11.63%	20.67%	46.51%	21.19%
Type II	Z0902c	*n.s.*	10.18%	15.95%	27.02%	46.84%
Type II	Z0416b	*n.s.*	8.18%	19.63%	33.47%	38.71%
Type II	Z0409b	*n.s.*	7.60%	31.47%	40.88%	20.05%
Type II	Z0423b1	*n.s.*	7.09%	11.08%	30.21%	51.62%
Type II	Z0409c	*n.s.*	5.07%	14.62%	54.03%	26.28%
Type II	Z0409d1	*n.s.*	4.48%	5.30%	50.21%	40.01%
Type II	D0408c1	*n.s.*	4.04%	49.54%	14.94%	31.48%
Type II	Z1217a	*n.s.*	2.19%	23.05%	32.75%	42.01%
Type II	Z0819b	*n.s.*	1.64%	2.35%	57.43%	38.58%
Type II	Z1209b	*n.s.*	0.94%	11.87%	33.79%	53.40%
Type II	Z1217b	*n.s.*	0.62%	9.06%	22.02%	68.30%
Type II	Z0407b	*n.s.*	28.54%	*n.s.*	20.23%	51.23%
Type II	Z0826c	*n.s.*	17.02%	*n.s.*	60.78%	22.20%
Type II	Z1217e	*n.s.*	12.66%	*n.s.*	42.35%	44.99%
Type II	Z0407c	*n.s.*	6.56%	*n.s.*	32.29%	61.15%
Type II	Z0414b	*n.s.*	4.78%	*n.s.*	8.14%	87.08%
Type II	Z0414c	*n.s.*	*n.s.*	30.90%	44.60%	24.50%
Type II	D0408b1	*n.s.*	*n.s.*	15.67%	29.12%	55.21%
Type II	Z0819c	*n.s.*	*n.s.*	15.23%	37.40%	47.38%
Type II	Z0414e	*n.s.*	*n.s.*	14.97%	30.97%	54.05%
Type II	Z0826b	*n.s.*	*n.s.*	14.22%	46.23%	39.54%
Type II	Z1208b	*n.s.*	*n.s.*	10.83%	51.75%	37.41%
Type II	Z1209e	*n.s.*	*n.s.*	*n.s.*	56.58%	43.42%
Type II	Z0416d	*n.s.*	*n.s.*	*n.s.*	50.06%	49.94%
Type II	Z0903d	*n.s.*	*n.s.*	*n.s.*	50.02%	49.98%
Type II	Z0820b	*n.s.*	*n.s.*	*n.s.*	46.82%	53.18%
Type II	Z1209a	*n.s.*	*n.s.*	*n.s.*	42.27%	57.73%
Type II	Z0409a	*n.s.*	*n.s.*	*n.s.*	33.46%	66.54%
Type II	Z0902b1	*n.s.*	*n.s.*	*n.s.*	29.28%	70.72%
Type II	Z1217f	*n.s.*	*n.s.*	*n.s.*	28.47%	71.53%
Type II	Z0416a	*n.s.*	*n.s.*	*n.s.*	26.53%	73.47%
Type II	Z1209f	*n.s.*	*n.s.*	*n.s.*	*n.s.*	100.00%

2.7 References

Bourassa J, Deschenes M (1995) Corticothalamic projections from the primary visual cortex in rats: a single fiber study using biocytin as an anterograde tracer. Neuroscience 66:253-263.

Briggs F, Callaway EM (2001) Layer-specific input to distinct cell types in layer 6 of monkey primary visual cortex. J Neurosci 21:3600-3608.

Briggs F, Callaway EM (2005) Laminar patterns of local excitatory input to layer 5 neurons in macaque primary visual cortex. Cereb Cortex 15:479-488.

Callaway EM (1998) Local circuits in primary visual cortex of the macaque monkey. Annu Rev Neurosci 21:47-74.

Callaway EM, Katz LC (1993) Photostimulation using caged glutamate reveals functional circuitry in living brain slices. Proc Natl Acad Sci U S A 90:7661-7665.

Clark DA, Mitra PP, Wang SS (2001) Scalable architecture in mammalian brains. Nature 411:189-193.

Dantzker JL, Callaway EM (2000) Laminar sources of synaptic input to cortical inhibitory interneurons and pyramidal neurons. Nat Neurosci 3:701-707.

Finlay BL, Darlington RB (1995) Linked regularities in the development and evolution of mammalian brains. Science 268:1578-1584.

Gilbert CD (1983) Microcircuitry of the visual cortex. Annu Rev Neurosci 6:217-247.

Gilbert CD, Wiesel TN (1983) Functional organization of the visual cortex. Prog Brain Res 58:209-218.

Guillery RW, Sherman SM (2002) Thalamic relay functions and their role in corticocortical communication: generalizations from the visual system. Neuron 33:163-175.

Herkenham M (1980) Laminar organization of thalamic projections to the rat neocortex. Science 207:532-535.

Katz LC, Dalva MB (1994) Scanning laser photostimulation: a new approach for analyzing brain circuits. J Neurosci Methods 54:205-218.

Lund JS, Lund RD (1970) The termination of callosal fibers in the paravisual cortex of the rat. Brain Res 17:25-45.

Lund JS, Lund RD, Hendrickson AE, Bunt AH, Fuchs AF (1975) The origin of efferent pathways from the primary visual cortex, area 17, of the macaque monkey as shown by retrograde transport of horseradish peroxidase. J Comp Neurol 164:287-303.

Mercer A, West DC, Morris OT, Kirchhecker S, Kerkhoff JE, Thomson AM (2005) Excitatory Connections Made by Presynaptic Cortico-Cortical Pyramidal Cells in Layer 6 of the Neocortex. Cereb Cortex.

Ogren MP, Hendrickson AE (1977) The distribution of pulvinar terminals in visual areas 17 and 18 of the monkey. Brain Res 137:343-350.

Olavarria J, Van Sluyters RC (1983) Widespread callosal connections in infragranular visual cortex of the rat. Brain Res 279:233-237.

Rezak M, Benevento LA (1979) A comparison of the organization of the projections of the dorsal lateral geniculate nucleus, the inferior pulvinar and adjacent lateral pulvinar to primary visual cortex (area 17) in the macaque monkey. Brain Res 167:19-40.

Sawatari A, Callaway EM (1996) Convergence of magno- and parvocellular pathways in layer 4B of macaque primary visual cortex. Nature 380:442-446.

Sawatari A, Callaway EM (2000) Diversity and cell type specificity of local excitatory connections to neurons in layer 3B of monkey primary visual cortex. Neuron 25:459-471.

Schubert D, Staiger JF, Cho N, Kotter R, Zilles K, Luhmann HJ (2001) Layer-specific intracolumnar and transcolumnar functional connectivity of layer V pyramidal cells in rat barrel cortex. J Neurosci 21:3580-3592.

van Brederode JF, Snyder GL (1992) A comparison of the electrophysiological properties of morphologically identified cells in layers 5B and 6 of the rat neocortex. Neuroscience 50:315-337.

West DC, Mercer A, Kirchhecker S, Morris OT, Thomson AM (2005) Layer 6 Cortico-thalamic Pyramidal Cells Preferentially Innervate Interneurons and Generate Facilitating EPSPs. Cereb Cortex.

Yabuta NH, Callaway EM (1998a) Cytochrome-oxidase blobs and intrinsic horizontal connections of layer 2/3 pyramidal neurons in primate V1. Vis Neurosci 15:1007-1027.

Yabuta NH, Callaway EM (1998b) Functional streams and local connections of layer 4C neurons in primary visual cortex of the macaque monkey. J Neurosci 18:9489-9499.

Yoshimura Y, Dantzker JL, Callaway EM (2005) Excitatory cortical neurons form fine-scale functional networks. Nature 433:868-873.

Zhang ZW, Deschenes M (1997) Intracortical axonal projections of lamina VI cells of the primary somatosensory cortex in the rat: a single-cell labeling study. J Neurosci 17:6365-6379.

Zhang ZW, Deschenes M (1998) Projections to layer VI of the posteromedial barrel field in the rat: a reappraisal of the role of corticothalamic pathways. Cereb Cortex 8:428-436.

Chapter 3

Local Connections to Specific Types of Layer 5 Neurons in the Rat Visual Cortex

3.1 Abstract

Previous studies have categorized layer 5 cells into two groups using either morphological criteria (short versus tall) or by physiological properties (regular spiking versus burst spiking). Here we present a study that shows that layer 5 cells can be split into three non-overlapping cell subtypes: (1) regular spiking short pyramidal cells, (2) regular spiking tall pyramidal cells, and (3) burst spiking tall pyramidal cells. Short pyramidal cells can be separated from other two populations based on morphology, but have a characteristic spike firing properties that further distinguishes them from the other two cell types. Burst spiking cells can be distinguished from regular spiking cells by a characteristic fast afterspike depolarization that delays the occurrence of the afterspike hyperpolarization. In addition to analyzing the spiking properties of these three cell groups we characterized their functional local input using laser-scanning photostimulation, and as in previous photostimulation studies, we found significant differences between cell types. Although all cell types received significant input from all layers, short pyramidal neurons received stronger input from layer 4 and weaker input from layer 5 than did tall pyramidal cells. However, we did not find any differences between two populations of tall pyramidal cells.

3.2 Introduction

Understanding the functional connectivity of cortical neurons is critical in deciphering how information processing occurs in the mammalian brain. Previous experiments have shown that morphologically categorized cell types have highly specific connection patterns (Mercer et al., 2005; Song et al., 2005; Morishima and Kawaguchi, 2006; West et al., 2006) and receive specific functional input patterns (Dantzker and Callaway, 2000; Schubert et al., 2001; Schubert et al., 2003; Yoshimura and Callaway, 2005; Yoshimura et al., 2005; Zarrinpar and Callaway, 2006) that distinguishes them from other cell types. Hence cells of different morphology have functional distinctions that arise from differences in their functional input and connectivity patterns.

In the rat, there are at least two morphologically distinct layer 5 cortical cells based on dendritic cytoarchitecture. Short pyramidal neurons which have an apical dendrite that ends before reaching layer 1 and tall pyramidal neurons which are characterized by a dendritic tuft with branches that terminate in layer 1 (Chagnac-Amitai et al., 1990; Koester and O'Leary, 1992; Kasper et al., 1994). These cells project axons to different regions; for example, in the rat visual cortex, short cells project to the contralateral visual cortex while tall cells project to the superior colliculus (Hallman et al., 1988; Koester and O'Leary, 1992; Kasper et al., 1994).

Layer 5 cells of the rat visual cortex can also be distinguished based on firing properties. A large population of cells in layer 5 intrinsically burst at suprathreshold potentials, while others are regular-spiking (Chagnac-Amitai et al., 1990; Kasper et al., 1994; Schubert et al., 2001; Morishima and Kawaguchi, 2006; Schubert et al., 2006). Chagnac-Amitai, et al. (1990) showed that short cells were regular-spiking and that

almost all tall cells were intrinsically bursting. In their study, only one tall cell was regular spiking, although in subsequent studies, more regular-spiking tall layer 5 cells have been illustrated (Schubert et al., 2001; Morishima and Kawaguchi, 2006; Schubert et al., 2006). It is unclear whether tall regular spiking cells are morphologically distinct from tall bursting cells since some studies have shown no difference (Schubert et al., 2006) while other have shown that tall regular spiking cells have, on average, smaller soma area, less apical dendritic length, and fewer apical dendritic branching than their bursting counterparts (Schubert et al., 2001; Morishima and Kawaguchi, 2006). However, none of these studies separated the regular-spiking short pyramidal cells from the tall regular spiking cells.

Recently, in the mouse somatosensory cortex three different layer 5 pyramidal cells were distinguished based on their dendritic and axonal morphologies: short pyramidal, tall simple, and tall tufted (Larsen and Callaway, 2006). Short pyramidal cells were characterized by having an apical dendrite that ended before layer 1 and having axon that projected to the superficial layers. Tall simple cells had an apical dendrite that had a small tuft at the top of layer 2/3 and into layer 1. They also had axons that projected into the superficial layers. Tall tufted cells also had a dendritic tuft in layer 2/3 that extended into layer 1, but they were characterized by having an apical dendritic length nearly twice that of the tall simple cells. Furthermore tall tufted cells had axons that projected almost exclusively to the deep layers. This study suggests that there are possibly three different cell types in the rat visual cortex as well.

Previous photostimulation experiments of the layer 5 in the rat have focused on the rat somatosensory cortex. Schubert, et al. (2001) distinguished between two cell

types in the rat somatosensory cortex, the intrinsically bursting (IB) cells and regular spiking (RS) cells found throughout layer 5. They performed a photostimulation experiment on their two populations and were able to find one subtle difference in intracolumnar input. IB cells received input from more photostimulation sites in layer 6 than RS cells did. However, it is not clear whether the strength of the input from layer 6 to IB cells is stronger than to RS cells. Furthermore, their study included few cells (7 IB cells, 8 RS cells) and it is unclear whether more differences will be apparent if a larger number of cells were used, or if the short cells were separated from the other RS cells. A later study by the same group which focused exclusively on layer 5A neurons found no differences between RS and IB neurons and input patterns very similar to those found in their first study (Schubert et al., 2006).

These studies, nevertheless, were important in helping our understanding of the functional role of layer 5 neurons. One model of cortical circuitry (Gilbert, 1983; Gilbert and Wiesel, 1983), based primarily on anatomical studies of the cat visual cortex, proposed that the main cortical input to layer 5 is layer 2/3 with little input from layer 4. More recent cortical circuitry models based on the macaque visual system (Callaway, 1998) proposed that layer 5 cells receive strong input from layer 4 and layer 2/3 but less so from layer 6. However, these studies of the rat somatosensory cortex, as well as photostimulation studies in the macaque (Briggs and Callaway, 2005) show that layer 5 cells receive input from all layers. In the rat somatosensory cortex, layer 2/3 had fewer sites that provided input to layer 5 cells, suggesting a weaker connection. Furthermore, the bursting cells of layer 5 received input from more sites in layer 6 than any other layer, suggesting a relative stronger input from that layer.

This study had two main objectives: to characterize the neurons of layer 5 based on morphology and firing pattern and to characterize the laminar organization of functional excitatory inputs to these subtypes. A comparison of our results to those of the somatosensory cortex will elucidate the extent of their homology and whether these two sensory systems use similar circuits.

3.3 Materials and Methods

3.3.1 Slice preparation

Vibratome-cut coronal slices (400 μm) were prepared from the primary visual cortex of P21-P28 Long-Evans rats. Slices were cut in ice cold oxygenated (95% O_2-5% CO_2) artificial cerebral spinal fluid (ACSF) [which contained (in mM) 125 NaCl, 5 KCl, 26 $NaHCO_3$, 1.25 KH_2PO_4, 1.33 $MgSO_4$, 10 D-(+)-glucose, 3.15 $CaCl_2$, and 1 kynurenic acid] and then maintained submerged in the same ACSF solution heated to 35–37°C.

3.3.2 Electrophysiology

Slices were placed in a submersion type chamber with continuous perfusion of aerated ACSF. We used an infrared Olympus DIC microscope with a 40x, 0.8 NA water-immersion lens to visualize and target layer 5 neurons for whole-cell recordings in living brain slices. Glass microelectrodes (5-10 MΩ resistance) filled with a potassium-gluconate-based intracellular solution (130 mM K-gluconate, 10 mM HEPES, 2 mM $MgCl_2$, 0.2 mM EGTA, 6 mM KCl, 2.5 mM Na_2ATP, 0.5 mM Na_2GTP, 10 mM K-Phosphocreatine) contained 0.5-1% biocytin for cell labeling. We recorded in both

current clamp (for spike shape analysis, see below) and voltage clamp modes (for measurement of evoked EPSCs).

3.3.3 Photostimulation and Input Maps

Local stimulation of presynaptic input neurons by light-evoked conversion of 'caged' glutamate to glutamate ("photostimulation") was used to map laminar sources of functional connections onto individual recorded neurons (Callaway and Katz, 1993; Katz and Dalva, 1994; Sawatari and Callaway, 1996; Dantzker and Callaway, 2000; Sawatari and Callaway, 2000; Briggs and Callaway, 2001, 2005; Yoshimura and Callaway, 2005; Yoshimura et al., 2005; Zarrinpar and Callaway, 2006). Brain slices were bathed in oxygentated ACSF (without kynurenic acid) containing ~85 μM 'caged' glutamate (4-methoxy-7-nitroindolinyl-caged L-glutamate – 'MNI-glutamate'; Tocris Biosciences, Ellisville, MO) at room temperature. Ultraviolet light (10-ms flash from an argon-ion laser) was focused to photostimulate a small discrete spot in the plane of the brain slice through a 40x microscope objective above the slice. Whole-cell voltage-clamp recordings (-65 mV) were made from two layer 5 postsynaptic neurons simultaneously, and inward excitatory postsynaptic currents (EPSCs) resulting from photostimulaion of presynaptic neurons was measured.

To map the locations of input, ~600-800 sites were stimulated sequentially in a pseudo-random pattern that covered all cortical layers. Stimulation sites were located throughout a rectangular area surrounding the recorded neuron, typically extending ~200 μm laterally on either side of the cell and vertically from the white matter to layer 1. After each photostimulation event, voltage clamp records were made for each stimulation

trial to detect EPSCs. In addition, photostimulation trials were interleaved with control trials (no stimulation) to obtain spontaneous EPSCs (sEPSCs). After completion of photostimulation and recordings from a cell, the laser was used to burn alignment sites (< 10 μm) into the slice so that x-y photostimulation coordinates could be assigned to their corresponding position in the tissue. Laminar borders were determined using cytochrome oxidase stain.

The spatial resolution of this technique allows mapping of laminar-specific excitatory input in rat visual cortex. We supplemented previously published measures (Dantzker and Callaway, 2000; Yoshimura and Callaway, 2005; Yoshimura et al., 2005) with a series of experiments to assess the spatial resolution of the laser-scanning photostimulation with our given parameters. This was also to ensure that the spatial resolution of cells did not differ between layers. Loose-patch extracellular recordings were made of cells throughout the cortical column (~3-5 cells in each layer). We recorded the frequency of action potentials after a photostimulation event and found that our results matched previously published experiments; cells fired action potentials when focal uncaging occurred within ~50 μm from cell soma.

3.3.4 Staining and Morphological Analysis

After photostimulation, slices were fixed with 4% paraformaldehyde in 0.1 M PBS for 12–24 h, then submerged in 30% sucrose in PBS. The slices were then stained whole-mount using a Cy3-conjugated streptavidin system (Jackson ImmunoResearch Laboratories, Inc, West Grove, PA). Cells were mounted using Vectashield (Vector Laboratories, Burlingame, CA), and morphological characteristics of the cells were

determined using confocal laser-scanning microscopy (TCS SP2 AOBS; Leica). Multiple images of the cell was taken, including the whole cell with a low-resolution objective [PL Fluotar 10x; NA 0.3; Leica]; the apical dendrites and cell bodies with a medium-resolution objective [PL Fluotar 20x; NA 0.5; Leica] and the cell bodies with a high-resolution objective [PLAN APO 40x; NA 0.85; Leica]. Images were acquired as stacked files through the whole section thickness (step size, ~1 μm for 10x; ~0.5 μm for 20x, ~0.1 μm for 40x).

Slices were then resectioned at 80 μm, and stained for cytochrome oxidase and biocytin to reveal laminar borders and neuronal morphology using methods previously described (Yabuta and Callaway, 1998a, 1998b). Cells that had an incomplete apical dendrite were excluded from all analysis. For all slices, the laminar borders near the cells were reconstructed with Neurolucida, a computerized system (MicroBrightField, Williston, VT). Each reconstruction showing the laminar borders and alignments sites were aligned with the coordinate map of stimulation sites using Adobe Illustrator (Adobe Systems, San Jose, CA). Each stimulation site was assigned to a layer using this method. However, photostimulation sites within 50 μm of the layer borders were excluded from analysis since they can stimulate presynaptic cells in two layers (Yoshimura and Callaway, 2005; Yoshimura et al., 2005).

3.3.5 Analysis of EPSCs

We analyzed EPSCs that occurred during the first 150 ms after photostimulation. This window was chosen because presynaptic neurons fired most of their APs during this time (Dantzker and Callaway, 2000; Yoshimura and Callaway, 2005; Yoshimura et al., 2005), indicating that shorter analysis windows would exclude photostimulation-evoked EPSCs. We distinguished direct effects of focal uncaging of glutamate on the recorded cell, which had a distinct shape (longer rise-time) and occurred immediately after glutamate uncaging (shorter latency) from EPSCs, and included only EPSCs in our analysis (see Fig 3.5 E, trace 3). After photostimulation, within ~50 μm of the recorded cell, direct currents sometimes exceeded 100 pA and decayed over 100 ms, preventing EPSCs from being separately identified at these locations, and thus these sites were excluded from analysis. The amplitudes and numbers of EPSCs were measured for every stimulation site and for the no-stimulation controls using peak analysis software from Synaptosoft (Leonia, New Jersey) and other custom software. Each trial was assigned a value in picoampere, equal to the sum of the peak amplitudes of all detectable EPSCs. Stimulation sites were then assigned to their correct cortical layer, and EPSC amplitudes for all stimulation sites within a layer were pooled together using custom Matlab programs. Laminar groupings of EPSC sum of amplitudes were then compared with spontaneous EPSCs to identify statistically significant differences in EPSCs from a particular layer using Mann Whitney U tests. We also calculated the mean value of summed EPSC amplitudes for that layer as well as for control trials, measuring spontaneous EPSCs. To quantify the evoked input (EI) from a particular layer, the mean sum of amplitudes of spontaneous events was subtracted from the mean sum of

amplitudes for each layer. The relative strength of excitatory input from each layer was calculated by dividing the EI for that layer by the sum of the EIs from all layers for that same cell. Cells were then grouped based on their morphological characteristics. In addition, if a cell did not receive significant input from a layer, the EI for that layer was set to 0 to avoid negative EI and EI percentages. Significant differences in layer specific EI percentages between cell types were determined using Mann Whitney U Test.

To illustrate input patterns for individual cells, smoothed graphs of excitatory input were generated using custom Matlab programs (see Fig. 3.5). Values of the sum of amplitudes for each individual stimulation site were used to create these smoothed plots using linear interpolation. These plots illustrate estimated evoked activity measured in a given cell (mean sum of EPSC amplitudes for simulated trials minus mean sum of EPSC amplitudes for spontaneous trials) after stimulation at various locations. These plots are purely for illustration of the source of input; no part of the quantitative analyses was based on these linear interpolations.

3.3.6 Spike Analysis

An illustration of some of the spike analysis measurements that we made can be found in Figure 3.1.

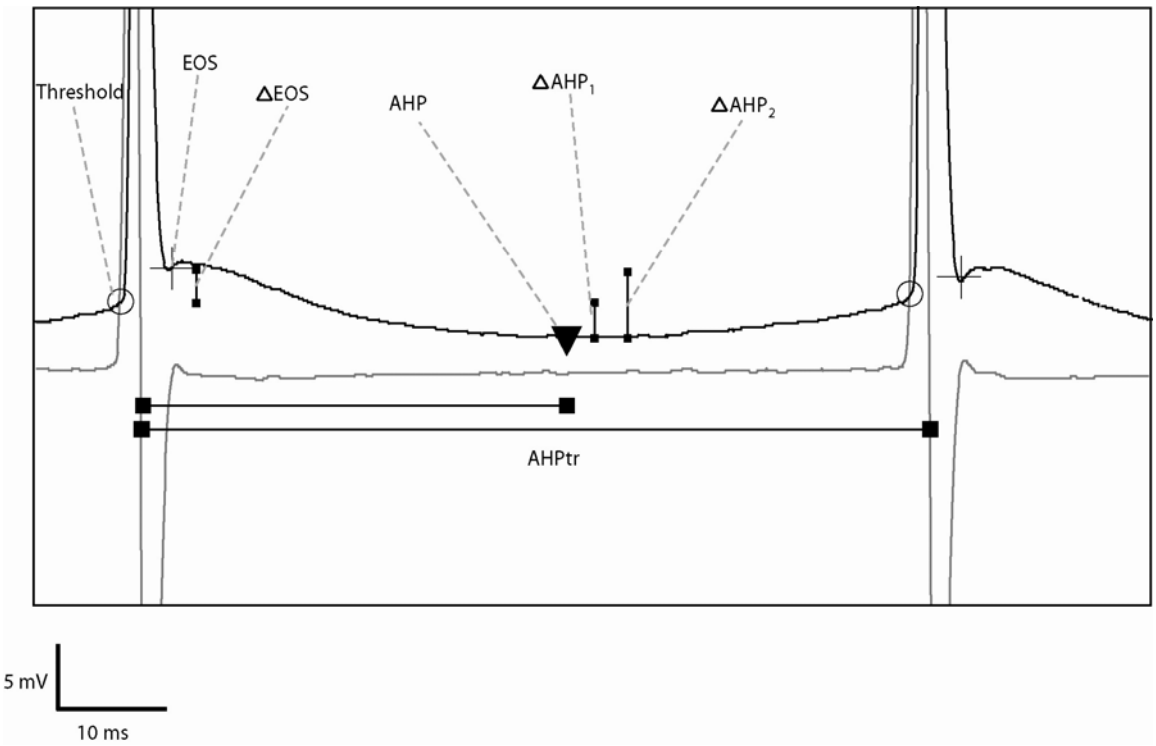

Figure 3.1: Spike Analysis Measurements. The threshold (open circle) was defined as the membrane potential at which the first derivate of the membrane potential (dV/dt) exceeded 10 V/s. The End of Spike (EOS; plus sign) is defined as the change in slope of the first derivative of the membrane potential (dV/dt) after the spike decreased by 90% (or when the post-peak maximum of the second derivative decreased by 90%). We also calculated an End of Spike potential (ΔEOS, in mV) by subtracting the threshold from the potential at which the spike ended. We defined the moment of the afterspike hyperpolarization (AHP; black triangle) as the minimum between the two peaks (dV/dt = 0). Two AHP potentials were calculated: ΔAHP_1 is the membrane potential difference between the spike threshold and absolute membrane potential minimum between spikes; ΔAHP_2 is the membrane potential difference between the EOS and the absolute membrane potential minimum between spikes. In addition an AHP time ration (AHPtr) was calculated where the time interval between the AHP and the peak of the spike was divided by the interspike interval.

Recorded spike trains were analyzed off-line using custom software written in Igor Pro (Wavemetrics, Lake Oswego, OR). Instantaneous firing rate was calculated as the reciprocal of the interspike interval and was assigned to all spikes except the first one in a train. To measure the fastest firing rate (FFR), we injected all cells the same amount of maximum current (20 pA) for 300 ms. We repeated this measure 20 or more times and chose the maximum firing frequency the cell attained. We calculated the adaptation coefficient which we defined as the ratio of the interspike interval of the penultimate pair of spikes to the last pair of spikes at the highest spiking frequency. Unless otherwise stated we did not use the first spike for each train in any of our analysis.

Action potential threshold was defined as the membrane potential at which the first derivate of the membrane potential (dV/dt) exceeded 10 V/s. Action potential height was defined from threshold to peak. Half peak width was calculated by measuring the width of the peak (in ms) at the point that was half the action potential height.

We calculated the point at which the spike ended (End of Spike, EOS) which we defined as the change in slope of the first derivative of the membrane potential (dV/dt) after the spike decreased by 90% (or when the post-peak maximum of the second derivative decreased by 90%). We also calculated an End of Spike potential (ΔEOS, in mV) by subtracting the threshold from the potential at which the spike ended. This value is positive if the spike is followed by a fast afterspike depolarization, and negative if the spike is followed with a fast afterspike hyperpolarization.

We defined the moment of the afterspike hyperpolarization (AHP) as the minimum between the two peaks (dV/dt = 0). AHP measurements for the last spike of a train were excluded from analysis. From this point, we calculated two AHP potentials:

ΔAHP_1 is the membrane potential difference between the spike threshold and absolute membrane potential minimum between spikes; ΔAHP_2 is the membrane potential difference between the EOS and the absolute membrane potential minimum between spikes. In addition an AHP time ration (AHPtr) was calculated where the time interval between the AHP and the peak of the spike was divided by the interspike interval. A low ratio would imply that the AHP occurred very close to the spike, whereas a larger number implies that the AHP is delayed. AHPtr was not calculated for the last spike in a train.

Finally, we defined the afterspike depolarization (ADP) as the maximum between the EOS and AHP. It should be noted that spikes that had a fast afterspike depolarization, and a high EOS (like some bursting cells) would sometimes have a value of 0 for ADP. This was mainly because the maximum between the EOS and AHP would be the EOS itself, causing EOS and ADP to be equal to each other, and their difference to be 0. The change in ADP potential (ΔADP) was calculated by subtracting EOS potential from the potential at the maximum between the EOS and AHP.

3.4 Results

3.4.1 Cell Classification

We intracellulary labeled and performed spike analysis for 87 layer 5 neurons. Three cells had aspiny dendrites, local pervasive axonal projections, nonpyramidal somata, and distinct firing patters and were classified as inhibitory interneurons. Since the morphology and spike analysis of each of the three interneurons was distinct, which implied that the group was comprised of different cell types, we excluded these cells from further analysis.

The remaining 84 cells were split into two main groups based on cell morphology. Cells that did not have an apical dendrite that reached layer 1 were labeled short pyramidal neurons (n = 16; Fig 3.2 A), and cells that had dendritic tufts that extended into layer 1 were classified as tall pyramidal neurons (n = 68; Fig 3.2, C & E). Great care was taken to ensure that the short pyramidal cells were not tall cells that had their apical dendrites cut. All cells within this category were regular spiking (Fig 3.2 B).

The tall pyramidal neurons were further subdivided into bursting and regular spiking subgroups (Fig. 3.2 C-F). While performing this task, we came across 6 cells that had a fast afterspike depolarization (high ΔEOS) that is characteristic of bursting cells (Chagnac-Amitai et al., 1990; Kasper et al., 1994), though they did not show any bursting per se (Fig. 3.4 AE). We initially analyzed the data set without these cells and found that, besides the high ΔEOS, they shared many spike features with bursting cells, and were remarkably different from the tall regular spiking cells in almost all variables except FFR (see below). Hence we reclassified these cells as tall bursting cells.

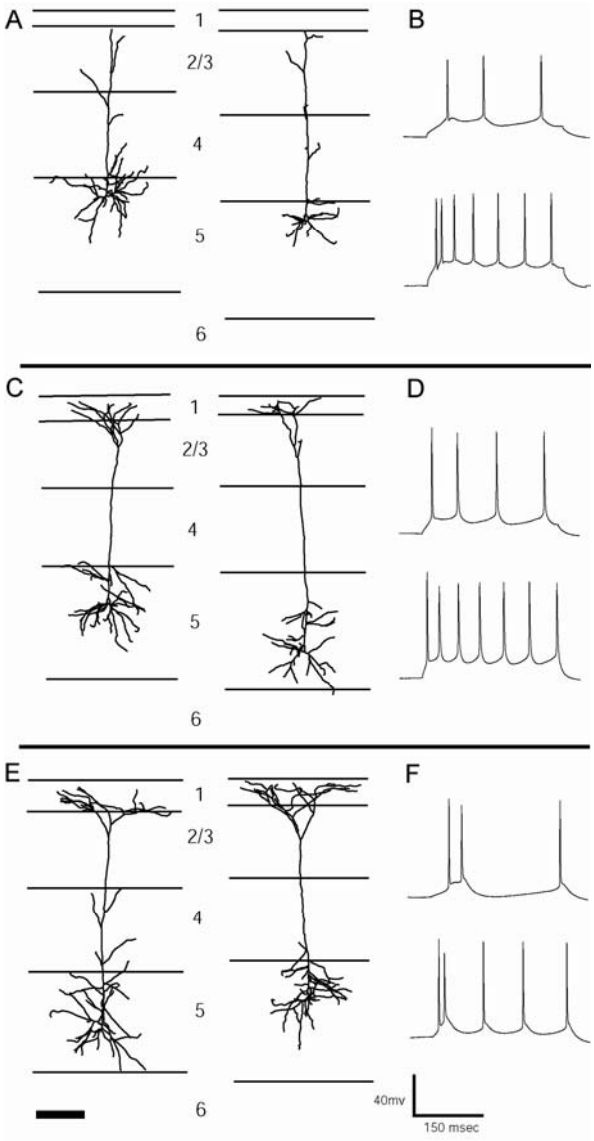

Figure 3.2: Examples of Cell Morphology of Layer 5 Pyramidal Cells. Neurolucida drawing 3 different neuron subtypes (with two examples each) differentiated based on dendritic morphology and cell spiking properties. Dark lines: dendrites; gray, somata. Axons have been excluded from the drawings. The sample traces are both from the same cell. Top traces are a response to a 10 pA current injection and the bottom trace is a response to 20 pA current injection. (A) Two examples of short pyramidal cells, identified by a lack of dendritic tuft and no dendritic branches or projections to layer 1. Although these two examples are from the top of layer 5, these cells were found throughout the entire cortex. (B) Sample spiking pattern from a short pyramidal cells. (C) Two examples of tall regular spiking pyramidal neurons, classified by their morphological characteristics (dendritic tuft that projects to and branches in layer 1) and spiking pattern (regular spiking). (D) Sample spiking pattern from a tall regular spiking pyramidal cell. (E) Two examples of tall burst spiking pyramidal neurons, classified by their morphological characteristics (dendritic tuft that projects to and branches in layer 1) and spiking pattern (burst spiking, followed by a fast afterspike depolarization). (F) Sample spiking pattern from a tall bursting cell. Scale bar in (E) represents 200 μm and applies to all drawings. Scale bars for the spike trains in (F) apply to all spike trains.

3.4.2. Spike Analysis

A summary of the spike features of the remaining cell types is provided in Table 3.1.

The three cell types differed from each other the most along two variables, ΔEOS and the FFR. Short pyramidal cells had the most negative ΔEOS of -3.042 (± 0.465; Mean ± SEM) and hence were rarely followed by a fast afterspike depolarization (Fig. 3.3 A). This ΔEOS was significantly more negative than both the tall regular spiking cells (-1.228 ± 0.370; $p < 0.005$, Mann Whitney U Test; Fig 3.3 B) and from the tall bursting cells (2.787 ± 0.411; $p < 5.0 \times 10^{-7}$, Mann Whitney U Test; Fig 3.3 C). The ΔEOS of tall regular spiking cells was also significantly more negative than those from the tall bursting cells ($p < 5.0 \times 10^{-8}$, Mann Whitney U Test; Fig 3.3.BC). Almost all of the tall bursting cells had a ΔEOS greater than 1 (n = 29/32, 91%; Fig 3.3 D) whereas only 8/52 (15%) of the other two cell types met this criteria ($p < 5.0 \times 10^{-12}$; Fisher Exact Test; for a closer look at the spikes from the exceptions, see Figure 3.4 BCE).

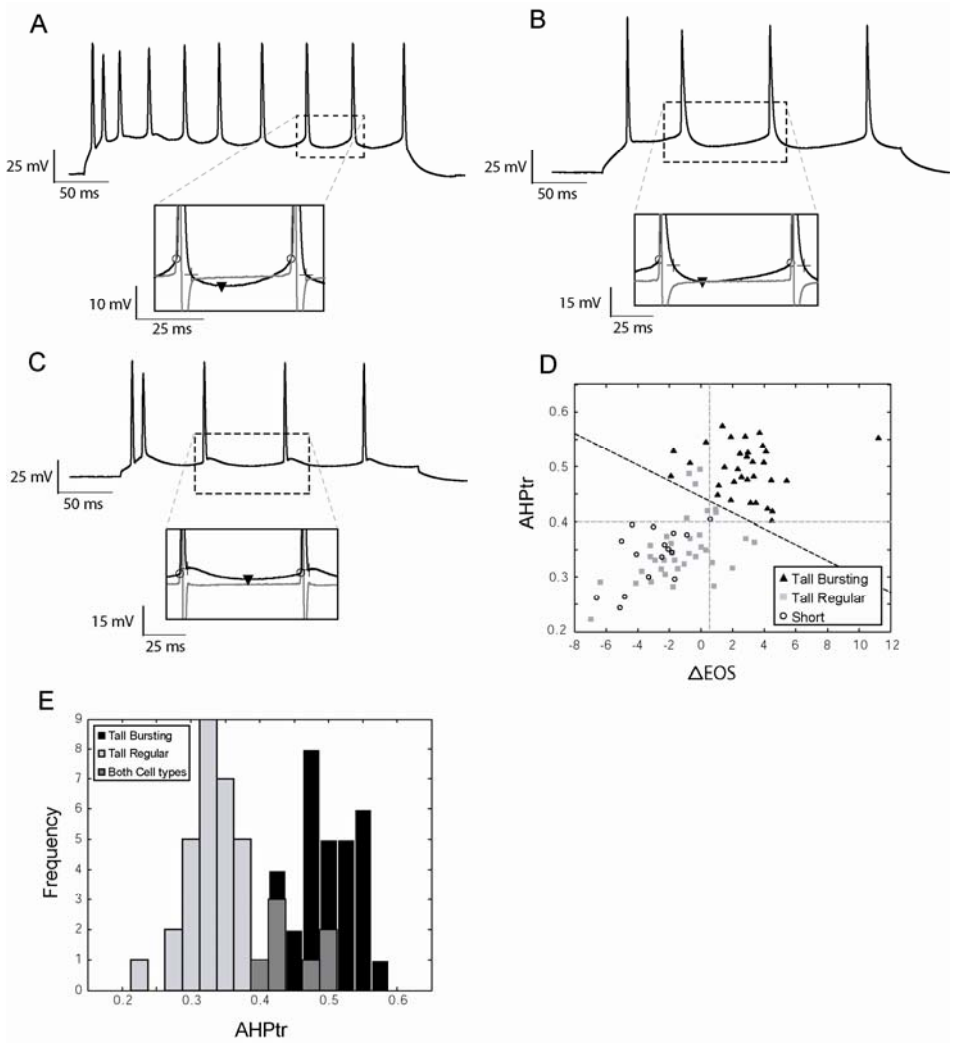

Figure 3.3: Spike Properties of the Three Subtypes of Layer 5 Pyramidal Neurons. (A-C) Example spike trains of three different subtypes with insets showing enlargements of the base of two spikes and interspike interval. In the insets, the threshold is represented by an open circle, the EOS as a plus sign, and the AHP as a black triangle. The gray line represents the first derivative (dV/dt) of the spike wave. (A) Spike train from a short pyramidal cell. These spikes are characterized by a higher FFR, most negative ΔEOS, least negative ΔAHP_2. Also their AHPtr was less than 0.4. (B) Spike train from a tall regular spiking cell. These spikes are characterized by a low FFR, slow adaptation, higher HPW, a negative ΔEOS, and the most negative ΔAHP_1. Similar to the short pyramidal cells, they also had a AHPtr that was less than 0.4. (C) Spike train from a tall bursting cell. These spikes are characterized by a high FFR (caused by the burst), a positive ΔEOS and an AHPtr that was greater than 0.4. (D) The relationship of ΔEOS and AHPtr. Tall bursting cells can be separated from the tall regular spiking cells and short pyramidal cells based on the AHPtr of 0.4 (horizontal dashed gray line), or on the ΔEOS of 1 (vertical dashed gray line) or a combination of the two [y = (-0.0138 * ΔEOS) + 0.4406; dashed black line; cells that fall below this line are regular spiking cells). (E) AHPtr was the best single factor that separated the tall bursting cells from the tall regular spiking cells. This frequency bar graph shows a clear bimodal distribution. The black bars represent tall bursting cells, the light grey are the tall regular spiking cells, and the dark grey is the area of overlap between the two distributions.

Surprisingly, the cells with the highest FFR were the short pyramidal cells (101.78 Hz ± 4.24) which were significantly higher than the tall regular spiking cells (47.45 Hz ± 4.41; $p < 5.0 \times 10^{-7}$, Mann Whitney U Test; Fig 3.3 A) and the tall bursting cells (84.63 Hz ± 4.84, $p < 0.05$, Mann Whitney U Test; Fig 3.3 C). As expected, the tall bursting cells had a faster firing rate than the tall regular spiking cells ($p < 5.0 \times 10^{-6}$; Mann Whitney U Test; Fig 3.3 B). A large majority of the tall regular spiking cells (n = 30/36; 83%) had a firing rate lower than 75 Hz, while only 9/32 (28%) of the tall bursting cells and none of the short pyramidal cells fired less than 75 Hz ($p < 5.0 \times 10^{-5}$, Fisher Exact Test; tall regular spiking versus both short and tall bursting).

The most striking feature of tall bursting pyramidal cells was AHPtr, which is the ratio of the time interval between the peak and AHP to the interspike interval time. Since tall bursting cells were followed by a fast afterspike depolarization and, hence, a rise in ΔEOS, this caused the AHP to occur later in the interspike interval. The AHPtr for tall bursting cells was 0.495 (± 0.008; Fig 3.3 CDE) which was significantly higher than those of tall regular spiking cells (0.351 ± 0.010; $p < 5.0 \times 10^{-10}$, Mann Whitney U Test; Fig. 3.3 BDE) and for short pyramidal cells (0.338 ± 0.013, $p < 5.0 \times 10^{-8}$, Mann Whitney U Test; Fig. 3.3 AD). For tall cells, a histogram of this measure gives a clear bimodal distribution (Fig. 3.3 E). All of the tall bursting cells had an AHPtr greater than 0.4, whereas only 1 short pyramidal cell and 7 tall regular spiking cells met this criteria ($p < 5.0 \times 10^{-16}$, Fisher Exact Test, Fig 3.3 DE), which made it a better predictor of burst spiking than the ΔEOS measure.

A combination of the ΔEOS and AHPtr was the best predictor of whether a cell was bursting or regular spiking cell. Using these two factors alone, we formulated an

equation [if AHPtr < (-0.0138 * ΔEOS) + 0.4406 was true, then the cell was regular spiking] that separated all the tall regular spiking cells from tall burst spiking ones. None of the short pyramidal cells and only 3 tall regular spiking were grouped with the burst spiking cells using this criteria ($p < 5.0 \times 10^{-20}$). A more detailed look at these 3 exceptional cases is provided in Figure 3.4 CDF.

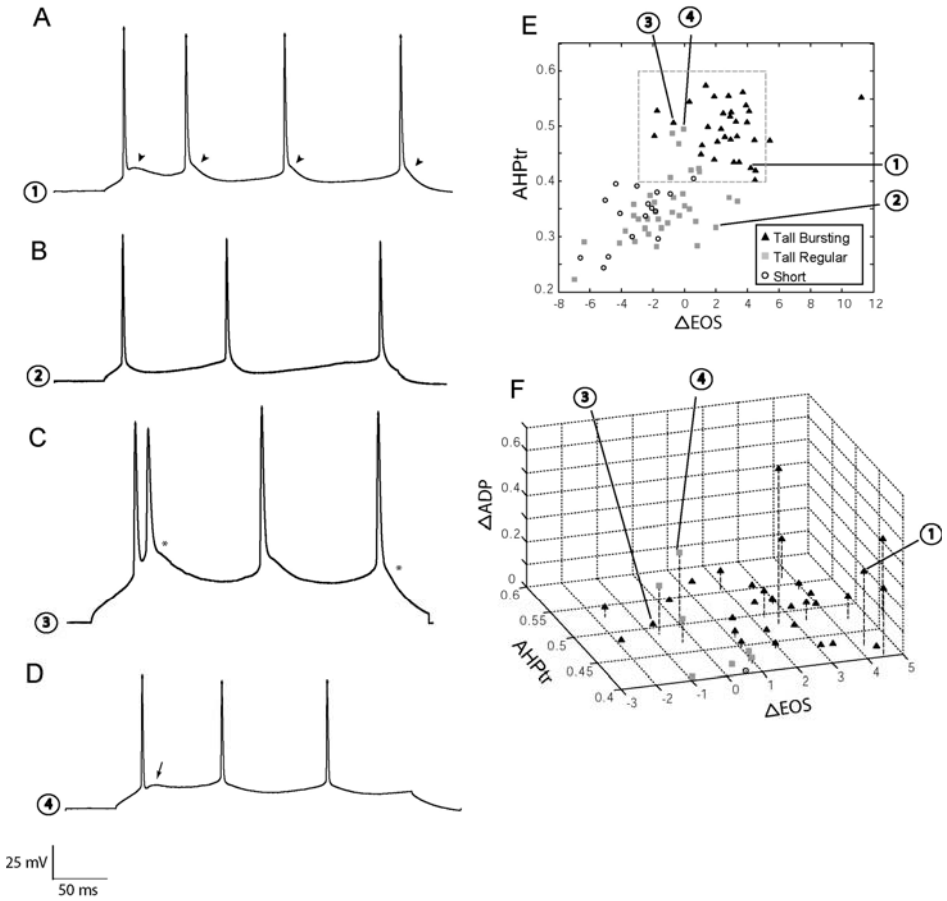

Figure 3.4: Exceptional Spiking Patterns. The spiking patterns of these cells straddled our main criteria we used for separating the tall pyramidal cells. Therefore we used additional criteria to place them in the correct group. (A) Example of tall bursting cell that did not burst. All spikes are followed by a fast afterspike depolarization (arrowheads), giving this cell a high, positive ΔEOS and high AHPtr. This trace corresponds to the cell labeled 1 in (E) and (F), showing this cell fits most criteria for tall bursting cells. (B) Example of a tall regular spiking cell with a high ΔEOS. Because of a widening at the base of the spikes EOS was detected higher than would be expected making it positive for this cell. However it is clear from the lack of fast afterspike depolarization, the lack of bursts, and the low AHPtr that this is a regular spiking cell. This trace corresponds to the cell labeled 2 in (E), showing that it fits most criteria for tall regular cells. (C) Example of a tall bursting cell with a low ΔEOS. Asterisks denote a spike with a negative ΔEOS. The second spike in this train occurred before a repolarization of the membrane, causing an artificially high threshold based on a shrinking of the dV/dt peak for this spike. Also for this cell, there were occasional instances where there was no fast afterspike depolarization (the second asterisk), causing the average ΔEOS to drop below 1. However, this cell is clearly a tall burst spiking cell because it bursts and it has AHPtr greater than 0.4. This trace corresponds to the cell labeled 3 in (E) and (F). (D) Example of tall regular spiking cell with a high AHPtr. Because this cell has a high, late ADP (arrow), on some of its spikes the AHP occurred later in some of the spikes in the train making the average AHPtr higher than would be expected. However, this cell is clearly a tall regular spiking cell because it does not burst, and has a low ΔEOS. It also has a high ADP compared to the tall bursting cells surrounding it (see F). This trace corresponds to the cell labeled 4 in (E) and (F). (E) Same scatterplot as 3.3 D, showing the relationship of ΔEOS and AHPtr. (F) Enlarged three dimensional plot of the boxed area in panel (E) showing the use of ADP as an additional criterion to separate some of the tall regular spiking cells, as in (D), from tall bursting cells, as in (C) that overlap in (E)

We found some more subtle differences between the spikes shapes of the three cell groups (see Table 3.1). We calculated the ΔAHP potential difference in two ways. We first calculated the difference between the membrane potential at threshold and subtracted the potential at AHP (a measure we called ΔAHP_1). Then we calculated the difference between the membrane potential at the EOS and subtracted the potential at AHP (a measure we called ΔAHP_2). We found that the tall regular spiking cells had a more negative ΔAHP_1 (-10.187 ± 0.439; Fig 3.3 B) than the other two cell types. This difference was significant between tall regular spiking cells and short pyramidal cells (-7.633 ± 0.644; $p < 0.005$, Mann Whitney U Test) as well as tall bursting cells (-6.698 ± 0.742, $p < 5.0 \times 10^{-5}$, Mann Whitney U Test). However, short pyramidal cells has a less negative ΔAHP_2 than the other two cell types (-4.591 ± 0.659; Fig 3.3 A). This difference was significant between short pyramidal cells and tall regular spiking cells (-8.960 ± 0.414, $p < 5.0 \times 10^{-5}$, Mann Whitney U Test) as well as tall bursting cells (-9.485 ± 0.881, $p < 5.0 \times 10^{-5}$, Mann Whitney U Test). The smaller drop in AHP for short pyramidal cells could contribute to their higher FFR. Tall regular spiking cells and tall bursting cells have a similar ΔAHP_2 perhaps suggesting a similar mechanism for their AHP. However, the fast afterspike depolarization that follows every spike of the tall bursting cells prevents the AHP from dropping too far from threshold, hence causing a significant difference between the two tall populations in ΔAHP_1.

Finally, we found two other differences between the tall regular spiking and tall bursting cells. Tall regular spiking cells had a larger half peak width compared to the tall bursting cells (2.180 ± 0.103 and 1.885 ± 0.084, for tall regular and tall burst spiking cells, respectively, $p < 0.05$, Mann Whitney U Test; Fig 3.3 BC). Short pyramidal cells

were insignificantly different from these two cell groups. Also, tall regular spiking had a smaller adaptation coefficient than the tall bursting cells (0.837 ± 0.018 and 0.904 ± 0.013, for tall regular and tall burst spiking cells, respectively, $p < 0.005$, Mann Whitney U Test). This suggests that spikes in the tall regular spiking cells adapted at a faster rate than spikes in tall bursting cells.

In conclusion, we were able to differentiate our tall cells into two different populations based on their spiking patterns and electrophysiological properties. Tall regular spiking cells had thicker spikes, a more negative ΔEOS, more negative ΔAHP_1, and an AHP that occurred closer to the spike (low AHPtr), and they adapted slowly. Tall bursting cells had a higher FFR (from the burst) and were characterized by having a fast afterspike depolarization that would end their spike sooner (positive ΔEOS). As a result, their AHP occurred much later (high AHPtr). Furthermore, we found further evidence that the short pyramidal cells, a population distinguished from the other two morphologically, has electrophysiological characteristics that are unique to it (such as higher FFR, more negative ΔEOS, and less negative ΔAHP_2).

3.4.3 Photostimulation Results

We used laser-scanning photostimulation to map local sources of excitatory input to all 84 layer 5 cells. This included 16 short pyramidal neurons, 36 tall regular neurons, and 32 tall bursting neurons. Complete tables of the photostimulation results for all of our cells are provided in Table 3.2, 3.3, and 3.4 with sample excitatory input patterns for each cell type provided in Figure 3.5.

As a whole, nearly all layer 5 neurons received significant input from all layers, and hence there was no significant difference between the cell types based on source of laminar input. Only 4 of the 84 cells (4.8%; 2 tall regular spiking and 2 tall burst spiking cells) did not receive significant input from layer 2/3, and 5 of 84 cells (6.0%; 2 short pyramidal cells, 1 tall regular spiking cells, and 2 tall bursting cells) did not receive input from layer 6. There were no significant differences between cell subtypes in this measure. All cells received input from at least three layers.

We analyzed the relative strength of excitatory input from each layer to the three different types of cells and found significant differences in the strength of input from certain layers between the short pyramidal cells and the two tall subtypes of pyramidal neurons. Short pyramidal neurons received their strongest input from layer 4 (38.9% ± 4.5%; mean ± SE) followed by layer 5 (34.8% ± 3.8%; Fig 3.5AB 3.6 A). Functional input from layer 2/3 and layer 6 was weaker, with layer 2/3 providing 17.0% ± 2.2% of evoked input and layer 6 providing 9.3% ± 1.8% input.

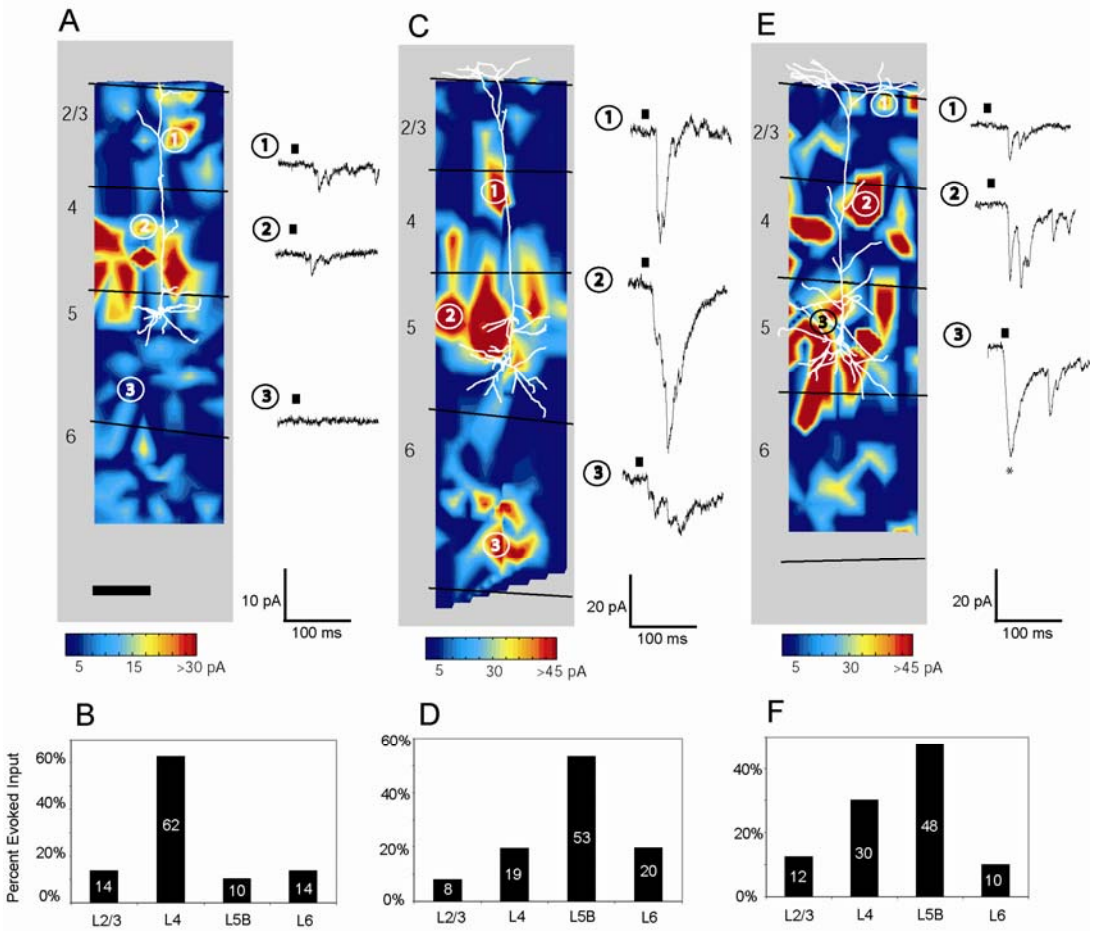

Figure 3.5: Examples of Laminar Excitatory Input to Three Individual Layer 5 Pyramidal Cells. Pseudo-colored input maps demonstrate representative patterns of excitatory input to three individual neurons. These input maps are linear interpolations of the sum of EPSC amplitude values (minus spontaneous EPSCs) measured following photostimulation at sites spaced ~50 microns apart. Colored horizontal scale bars indicate the corresponding sum of EPSC amplitude values for input maps above. Camera lucida drawings of dendrites (white lines) and soma (white) are overlaid onto plots. Gray areas are present so that neuronal processes can be seen against otherwise white background. Laminar borders are represented by horizontal black lines and labeled on the left. To the right of each input map are example voltage-clamp recordings (-65 mV holding potential) made while stimulating presynaptic regions signified by the corresponding circled numbers. Short dashes above each trace show the duration of photostimulation and onset of glutamate activation. The current marked with an asterisk (*) shows a direct response to glutamate uncaging and is omitted from analysis. Percentage of evoked excitatory input (EI, see text) from each layer is illustrated in the bar graphs below each plot. (A) Short pyramidal neuron that received significant input from all layers. (B) Bar graph representing the percent of total evoked input from each layer for cell in (A). In this case the strongest input came from layer 4 followed by layers 2/3 and 6. The weakest significant input came from layer 5. (C) Tall burst spiking pyramidal neuron that received significant input from all layers. (D) Bar graph representing the percent of total evoked input from each layer for cell in (C). In this case the strongest input came from layer 5 followed by layer 6. (E) Tall regular spiking pyramidal cell that received significant input from all layers. (F) Bar graph representing the percent of total evoked input from each layer for cell in (E). In this case, the strongest input was from layer 5 followed by layer 4. Black scale bar in (A) represents 200 microns.

Tall regular spiking pyramidal cells, on the other hand, received their strongest input from layer 5 (47.0% ± 2.5%; Fig 3.5 CD, 3.6 A). This input was significantly greater than the layer 5 input to short pyramidal cells ($p < 0.01$, Mann Whitney U Test). Tall regular-spiking cells also received strong input from layer 4 (26.5% ± 2.3%), though this was significantly lower than the strength of input to the short pyramidal neurons ($p < 0.05$, Mann Whitney U Test). Similar to short pyramidal cells, they received weaker input from layer 2/3 (12.7% ± 1.4%) and layer 6 (13.8% ± 1.7%). The input from these two latter layers was insignificantly different from those to the short pyramidal neurons, though input from layer 6 was close to significance ($p = 0.08$, Mann Whitney U Test).

The strength of laminar input to the tall bursting pyramidal cells was also significantly different from short pyramidal cells, but nearly identical to the values from the tall regular-spiking cells (Fig 3.5 EF, 3.6A). Similar to the tall regular-spiking cells, the tall bursting cells received their strongest input from layer 5 (48.9% ± 2.7%). This was significantly different from the short pyramidal cells ($p < 0.05$, Mann Whitney U Test) but not from the tall regular-spiking cells ($p = 0.86$ Mann Whitney U Test). Tall bursting pyramidal cells also received input from layer 4 (26.8% ± 1.9%) which was significantly different from short pyramidal neurons ($p < 0.05$, Mann Whitney U Test), but not from tall regular spiking cells ($p = 0.50$, Mann Whitney U Test). Similar to tall regular spiking and short pyramidal cells, tall bursting cells received 13.1% ± 1.4% of their input from layer 2/3 and 11.2% ± 1.1% of their input from layer 6. These values were insignificantly different from the other cell types.

Since the values of the two tall cells were very similar to each other, we decided to group the two tall subtypes together and compare them to the short pyramidal cells.

As expected there was a significant difference between the short pyramidal and the tall pyramidal cells from layer 4 ($p < 0.05$, Mann Whitney U Test) and from layer 5 ($p < 0.005$, Mann Whitney U Test). However, there was no significant difference between the two groups in the strength of input from layer 2/3 ($p = 0.11$, Mann Whitney U Test) and layer 6 ($p = 0.12$, Mann Whitney U Test).

For all cell types we also calculated the ratio of layer 4 input to the total input from layers 4 and 5. For this value, a ratio of 1 would imply that the cell received input from layer 4 but not 5, a ratio of 0 would imply that the cell received input from layer 5 but not 4, and a ratio of 0.5 would imply that the cell received equal input from layer 4 and layer 5. The layer 4 input ratio for short pyramidal cells was 0.52 (± 0.05) suggesting that they receive input evenly from layers 4 and 5. This ratio was significantly higher than that of tall regular spiking cells (0.36 ± 0.03, $p < 0.05$, Mann Whitney U Test) and the tall bursting cells (0.36 ± 0.03, $p < 0.05$, Mann Whitney U Test), and to the population of tall cells as a whole (0.36 ± 0.02, $p < 0.05$, Mann Whitney U Test). Unlike short cells, tall cells receive twice as much layer 5 input than they do from layer 4.

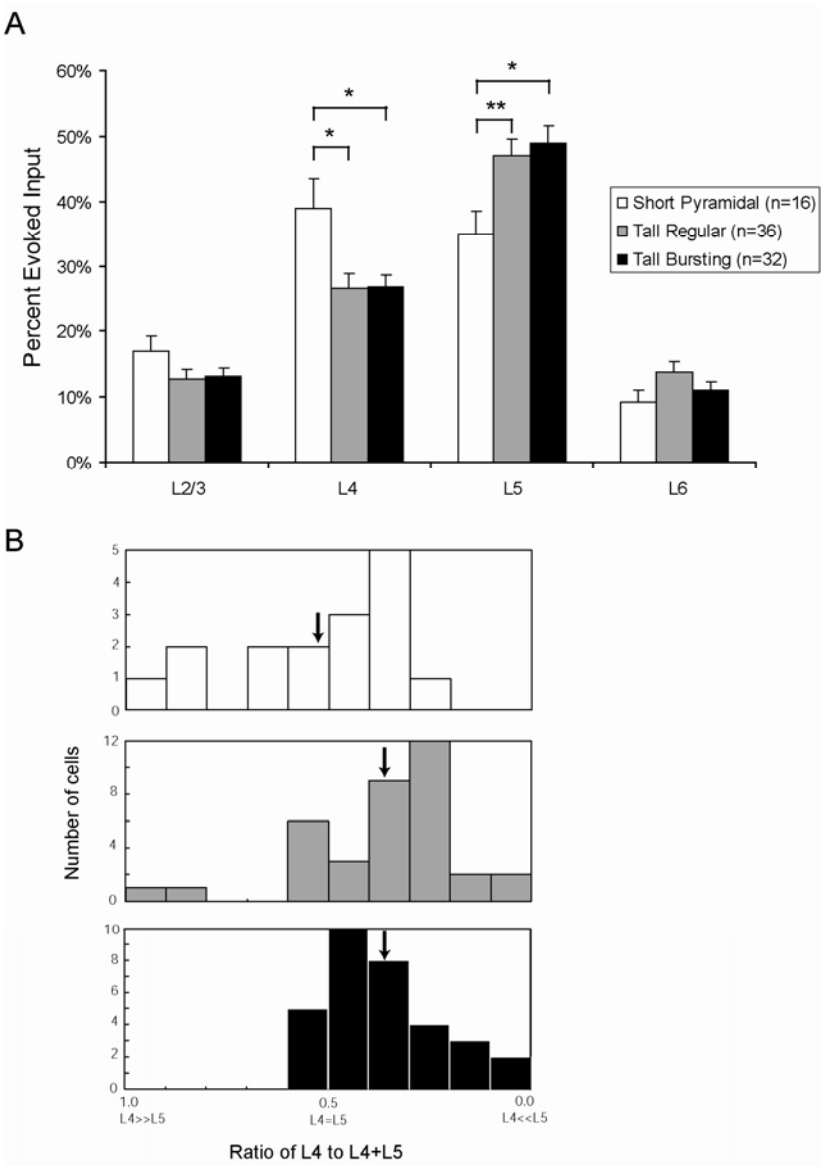

Figure 3.6. Laminar input to the three types of layer 5 neurons. (A) Mean ± SEM percent of total evoked input for each layer for the three subtypes of layer 5 cells. Short pyramidal neurons received a larger percentage of evoked input from layer 4 than other cell types (Mann Whitney U test, tall regular, $p < 0.05$, tall bursting, $p < 0.05$). However, they also received relatively weaker input from layer 5 than did the two tall cells (Mann Whitney U test, tall regular $p < 0.01$, tall bursting cells, $p < 0.05$). The inputs to the two tall cells were insignificantly different from each other. * denotes a significance of $p < 0.05$; ** denotes a significance of $p < 0.01$. (B) Frequency bar graphs for each cell type showing the ratio of L4 input to total input from L4 and L5. A value near 1.0 (toward the left) implies that the cell received much more L4 input than L5; a value near 0 (toward the right) implies that the cell received much more L5 input than L5. Arrows point to the mean of the distribution for each cell types. The means of the two tall populations are nearly identical, but the mean of the short pyramidal cells is shifted to the left.

3.5 Discussion

3.5.1 Cell Classification and Potential Projections

Layer 5 pyramidal neurons have been studied in the rat across different cortical regions, such as the visual cortex (Kasper et al., 1994), somatosensory cortex (Schubert et al., 2001; Schubert et al., 2006), motor cortex (Angulo et al., 2003), and the frontal cortex (Morishima and Kawaguchi, 2006). In these and other studies of layer 5 pyramidal neurons, cells were either characterized by their morphological characteristics (short vs tall) or physiological characteristics (regular spiking v burst spiking). Using either one of these criteria would yield two subtypes of neurons. Chagnac-Amitai, et al. (1990) published a study that showed that all bursting cells had a tall pyramidal cell morphology. They also found that a large majority of their 9 reconstructed cells had a short pyramidal morphology. Although these two main findings justify a two subtype classification of layer 5 cells, Chagnac-Amitai, et al. also report finding a cell (1/9) that had a morphology that was indistinguishable from the tall bursting cells but was characterized as regular spiking. The low number of tall regular spiking cells may have been because of the brain region they chose to prepare their slices (parietal cortex).

In the mouse somatosensory cortex, three layer 5 cells have been identified based on dendritic and axonal morphology: tall tufted, tall-simple, and short pyramidal (Larsen and Callaway, 2006). The apical dendrite of short pyramidal cells did not enter layer 1 and often ended midway through layer 2/3. Furthermore, short pyramidal cells often did not have a tuft or branching at the end of the apical dendrite. These cells also had extensive axonal projections to the superficial layers. On the other hand, tall tufted and tall simple cells had apical dendritic branches that reached the top of layer 2/3 and layer

1. However, tall tufted cells were characterized by having axons that arborized exclusively within the deep layers, but tall simple, on the other hand, projected axons to the superficial layers. Furthermore, earlier exhaustive studies of the spike shape of the rat sensorimotor cortex report three different spiking patterns: fast adapting regular spiking cells, slow adapting regular spiking cells, and burst spiking cells (Franceschetti et al., 1995; Schwindt et al., 1997). Multiple types of spikes patterns have also been observed in layer 5 of cat visual cortex (Nowak et al., 2003).

In our study we first investigated whether our cells fall into two or three subtypes. First we considered the morphological properties of cells, which clearly divided our cell population into two subtypes. One subtype, the short pyramidal cells, had apical dendrites that ended before reaching layer 1. The other subtype, the tall pyramidal cells, had apical tufts in layer 2/3 with extensive branching in layer 1. All short pyramidal cells are regular spiking cells.

However, a closer look at the tall pyramidal cells revealed that they can be separated into two groups based on their firing patterns and spike shape. About half of our tall pyramidal cells were burst spiking and the others regular spiking. As reported by Chagnac-Amitai, et al. tall bursting cells have a characteristic fast afterspike depolarization. This fast afterspike depolarization caused interesting changed in the spike shape properties. For example it shrunk the potential difference between the threshold and the afterspike hyperpolarization, and caused it to occur later in the interspike interval. Furthermore, tall regular spiking cells adapted more slowly, had a slower firing rate, and a longer half peak width.

The mechanism for the fast afterspike depolarization of the tall bursting cells of layer 5 has been the focus of a handful of studies (Franceschetti et al., 1995; Schwindt et al., 1997; Schwindt and Crill, 1999). This depolarization is calcium dependent and results from by sodium activated calcium channels in the dendrites of some layer 5 tall pyramidal cells (Franceschetti et al., 1995; Schwindt and Crill, 1999). When these cells received a large enough suprathreshold depolarization, these calcium channels can mediate a state of prolonged depolarization to cause the cells to burst.

We also found significant differences in the spike shape of the short pyramidal neurons and the other two cell types. Most strikingly, short pyramidal cells fired faster than the other two cells, and had a less negative afterspike hyperpolarization. Furthermore, the end of the spike was significantly more negative when compared to the other two cell types. The firing pattern of these cells was similar to the regular spiking fast adapting cells reported in other studies (Franceschetti et al., 1995).

Because of the morphological and physiological differences shown above, pyramidal neurons in the rat visual cortex can be differentiated into three different subtypes. The first of the three, tall bursting cells, often called tall tufted, or intrinsically bursting cells, project to subcortical targets, such as the superior colliculus and pontine nuclei as well as other areas (Hallman et al., 1988; Hubener and Bolz, 1988; Larkman and Mason, 1990).

The second of the three cells, the tall regular spiking cells, which are also called tall simple cells, have been mentioned in several articles but are usually identified by their intrinsic firing properties (Schubert et al., 2001; Schubert et al., 2006). Recent studies in the rat prefrontal cortex show convincingly that cells that have morphology and

physiological properties similar to tall regular spiking cells project to the corpus callosum (Morishima and Kawaguchi, 2006). Furthermore, cells that have a similar morphology and firing pattern have been identified in a transgenic mouse line expressing YFP under the control of Kv3.1 promoter (Akemann et al., 2004). These YFP-labeled cells similar to our tall regular spiking cells project to other cortical areas instead of subcortical targets, and probably play a similar role in the rat visual cortex.

Our final cell type are the short pyramidal cells, which are similar to the corticocortical projecting regular spiking cells described in several anatomical studies of layer 5 cells (Hallman et al., 1988; Hubener and Bolz, 1988; Larkman and Mason, 1990; Kasper et al., 1994). It is currently unclear whether the tall regular spiking cells and short pyramidal cells project to the same cortical areas. More anatomical studies need to be performed to distinguish between the projections of these cell types.

3.5.2 Functional Input and Role in Cortical Circuitry

In addition to our anatomical findings we identified the laminar sources of functional excitatory input to individual neurons (see Fig. 3.7 for summary). Nearly all of our cells received input from all of the layers. Short pyramidal neurons received input mainly from layer 4, with almost the same strength of input from layer 5. They had weaker input from layers 2/3 and 6 though this input was greatly significant. Their input was remarkably different from that of the tall cells. The two tall subtypes of layer 5 neurons had identical input patterns. Both received the strongest input from layer 5 followed by layer 4, and weaker input from layer 2/3 and 6. See Figure 3.7 for summary.

The tall cells received nearly twice as much input from layer 5 than they did from

layer 4. The short cells, on the other hand, received nearly equal strength input from layer 4 and layer 5. This observation, in addition to the fact that short pyramidal cells do not have dendritic branches in layer 1, suggests that perhaps one of the sources of layer 5 input to tall cells is through synapses located in layer 1. Tall regular spiking cells and short pyramidal cells are the only layer 5 cell types that project axons to the superficial layers suggesting that the higher input to these layers to layer 5 tall cells could be selectively from the these particular cell types.

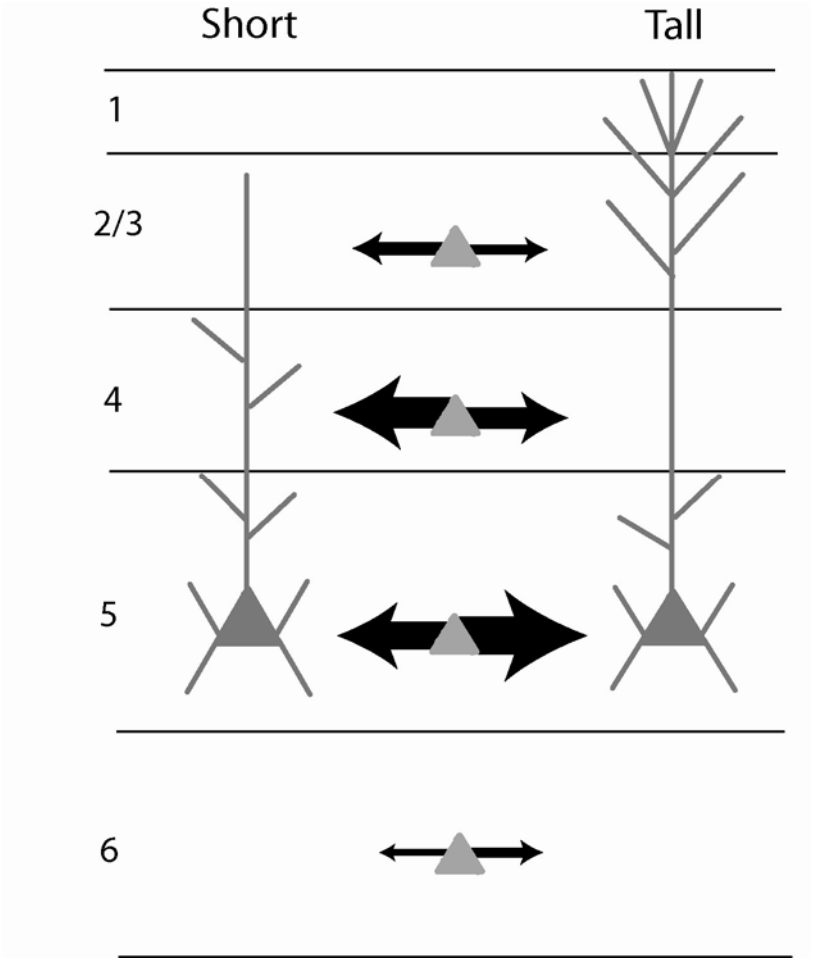

Figure 3.7: Schematic diagram summarizing the functional input to short and tall pyramidal cells of layer 5. Thickness of black arrows represents the strength and directionality of the source of local excitatory input to the two different cell subtypes. Short pyramidal cells receive significant local input from all layers. The inputs from layers 2/3 and 6 are weaker than those from layers 4 and 5. Short cells receive stronger input from layer 4 than they do from layer 5. Tall pyramidal cells also receive significant local input from all layers. Like short cells they receive weaker input from layers 2/3 and 6 than they do from layer 4 and 5. However, a key difference between the two cell types is that tall cells receive stronger layer 5 input than they do from layer 4.

Different cortical circuitry models have proposed different roles for layer 5 pyramidal neurons. Gilbert and Wiesel (1983), in a model based on the anatomical studies of cat visual cortex, predicted that the layer with the strongest input to layer 5 cells would be layer 2/3 with little or not input from layer 4. Callaway (1998), in a model based on the anatomical and photostimulation studies of the macaque visual cortex, predicted that layer 5 input would be from layer 4 and layer 2/3. Our findings are more in line with the latter model since, beside layer 5, the strongest input to layer 5 cells was from layer 4 cells for all cell types. However, neither model predicted the significant input from layer 6 cells.

3.5.3 Comparison to Rat Somatosensory Cortex

Our study is not the only photostimulation study of layer 5 pyramidal neurons. Schubert, et al. (2001) distinguished between two cell types in the rat somatosensory cortex, the intrinsically bust spiking cells (IB) and regular spiking cells (RS). In this experiment they chose cells that were located throughout layer 5 but underneath columns. They showed that these two cells are morphologically distinct, where IB cells had larger soma, apical dendritic length, apical dendritic branches, and maximal apical trunk diameter compared to RS cells. However, only a few cells were used for their morphological analysis (7 IB and 5 RS). We believe these two cells correspond to our two tall cell populations, with IB cells corresponding to tall bursting cells, and the RS cells corresponding to tall regular spiking cells. Photostimulation results of the two populations found that these two groups had very similar intracolumnar input, with one difference. IB cells received input from more photostimulation sites in layer 6 than RS

cells did. However, they again used only a few cells (7 IB cells, 8 RS cells). One problem with this study is that their analysis of photostimulation input does not allow direct comparison of the strength of input between layers. Although there may be more input from layer 6 sites, perhaps the size of these inputs are smaller than the few that were detected for the RS cells.

The photostimulation results of this experiment are very similar to our findings. Layer 5 cells in the somatosensory cortex receive widespread input from layer 5 and layer 4 with less widespread input from layer 2/3 with little difference between the two cell populations in the level of input from these layers. These are nearly identical to our findings. However, one key difference is that, although RS cells received the least widespread (and perhaps weakest) input from layer 6 (similar to both populations of our tall pyramidal cells), the IB cells received their most widespread (and perhaps strongest) input from layer 6. This most likely explanation for this difference between our observations and those of the Schubert, et al. group is that there are some key differences in the circuitry of the two sensory cortices. However, these differences could also be caused by a sampling bias since they only used 7 IB cells compared to our 32.

In a later study focusing only in pyramidal cells in layer 5A located below the barrels of the rat somatosensory cortex, Schubert, et al. (2006) found two cell types which they distinguished based on their firing properties (regular and bursting). These two cell types could not be distinguished from each other based on morphological measurements. Their photostimulation study of these cells revealed that two cell populations did not receive different patterns of input. The input to these cell types was indistinguishable from each other and remarkably similar to what the same group found

in layer 5B, with only one key difference. Although IB in layer 5B received more input from layer 6 than regular-spiking cells did, the bursting cells in layer 5A received the same amount of input from layer 6. In this study the used slightly more cells in their photostimulation results (12 RS and 7 IB cells). Their results for this study are nearly identical to the results we found for the two tall populations. The most widespread (and presumably the strongest) input came from layer 5 followed by layer 4 and layers 2/3 and 6. It is unclear whether the short pyramidal cells were included in either one of these studies as part of the regular spiking cell population.

These studies suggest there is a strong homology between the visual and somatosensory cortices. The only difference between the cortices is that the tall bursting cells receive stronger input from layer 6 in the somatosensory cortex than they do in the visual cortex. An increased input from layer 6 pyramidal cells suggests that there is greater coordination and communication between these two layers. In the rat somatosensory cortex, half of the corticothalamic cells (Zhang and Deschenes, 1997) as well as the corticopontine/corticotectal layer 5 cells (Mason and Groos, 1981) project to the higher-order sensory nucleus of the thalamus (for the rat somatosensory cortex this is the posterior nucleus). However, in the rat visual cortex, there are probably fewer layer 6 corticothalamic cells that project to the higher-order sensory nucleus of the thalamus (Zarrinpar and Callaway, 2006). This may explain why the input from layer 6 to layer 5 bursting cells is much weaker.

Perhaps the one surprising finding of this study is that we could not find any significant differences between two cell populations (the tall regular spiking and tall bursting cells). This is quite different from previous photostimulation experiments that

showed cell groups play specific roles in the cortical circuitry and receive different functional local laminar inputs. Future studies should investigate whether the tall bursting cells and tall regular spiking cells do indeed get input from two different population of cells. We partially address this specific issue in our next chapter.

3.6 Acknowledgements

The text of Chapter 3, in full, is a reprint of material that is in preparation for submission as a manuscript. I was the primary investigator and will be the first author on the manuscript and Edward M. Callaway, the second-author, directed and supervised the research. This study was also funded by National Institute of Health Grants EY-10742 and MH-63912. I would like to acknowledge Takuma Mori for his generous help with writing some of the spike analysis programs, Martha Bagnall and Aryn Gittis whose discussions were extremely helpful in developing our spike analysis and interpreting their results, and Rose Z. Zarrinpar for helping analyze a significant portion of the data collected for this study.

Table 3.1: Spike analysis properties for different layer 5 cell types
[1] Significant difference ($p < 0.05$) between short pyramidal and tall bursting cells.
[2] Significant difference ($p < 0.05$) between tall regular spiking and tall bursting cells.
[3] Significant difference ($p < 0.05$) between short pyramidal and tall regular cells.
Values are Mean ± SEM.

Cell Type	Short	Tall Regular	Tall Bursting
End of Spike from threshold (ΔEOS, in mV)	-3.042[1,3] ± 0.465	-1.228[2,3] ± 0.370	2.787[1,2] ± 0.411
Half Peak Width (HPW, in ms)	2.001 ± 0.096	2.180[2] ± 0.103	1.885[2] ± 0.084
Afterspike Depolarization (ΔADP, in mV for all spikes)	0.067 ± 0.021	0.053 ± 0.015	0.075 ± 0.026
Afterspike Hyperpolarization from threshold (ΔAHP_1, in mV)	-7.633[3] ± 0.644	-10.187[2,3] ± 0.439	-6.698[2] ± 0.742
Afterspike Hyperpolarization from EOS (ΔAHP_2 in mV)	-4.591[1,3] ± 0.659	-8.960[3] ± 0.414	-9.485[1] ± 0.881
Afterspike Hyperpolarization Time Ratio (AHPtr)	0.338[1] ± 0.013	0.351[2] ± 0.010	0.495[1,2] ± 0.008
Fastest Firing Speed (FFR, in Hz)	101.78[1,3] ± 4.24	47.45[2,3] ± 4.41	84.63[1,2] ± 4.84
Adaptation Coefficient	0.900 ± 0.026	0.837[2] ± 0.018	0.904[2] ± 0.013

Table 3.2: Laminar Sources of Evoked Excitatory Input for Short Pyramidal Cells. Layers with significant input to the cell show a percentage signifying the proportion of total evoked excitatory input that originated from that layer. Layers that provided non-significant input are denoted by *n.s.*

Cell Type	Cell Number	L2/3 Input	L4 Input	L5 Input	L6 Input
short pyramidal	C920A	18.26%	35.35%	33.48%	12.92%
short pyramidal	C920AB	30.19%	23.58%	33.28%	12.94%
short pyramidal	C1003A	19.51%	23.58%	44.07%	12.85%
short pyramidal	C1003AB	11.58%	41.39%	44.56%	2.47%
short pyramidal	C1207C	7.07%	59.12%	11.10%	22.72%
short pyramidal	C112B	8.70%	30.14%	54.71%	6.44%
short pyramidal	C112BB	12.81%	25.31%	54.97%	6.92%
short pyramidal	C209CB	20.29%	13.28%	41.18%	25.24%
short pyramidal	C216BB	37.39%	29.50%	33.11%	*n.s.*
short pyramidal	C216CB	14.58%	75.17%	6.83%	3.42%
short pyramidal	C228A	13.72%	62.40%	10.23%	13.66%
short pyramidal	C228AB	8.60%	63.29%	28.11%	*n.s.*
short pyramidal	C301A	14.44%	27.38%	50.24%	7.94%
short pyramidal	C307BB	6.78%	52.27%	30.89%	10.06%
short pyramidal	C308BB	27.41%	23.39%	45.19%	4.01%
short pyramidal	C309C	20.34%	37.40%	35.01%	7.25%

Table 3.3: Laminar Sources of Evoked Excitatory Input for Tall Regular Spiking Pyramidal Cells. Layers with significant input to the cell show a percentage signifying the proportion of total evoked excitatory input that originated from that layer. Layers that provided non-significant input are denoted by *n.s.*

Cell Type	Cell Number	L2/3 Input	L4 Input	L5 Input	L6 Input
tall regular	C919A	12.50%	9.72%	62.84%	14.94%
tall regular	C919AB	8.64%	29.39%	55.53%	6.44%
tall regular	C1012A	21.60%	17.07%	30.71%	30.61%
tall regular	C1012AB	26.63%	31.58%	26.63%	15.16%
tall regular	C1202B	2.02%	2.97%	48.72%	46.30%
tall regular	C1202BB	0.95%	5.19%	57.21%	36.64%
tall regular	C1207AB	18.78%	28.23%	45.84%	7.15%
tall regular	C1207B	21.79%	14.22%	58.37%	5.61%
tall regular	C1207CB	2.29%	41.25%	46.22%	10.24%
tall regular	C105A	10.09%	18.29%	62.42%	9.20%
tall regular	C105B	11.58%	23.88%	59.51%	5.02%
tall regular	C105BB	4.09%	41.57%	48.51%	5.83%
tall regular	C110B	*n.s.*	24.45%	71.21%	4.35%
tall regular	C111B	5.24%	20.00%	64.72%	10.04%
tall regular	C111BB	5.95%	33.53%	46.78%	13.74%
tall regular	C111D	*n.s.*	24.87%	61.28%	13.86%
tall regular	C112A	26.71%	18.13%	45.98%	9.17%
tall regular	C112AB	14.79%	39.84%	31.41%	13.96%
tall regular	C208A	7.59%	56.98%	14.11%	21.33%
tall regular	C208AB	7.32%	71.26%	6.95%	14.46%
tall regular	C209A	17.10%	23.78%	41.97%	17.15%
tall regular	C209AB	13.71%	38.67%	33.70%	13.92%
tall regular	C209C	16.34%	15.21%	51.40%	17.05%
tall regular	C216B	21.85%	22.60%	48.34%	7.21%
tall regular	C301AB	34.33%	10.87%	40.39%	14.41%
tall regular	C301C	12.09%	22.37%	34.29%	31.25%
tall regular	C301CB	25.52%	25.51%	20.85%	28.12%
tall regular	C302CB	12.34%	24.98%	57.25%	5.43%
tall regular	C302D	7.89%	19.47%	53.01%	19.64%
tall regular	C302DB	9.04%	48.46%	37.37%	5.13%
tall regular	C307B	9.19%	18.89%	71.92%	*n.s.*
tall regular	C308A	7.77%	28.80%	56.98%	6.45%
tall regular	C308AB	7.98%	21.71%	61.86%	8.45%
tall regular	C308B	17.70%	19.18%	57.60%	5.52%
tall regular	C404AB	9.22%	39.52%	37.78%	13.48%
tall regular	C404C	26.17%	22.78%	41.03%	10.02%

Table 3.4: Laminar Sources of Evoked Excitatory Input for Tall Burst Spiking Pyramidal Cells. Layers with significant input to the cell show a percentage signifying the proportion of total evoked excitatory input that originated from that layer. Layers that provided non-significant input are denoted by *n.s.*

Cell Type	Cell Number	L2/3 Input	L4 Input	L5 Input	L6 Input
tall bursting	C1004B	*n.s.*	21.56%	51.65%	26.78%
tall bursting	C1004BB	13.07%	14.65%	54.96%	17.31%
tall bursting	C1004C2	2.15%	15.86%	71.75%	10.25%
tall bursting	C1004C2B	12.68%	17.43%	62.71%	7.17%
tall bursting	C1207A	8.69%	41.03%	41.16%	9.12%
tall bursting	C1207BB	9.78%	26.26%	46.64%	17.32%
tall bursting	C105AB	3.07%	4.54%	83.27%	9.11%
tall bursting	C105C	8.18%	31.71%	43.04%	17.08%
tall bursting	C105CB	13.15%	19.92%	43.72%	23.21%
tall bursting	C111DB	20.58%	39.54%	32.45%	7.43%
tall bursting	C208B	3.48%	12.45%	76.83%	7.24%
tall bursting	C208BB	4.79%	3.23%	80.30%	11.68%
tall bursting	C208C	20.75%	21.02%	35.57%	22.65%
tall bursting	C208CB	20.58%	35.33%	27.04%	17.05%
tall bursting	C209B	11.54%	37.01%	48.36%	3.10%
tall bursting	C209BB	12.70%	35.29%	48.36%	3.65%
tall bursting	C216A	21.49%	20.43%	40.88%	17.20%
tall bursting	C216AB	17.49%	29.04%	47.54%	5.93%
tall bursting	C217A	12.49%	30.02%	47.57%	9.92%
tall bursting	C217AB	10.09%	27.23%	54.64%	8.04%
tall bursting	C217B	*n.s.*	48.13%	35.42%	16.44%
tall bursting	C302A	25.31%	30.90%	35.52%	8.27%
tall bursting	C302AB	29.28%	27.38%	33.69%	9.66%
tall bursting	C302B	28.05%	27.02%	38.27%	6.66%
tall bursting	C302BB	20.18%	43.54%	34.12%	2.16%
tall bursting	C308C	8.07%	29.62%	51.39%	10.92%
tall bursting	C309CB	17.12%	37.75%	31.87%	13.26%
tall bursting	C404A	9.47%	11.96%	78.57%	*n.s.*
tall bursting	C404B	10.66%	32.60%	46.49%	10.25%
tall bursting	C404BB	23.27%	25.29%	32.33%	19.10%
tall bursting	C404CB	7.09%	19.22%	64.65%	9.05%
tall bursting	C406BB	15.30%	40.48%	44.23%	*n.s.*

3.7 References

Akemann W, Zhong YM, Ichinohe N, Rockland KS, Knopfel T (2004) Transgenic mice expressing a fluorescent in vivo label in a distinct subpopulation of neocortical layer 5 pyramidal cells. J Comp Neurol 480:72-88.

Angulo MC, Staiger JF, Rossier J, Audinat E (2003) Distinct local circuits between neocortical pyramidal cells and fast-spiking interneurons in young adult rats. J Neurophysiol 89:943-953.

Briggs F, Callaway EM (2001) Layer-specific input to distinct cell types in layer 6 of monkey primary visual cortex. J Neurosci 21:3600-3608.

Briggs F, Callaway EM (2005) Laminar patterns of local excitatory input to layer 5 neurons in macaque primary visual cortex. Cereb Cortex 15:479-488.

Callaway EM (1998) Local circuits in primary visual cortex of the macaque monkey. Annu Rev Neurosci 21:47-74.

Callaway EM, Katz LC (1993) Photostimulation using caged glutamate reveals functional circuitry in living brain slices. Proc Natl Acad Sci U S A 90:7661-7665.

Chagnac-Amitai Y, Luhmann HJ, Prince DA (1990) Burst generating and regular spiking layer 5 pyramidal neurons of rat neocortex have different morphological features. J Comp Neurol 296:598-613.

Dantzker JL, Callaway EM (2000) Laminar sources of synaptic input to cortical inhibitory interneurons and pyramidal neurons. Nat Neurosci 3:701-707.

Franceschetti S, Guatteo E, Panzica F, Sancini G, Wanke E, Avanzini G (1995) Ionic mechanisms underlying burst firing in pyramidal neurons: intracellular study in rat sensorimotor cortex. Brain Res 696:127-139.

Gilbert CD (1983) Microcircuitry of the visual cortex. Annu Rev Neurosci 6:217-247.

Gilbert CD, Wiesel TN (1983) Functional organization of the visual cortex. Prog Brain Res 58:209-218.

Hallman LE, Schofield BR, Lin CS (1988) Dendritic morphology and axon collaterals of corticotectal, corticopontine, and callosal neurons in layer V of primary visual cortex of the hooded rat. J Comp Neurol 272:149-160.

Hubener M, Bolz J (1988) Morphology of identified projection neurons in layer 5 of rat visual cortex. Neurosci Lett 94:76-81.

Kasper EM, Larkman AU, Lubke J, Blakemore C (1994) Pyramidal neurons in layer 5 of the rat visual cortex. I. Correlation among cell morphology, intrinsic electrophysiological properties, and axon targets. J Comp Neurol 339:459-474.

Katz LC, Dalva MB (1994) Scanning laser photostimulation: a new approach for analyzing brain circuits. J Neurosci Methods 54:205-218.

Koester SE, O'Leary DD (1992) Functional classes of cortical projection neurons develop dendritic distinctions by class-specific sculpting of an early common pattern. J Neurosci 12:1382-1393.

Larkman A, Mason A (1990) Correlations between morphology and electrophysiology of pyramidal neurons in slices of rat visual cortex. I. Establishment of cell classes. J Neurosci 10:1407-1414.

Larsen DD, Callaway EM (2006) Development of layer-specific axonal arborizations in mouse primary somatosensory cortex. J Comp Neurol 494:398-414.

Mason R, Groos GA (1981) Cortico-recipient and tecto-recipient visual zones in the rat's lateral posterior (pulvinar) nucleus: an anatomical study. Neurosci Lett 25:107-112.

Mercer A, West DC, Morris OT, Kirchhecker S, Kerkhoff JE, Thomson AM (2005) Excitatory connections made by presynaptic cortico-cortical pyramidal cells in layer 6 of the neocortex. Cereb Cortex 15:1485-1496.

Morishima M, Kawaguchi Y (2006) Recurrent connection patterns of corticostriatal pyramidal cells in frontal cortex. J Neurosci 26:4394-4405.

Nowak LG, Azouz R, Sanchez-Vives MV, Gray CM, McCormick DA (2003) Electrophysiological classes of cat primary visual cortical neurons in vivo as revealed by quantitative analyses. J Neurophysiol 89:1541-1566.

Sawatari A, Callaway EM (1996) Convergence of magno- and parvocellular pathways in layer 4B of macaque primary visual cortex. Nature 380:442-446.

Sawatari A, Callaway EM (2000) Diversity and cell type specificity of local excitatory connections to neurons in layer 3B of monkey primary visual cortex. Neuron 25:459-471.

Schubert D, Kotter R, Luhmann HJ, Staiger JF (2006) Morphology, electrophysiology and functional input connectivity of pyramidal neurons characterizes a genuine layer va in the primary somatosensory cortex. Cereb Cortex 16:223-236.

Schubert D, Kotter R, Zilles K, Luhmann HJ, Staiger JF (2003) Cell type-specific circuits of cortical layer IV spiny neurons. J Neurosci 23:2961-2970.

Schubert D, Staiger JF, Cho N, Kotter R, Zilles K, Luhmann HJ (2001) Layer-specific intracolumnar and transcolumnar functional connectivity of layer V pyramidal cells in rat barrel cortex. J Neurosci 21:3580-3592.

Schwindt P, Crill W (1999) Mechanisms underlying burst and regular spiking evoked by dendritic depolarization in layer 5 cortical pyramidal neurons. J Neurophysiol 81:1341-1354.

Schwindt P, O'Brien JA, Crill W (1997) Quantitative analysis of firing properties of pyramidal neurons from layer 5 of rat sensorimotor cortex. J Neurophysiol 77:2484-2498.

Song S, Sjostrom PJ, Reigl M, Nelson S, Chklovskii DB (2005) Highly nonrandom features of synaptic connectivity in local cortical circuits. PLoS Biol 3:e68.

West DC, Mercer A, Kirchhecker S, Morris OT, Thomson AM (2006) Layer 6 cortico-thalamic pyramidal cells preferentially innervate interneurons and generate facilitating EPSPs. Cereb Cortex 16:200-211.

Yabuta NH, Callaway EM (1998a) Cytochrome-oxidase blobs and intrinsic horizontal connections of layer 2/3 pyramidal neurons in primate V1. Vis Neurosci 15:1007-1027.

Yabuta NH, Callaway EM (1998b) Functional streams and local connections of layer 4C neurons in primary visual cortex of the macaque monkey. J Neurosci 18:9489-9499.

Yoshimura Y, Callaway EM (2005) Fine-scale specificity of cortical networks depends on inhibitory cell type and connectivity. Nat Neurosci 8:1552-1559.

Yoshimura Y, Dantzker JL, Callaway EM (2005) Excitatory cortical neurons form fine-scale functional networks. Nature 433:868-873.

Zarrinpar A, Callaway EM (2006) Local connections to specific types of layer 6 neurons in the rat visual cortex. J Neurophysiol 95:1751-1761.

Zhang ZW, Deschenes M (1997) Intracortical axonal projections of lamina VI cells of the primary somatosensory cortex in the rat: a single-cell labeling study. J Neurosci 17:6365-6379.

Chapter 4

Connection specificity to similar and different pairs of layer 5 excitatory neurons of the rat visual cortex

4.1 Abstract

In the previous chapter, although we distinguished between two cell types, the tall bursting and tall regular spiking cells, we did not see any major difference in their laminar input. We decided to calculate a correlation probability (CP) as a measure of synchronous activity in our cell types, and to see if our cells get input from distinct populations of cells within layer 5. If a single presynaptic neuron is stimulated and it provides input to both recorded cells it will generate synchronous synaptic currents and a high CP; inputs from different presynaptic neurons that fire action potentials asynchronously will generate asynchronous synaptic currents and a low CP. We found that if a tall regular spiking cell is matched with another tall regular spiking cell it was more than twice as likely to get synchronous input from layer 5 and more than four times as like to get synchronous input from layer 6. We found similar results for tall burst spiking cells, where two tall bursting cells were three times more likely to get input from layer 5, but not from layer 6. Pairs of short pyramidal neuron did not have any differences in their laminar CPs when compared to their unmatched cohorts. Although the two types of tall pyramidal neurons receive the same laminar input patterns, they receive input from different cell populations within those layers.

4.2 Introduction

We found part of the results in the previous chapter quite surprising. We identified two cell types, tall regular spiking and tall bursting cells, based on their firing properties. Although these cells had remarkable differences in their spike shape and firing properties, they had similar morphological characteristics. Furthermore, they had indistinguishable input patterns. These results run counter to some of our earlier principles of cortical circuitry discussed in the introduction, that different cell types play different roles in the cortical circuitry. If this principle is true, then one could conclude that these two cell types are not different from each other, since they share the same laminar inputs and have similar morphologies.

Previous research suggests that these cells are in fact projecting to different subcortical areas (Kasper et al., 1994; Morishima and Kawaguchi, 2006). Tall regular spiking cells project to the corpus callosum, whereas bursting cells project to the superior colliculus, LP, and pontine nuclei. However, if they are the same cell type, it would be more evolutionarily advantageous to have one cell type that has a single axon that projects to the two areas. Therefore there must me more subtle differences between the input to the two cell types that we cannot detect from single cell photostimulation but may be detected by collecting photostimulation data from two cells simultaneously and looking for correlated input to these two different cell types.

To address this issue, we took advantage of the ability of focal uncaging to generate asynchronous action potentials in a small, spatially restricted population of neurons in the rat visual cortex brain slices (see Fig. 4.1). By combining this type of stimulation with intracellular recordings of excitatory synaptic currents to layer 5

pyramidal neurons, we were able to use the timing of evoked synaptic currents to infer whether individual stimulated neurons provided common input to both recorded cells or if instead the recorded cells received input from separate neuronal populations. If a single presynaptic neuron is stimulated and it provides input to both recorded cells it will generate synchronous synaptic currents (Fig 4.1 A); inputs from different presynaptic neurons that fire action potentials asynchronously will generate asynchronous synaptic currents (Fig 4.1 B).

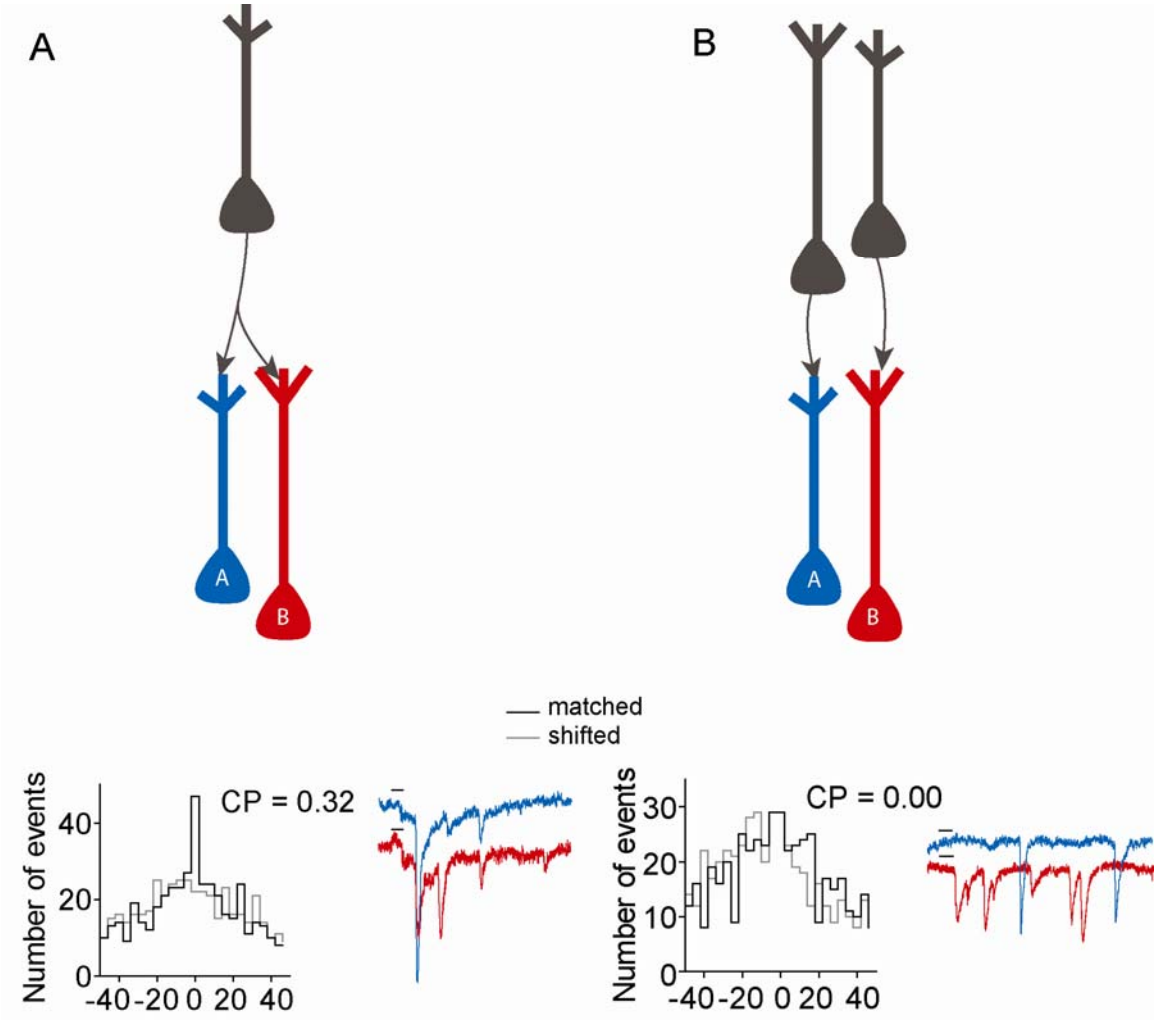

Figure 4.1: Explanation of Correlation Probability. (A) If a single presynaptic neuron (black cell) is stimulated and it provides input to both recorded cells (blue cell labeled A and red cell labeled B), it will generate synchronous synaptic currents such as the blue and red traces (short dashes above trace show the duration of photostimulation and onset of glutamate activation). The correlation probability (CP) closely estimated the probability that when a photostimulated presynaptic neuron fires an action potential and evoked a synaptic current in one of the two recoded layer 5 pyramidal cell, the same presynaptic neuron will also evoke a synaptic current in the second recorded neuron. Hence for a scenario illustrated in (A) the CP will be relatively high. (B) Inputs from different presynaptic neurons that fire action potentials asynchronously will generate asynchronous synaptic currents. Hence their Correlation probability will be low.

We used established cross-correlation analysis methods (Aertsen et al., 1989; Yoshimura and Callaway, 2005; Yoshimura et al., 2005) to normalize for synchrony resulting from time-locking of action potential generation to the stimulus. To obtain correlation probabilities, the numbers of synchronous synaptic currents attributable to shared input were expressed as a proportion of the total numbers of evoked synaptic currents from each cell. The correlation probability (CP) closely estimated the probability that when a photostimulated presynaptic neuron fires an action potential and evoked a synaptic current in one of the two recoded layer 5 pyramidal cell, the same presynaptic neuron will also evoke a synaptic current in the second recorded neuron. To determine the extent of shared input from the different laminar sources to each pair of recorded layer 5 pyramidal cells, separate calculations of CP were made based on stimulation sites in each cortical layer.

By comparing the correlation probabilities of pairs of layer 5 cells that are the same or different subtypes we can deduce whether these two populations get input from different populations of pyramidal cells. That is, if tall regular spiking cells or tall bursting cells are indeed a different population of cells than tall burst spiking cells, then they would share input from the same presynaptic cells (and have a higher CP) than when they are paired with a different cell type.

4.3 Materials and Methods

We used the same data that was collected as described in Chapter 3. We briefly describe the procedure for data collection again here, followed with a description of correlation analysis:

4.3.1 Slice preparation

Vibratome-cut coronal slices (400 μm) were prepared from the primary visual cortex of P21-P28 Long-Evans rats. Slices were cut in ice cold oxygenated (95% O2-5% CO2) artificial cerebral spinal fluid (ACSF) [which contained (in mM) 125 NaCl, 5 KCl, 26 $NaHCO_3$, 1.25 KH_2PO_4, 1.33 $MgSO_4$, 10 D-(+)-glucose, 3.15 $CaCl_2$, and 1 kynurenic acid] and then maintained submerged in the same ACSF solution heated to 35–37°C.

4.3.2 Electrophysiology

Slices were placed in a submersion type chamber with continuous perfusion of aerated ACSF. We used an infrared Olympus DIC microscope with a 40x, 0.8 NA water-immersion lens to visualize and target layer 5 neurons for whole-cell recordings in living brain slices. Glass microelectrodes (5-10 MΩ resistance) filled with a potassium-gluconate-based intracellular solution (130 mM K-gluconate, 10 mM HEPES, 2 mM $MgCl_2$, 0.2 mM EGTA, 6 mM KCl, 2.5 mM Na_2ATP, 0.5 mM Na_2GTP, 10 mM K-Phosphocreatine) contained 0.5-1% biocytin for cell labeling. We recorded in both current clamp (for spike shape analysis, see below) and voltage clamp modes (for measurement of evoked EPSCs)

4.3.3 Photostimulation and Input Maps

Local stimulation of presynaptic input neurons by light-evoked conversion of ‘caged’ glutamate to glutamate (“photostimulation”) was used to map laminar sources of functional connections onto individual recorded neurons (Callaway and Katz, 1993; Katz

and Dalva, 1994; Sawatari and Callaway, 1996; Dantzker and Callaway, 2000; Sawatari and Callaway, 2000; Briggs and Callaway, 2001, 2005; Yoshimura and Callaway, 2005; Yoshimura et al., 2005; Zarrinpar and Callaway, 2006). Brain slices were bathed in oxygentated ACSF (without Kynurenic acid) containing ~85 μM 'caged' glutamate (4-Methoxy-7-nitroindolinyl-caged L-glutamate – 'MNI-glutamate'; Tocris Biosciences, Ellisville, MO) at room temperature. Ultraviolet light (10-ms flash from an argon-ion laser) was focused to photostimulate a small discrete spot in the plane of the brain slice through a 40x microscope objective above the slice. Whole-cell voltage-clamp recordings (-65 mV) were made from two layer 5 postsynaptic neurons simultaneously, and inward excitatory postsynaptic currents (EPSCs) resulting from photostimulaion of presynaptic neurons was measured.

To map the locations of input, ~600-800 sites were stimulated sequentially in a pseudo-random pattern that covered all cortical layers. Stimulation sites were located throughout a rectangular area surrounding the recorded neuron, typically extending ~200 μm laterally on either side of the cell and vertically from the white matter to layer 1. After each photostimulation event, voltage clamp records were made for each stimulation trial to detect EPSCs. In addition, photostimulation trials were interleaved with control trials (no stimulation) to obtain spontaneous EPSCs (sEPSCs). After completion of photostimulation and recordings from a cell, the laser was used to burn alignment sites (< 10 μm) into the slice so that x-y photostimulation coordinates could be assigned to their corresponding position in the tissue. Laminar borders were determined using cytochrome oxidase stain.

4.3.4 Staining and Morphological Analysis

After photostimulation, slices were fixed with 4% paraformaldehyde in 0.1 M PBS for 12–24 h, then submerged in 30% sucrose in PBS. The slices were then stained whole-mount using a Cy3-conjugated streptavidin system (Jackson ImmunoResearch Laboratories, Inc, West Grove, PA). Cells were mounted using Vectashield (Vector Laboratories, Burlingame, CA), and morphological characteristics of the cells were determined using confocal laser-scanning microscopy (TCS SP2 AOBS; Leica). Multiple images of the cell was taken, including the whole cell with a low-resolution objective [PL Fluotar 10x; NA 0.3; Leica]; the apical dendrites and cell bodies with a medium-resolution objective [PL Fluotar 20x; NA 0.5; Leica] and the cell bodies with a high-resolution objective [PLAN APO 40x; NA 0.85; Leica]. Images were acquired as stacked files through the whole section thickness (step size, 0.11 μm).

Slices were then resectioned at 80 μm, and stained for cytochrome oxidase and biocytin to reveal laminar borders and neuronal morphology using methods previously described (Yabuta and Callaway, 1998a, 1998b). Cells that had an incomplete apical dendrite were excluded from all analysis. For all slices, the laminar borders near the cells were reconstructed with Neurolucida, a computerized system (MicroBrightField, Williston, VT). Each neuronal reconstruction, showing the laminar borders and alignments sites were aligned with the coordinate map of stimulation sites using Adobe Illustrator (Adobe Systems, San Jose, CA). Each stimulation site was assigned to a layer using this method. However, photostimulation sites within 50 μm of the layer borders were excluded from analysis since they can stimulate presynaptic cells in two layers (Yoshimura and Callaway, 2005; Yoshimura et al., 2005).

4.3.5 Cross Correlation Analysis

Cross-correlograms of EPSCs were computed for each pair of simultaneously recorded layer 5 cells. Separate correlograms were computed for stimulation sites from each cortical layer (layer 2/3, 4, and 5). Cross-correlation data were binned into histograms using 4 ms bins; the central bin included values of 0 ± 2 ms. Data from stimulation trials (from the same layer) were also used to create shifted correlograms for each layer and cell pairs. To calculate the CP, the shifted correlogram was subtracted from the unshifted correlogram for the corresponding layer, and then the value in the central bin was divided by the average estimated total number of evoked EPSCs (for the two cells) observed for all trials in the relevant layer. The average number of evoked EPSCs was calculated as the total number of measured EPSCs for Cell A minus the expected number of spontaneous EPSCs for that cell, plus the same value calculated for Cell B. This total was then divided by 2.

For some layers, the amount of input that occurred within 50 msecs of each other was so scant that an appropriate CP analysis could not be done accurately. The CP from these layers was either artificially too high or too low. Hence, we excluded CP data from layers of input where the pair of cells had fewer than 75 total EPSCs within 50 msecs of each other.

4.4 Results

We tested 41 pairs of layer 5 pyramidal cells from the pool of cells presented in the previous chapter. Since these cells were the same as the ones reported in that chapter,

the same criteria still applied for cell classification into three subtypes, tall regular spiking cells (TR), tall burst spiking cells (TB), and short pyramidal cells (SH). A complete table of our results is presented in Table 4.1. Of the 41 pairs of cells, we only had one connected pair, a reciprocal connection between a tall regular and tall bursting cell. Since previous research has shown that connected cells may receive different CP patterns than unconnected pairs (Yoshimura and Callaway, 2005; Yoshimura et al., 2005), we chose to exclude this cell from our analysis.

We were able to compute the layer 5 CP of 9 pairs of TR-TR cells and 12 pairs where a TR was matched with a cell of another type (TR-X). On average, the layer 5 CP TR-TR pairs was 0.071 ± 0.010 (Mean ± SEM; Fig 4.2 A), which means that for 7% of cases in which a layer 5 neuron was photostimulated and evoked an EPSC in one TR cell, that same layer 5 neuron also evoked a synchronous EPSC that was detected other TR cell. This CP value was significantly higher from that of TR-X pairs (CP = 0.030 ± 0.008; $p < 0.05$, Mann Whitney U Test). We also calculated the layer 6 CP for TR-TR pairs (n = 6 pairs; Fig 4.2 B). These pairs had a relatively high CP (0.077 ± 0.018) that was significantly different from TR-X pairs (0.017 ± 0.030; $p = 0.05$, Mann Whitney U Test). It seems clear that TR-TR pairs get a higher CP, and hence have a higher proportion of shared presynaptic neurons from both layers 5 and 6, compared to their unmantched counterparts. We were not able to detect any significant differences between the CP of the TR-TR pairs and TR-X pairs from the superficial layers, though this may be caused by the few number of calculable CPs from the superficial layers.

We were also able to compute the layer 5 CP of 11 pairs of TB-TB cells and 8 pairs where a TB cell was matched with another cell type (TB-X cells; Fig 4.2 A). On

average, the layer 5 CP for TB-TB pair was 0.070 ± 0.013 which was also significantly higher from the TB-X pairs (0.026 ± 0.008; $p < 0.05$, Mann Whitney U Test). However, unlike TR-TR pairs, TB-TB pairs did not have any significant differences between their layer 6 CP and those of found for TB-X pairs (0.030 ± 0.013 for TB-TB pairs and 0.035 ± 0.031 for TB-X cells, $p = 0.57$; Fig 4.2 B). Furthermore, we could not detect any other significant differences between the CP from the other layers of TB-TB pairs and those found for TB-X cells.

Since we were concerned about whether TR and TB cells were indeed different cell types we decided to do a direct comparison between matching pair of tall cells (TR-TR or TB-TB cells) to unmatched pairs of tall cells (TR-TB). Of the TR-X cell pairs, 5 pairs were TR-TB cells with a layer 5 CP of 0.032 ± 0.010. Both, the TR-TR cell pair CP was significantly higher than TR-TB cell pairs ($p = 0.05$, Mann Whitney U Test), as were the CP of TB-TB pairs ($p < 0.05$, Mann Whitney U Test). We were not able to detect any other significant differences in the CP of the other layer between either one of the matching tall cell subsets (TR-TR or TB-TB) and TR-TB cells.

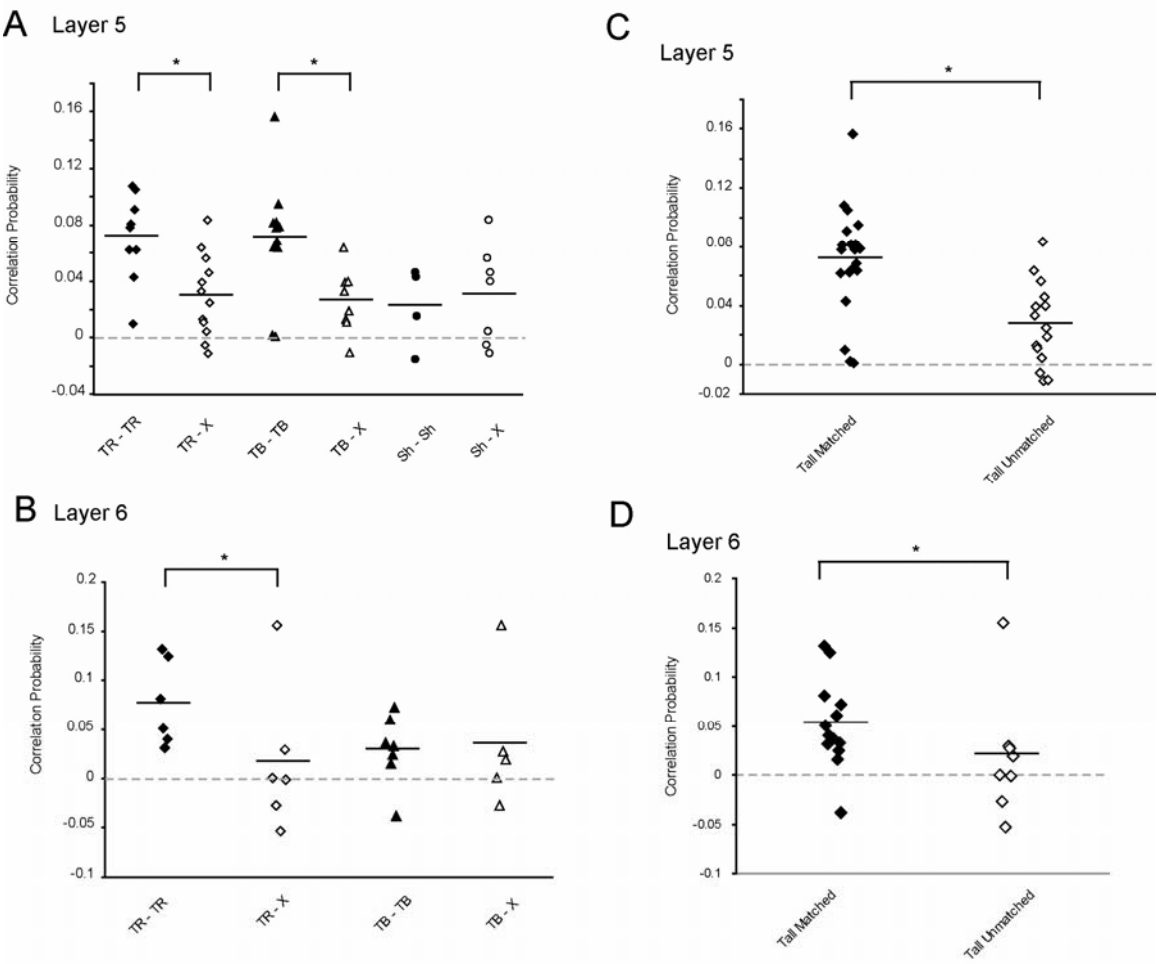

Figure 4.2 Correlation Probabilities for Different Cell Groups. (A) There are significant differences in the correlation probability (CP) from layer 5 between matched tall regular spiking cells (TR-TR) and their respective unmatched cohorts (TR-X; $p < 0.05$) as well as matched tall spiking cells (TB-TB) and their respective unmatched cohorts (TB-X; $p < 0.05$). There were no significant difference between matched short pyramidal cells (SH-SH) and their respective unmatched cohorts (SH-X). (B) There was a significant overall effect between matching pairs of tall cells (TR-TR and TB-TB) and unmatched tall cells (TR-X or TB-X; $p < 0.05$). (C) There are significant differences in the correlation probability (CP) from layer 6 between matched tall regular spiking cells (TR-TR) and their respective unmatched cohorts (TR-X; $p = 0.05$). However, there was no significant difference between matched tall bursting cells. (D) There was a significant overall effect between matched tall cells (TR-TR and TB-TB) and unmatched tall cells (TR-X or TB-X; $p < 0.05$).

Interestingly, SH-SH pairs (4 pairs) did not have as high of a CP as their matching tall counterparts. Their layer 5 CP was 0.022 ± 0.014 which was insignificantly different from that of SH cells matched with some other cell type (SH-X; n = 7 pairs; 0.031 ± 0.013; p = 0.68, Mann Whitney U Test; Fig 4.2 A). Furthermore, no significant differences existed between SH-SH and SH-X cells in CP from other layers. SH-SH low CP from layer 5 differed significantly from those of tall matched pairs (TR-TR and TB-TB). These values were 0.022 ± 0.014 for SH-SH cells and 0.071 ± 0.008 for tall matched pairs ($p < 0.05$, Mann Whitney U Test). We were unable to calculate layer 6 CP for any of the SH-SH pairs and hence were unable to do any comparisons with this pair group in that layer.

Ultimately we decided to pool data from the tall matching pairs (TR-TR and TB-TB; n = 20) and compare them to all tall unmatched pairs (TB-X or TR-X cells; n = 15). Tall matching pairs had significantly higher CPs from layer 5 (0.071 ± 0.008 for matched tall pairs; 0.027 ± 0.007 for unmatched tall pairs; $p < 0.005$, Mann Whitney U Test, Fig 4.2 C). We then compared the tall matched pairs to a subset of the tall unmatched where both cells were tall (TR-TB; n = 5). We also found a significant difference between these two populations ($p < 0.05$, Mann Whitney U Test). Furthermore, tall matching pairs had higher layer 6 CP than tall unmatched pairs (0.051 ± 0.012 for tall matched; 0.019 ± 0.022 for tall unmatched pairs; $p < 0.05$, Mann Whitney U Test; Fig 4.2 D). We were not able to find any significant differences in the CP of other layers between the tall matched and tall unmatched groups.

4.5 Discussion

Our findings in the earlier chapter challenged a long standing assumption of cortical circuitry models. In that study, we characterized two distinct cell types that had received identical functional laminar input patterns. The assumption that this finding challenged was that each cell type plays a unique role in cortical circuitry. Although there was a possibility that these cells received differential input from non-local areas (for example cortico-cortical projections to distal apical dendrites), we thought that the correlation probability experiment would elucidate whether these cells received input from different populations of cell or from the same population of cells.

Previous research suggests that these two cells project to different areas of the brain. The tall bursting cells project to subcortical nuclei, such as the lateral posterior nucleus (LP), the superior colliculus, the pontine nuclei and other areas (Mason and Groos, 1981), while tall regular spiking cells probably project to the corpus callosum (Morishima and Kawaguchi, 2006). Having two cells that get the same input but project to two different areas is not evolutionarily advantageous because it is not as economical as a system where the same cell projects to both areas.

We to address this specific issue, we calculated a correlation probability for matched and unmatched cell pairs. The correlation probability is a measure of synchronous EPSCs in a pair of neurons, and a predictor of the number of shared presynaptic neurons between them. Our results show clearly these cells receive a small amount of their input from two different populations of cells, especially from layer 5. Tall regular spiking cells receive more than twice as much synchronous input from layer 5 when they are matched up with another tall regular spiking cell. This observation was

also true for the layer 5 CP of the tall bursting cells; when they were matched with another tall bursting cell, they received more nearly three times as much synchronous input. Interestingly, we did not observe the same trend in the layer 5 CP of the matched pairs of short-short pyramidal neurons.

In addition to finding differences in the layer 5 CP of the tall matched and tall unmatched groups, we found similar differences in the layer 6 CP. Tall regular spiking cells receive more than four time higher increase in CP from layer 6 when compared to their unmatched cohorts. However, tall bursting cells did not have a significant difference in layer 6 CP. This suggests that tall regular spiking cells receive input from a select subpopulation of layer 6 cells that are selectively connected to them.

Our CP are quite low when compared to the ones found in connected pairs of layer 2/3 neurons (Yoshimura and Callaway, 2005; Yoshimura et al., 2005). The high CP between connected cells in the layer 2/3 of the rat visual cortex suggested fine scale specificity in the network of these cells. Because our CPs are low, it does not demonstrate a fine scale specificity in the layer 5 network. However, earlier studies of layer 5 in the rat prefrontal cortex show that there are selective connections between different cell types. For example, cells equivalent to our tall regular spiking cells synapse onto other tall regular spiking cells and to cells equivalent to our tall bursting cells with similar frequency (~10% probability of connection). However, the tall bursting cells rarely synapse onto other the tall regular spiking cells (~1%). Their finding, in addition to the difference in CP we observed in our study, implies that selective connections between different types of layer 5 pyramidal cells is based on the genetic differences between cell types. That is, cells selectively synapse onto other cells based on what cell

type they are. Cells in layer 2/3 do not appear to be genetically different from each other, and hence connections between cells are a result of activity dependent forces.

Although our study does not suggest that there is fine scale specificity in layer 5 of the rat visual cortex, other pieces of evidence strongly suggest that it does exist. Simultaneous recordings from multiple cells in layer 5 showed that if Cell A is connected to Cell B and to Cell C, Cell B and C have much greater than random chance of being connected to each other. Hence we see cluster of cells within layer 5 that are selectively connected to each other. Furthermore, in our study, the one connected pair of cells, comprised of a tall regular spiking cell and tall bursting cell (an unmatched pair) has a layer 5 CP that was 2.5 times more than the highest unmatched pair (unconnected) pair of cells and was the highest CP we recorded between any pair of cells from any layer. Although these two pieces of evidence are hardly proof of fine scale specificity in layer 5, they are strong suggestions.

In conclusion, we speculate that cells in layer 5 of pyramidal cortex are probably connected to each other based on genetic factors (that is, synapses are selective to certain cell types), and based on activity dependent factors. Since cells in layer 2/3 do not fall into genetically different cell subtypes, specificity in their network of cells relies solely on activity dependent means. Furthermore, this study shows that, although superficially it may appear that the tall regular spiking cells and tall bursting cells receive the same pattern of functional local input, they receive input from two distinct populations of cells, at least from layer 5 and layer 6. Indeed, these cells are receive functional input from different cell types and serve a different role from each other in the cortical circuit.

4.6 Acknowledgements

The text of Chapter 4, in part, will be combined and published with those of chapter 3. I was the primary investigator and first author of this chapter and Edward M. Callaway, will be the second author for his role in directing and supervising this project, and for writing a portion of the introduction. This study was also funded by National Institute of Health Grants EY-10742 and MH-63912. The authors would like to acknowledge Rose Z. Zarrinpar for helping analyze a significant portion of the data collected for this study.

Table 4.1: Correlation Probability from Each Layer to Matched Pairs of Cells. Dashed lines represent blocks were there was not enough input to do an adequate correlation probability measure.

Cell Type A	Cell Type B	L2/3 CP	L4 CP	L5 CP	L6 CP
Tall Regular	Tall Regular	-	-	0.105	-
Tall Regular	Tall Regular	0.014	0.045	0.062	0.081
Tall Regular	Tall Regular	-	-	0.081	0.051
Tall Regular	Tall Regular	-	0.083	0.091	0.125
Tall Regular	Tall Regular	-	0.091	0.063	-
Tall Regular	Tall Regular	0.079	0.029	0.078	0.132
Tall Regular	Tall Regular	-	-	-	-
Tall Regular	Tall Regular	0.080	0.033	0.108	0.031
Tall Regular	Tall Regular	-	0.036	0.010	-
Tall Regular	Tall Regular	0.124	0.033	0.043	0.040
Tall Bursting	Tall Bursting	-	-	0.002	-
Tall Bursting	Tall Bursting	0.066	0.061	0.078	0.060
Tall Bursting	Tall Bursting	-	-	0.001	-
Tall Bursting	Tall Bursting	-	-	0.079	-0.038
Tall Bursting	Tall Bursting	0.063	0.091	0.095	0.072
Tall Bursting	Tall Bursting	0.037	-0.016	0.156	-
Tall Bursting	Tall Bursting	-	-	0.065	-
Tall Bursting	Tall Bursting	-	0.067	0.064	0.033
Tall Bursting	Tall Bursting	0.043	0.085	0.082	0.015
Tall Bursting	Tall Bursting	0.109	0.026	0.082	0.037
Tall Bursting	Tall Bursting	0.021	0.052	0.069	0.024
Short Pyramidal	Short Pyramidal	-0.032	-0.010	0.043	-
Short Pyramidal	Short Pyramidal	-	0.046	0.015	-
Short Pyramidal	Short Pyramidal	-	0.028	0.046	-
Short Pyramidal	Short Pyramidal	-	0.018	-0.015	-

Table 4.2: Correlation Probability from Each Layer to Unmatched Pairs of Cells. Dashed lines represent blocks were there was not enough input to do an adequate correlation probability measure.

Cell Type A	Cell Type B	L2/3 CP	L4 CP	L5 CP	L6 CP
Tall Bursting	Tall Regular	-	-0.002	0.013	-0.027
Tall Bursting	Tall Regular	-	0.035	0.033	-
Tall Bursting	Tall Regular	-	-	**0.160**	**0.008**
Tall Bursting	Tall Regular	-	0.068	0.011	0.156
Tall Bursting	Tall Regular	-	-	0.039	-
Tall Bursting	Tall Regular	0.011	-0.025	0.064	0.000
Short Pyramidal	Tall Regular		0.073	-0.005	-
Short Pyramidal	Tall Regular	0.018	0.094	0.057	-0.053
Short Pyramidal	Tall Regular	0.001	-0.062	-0.011	-
Short Pyramidal	Tall Regular	-	-	0.046	0.029
Short Pyramidal	Tall Regular	-	-0.041	0.005	-
Short Pyramidal	Tall Regular	0.039	0.000	0.084	-
Short Pyramidal	Tall Bursting	0.127	0.042	0.040	0.027
INT	Tall Regular	-	-	0.025	-0.001
INT	Tall Bursting	-	0.032	-0.010	0.019
INT	Tall Bursting	0.031	-	0.019	-

4.7 References

Aertsen AM, Gerstein GL, Habib MK, Palm G (1989) Dynamics of neuronal firing correlation: modulation of "effective connectivity". J Neurophysiol 61:900-917.

Briggs F, Callaway EM (2001) Layer-specific input to distinct cell types in layer 6 of monkey primary visual cortex. J Neurosci 21:3600-3608.

Briggs F, Callaway EM (2005) Laminar patterns of local excitatory input to layer 5 neurons in macaque primary visual cortex. Cereb Cortex 15:479-488.

Callaway EM, Katz LC (1993) Photostimulation using caged glutamate reveals functional circuitry in living brain slices. Proc Natl Acad Sci U S A 90:7661-7665.

Dantzker JL, Callaway EM (2000) Laminar sources of synaptic input to cortical inhibitory interneurons and pyramidal neurons. Nat Neurosci 3:701-707.

Kasper EM, Larkman AU, Lubke J, Blakemore C (1994) Pyramidal neurons in layer 5 of the rat visual cortex. I. Correlation among cell morphology, intrinsic electrophysiological properties, and axon targets. J Comp Neurol 339:459-474.

Katz LC, Dalva MB (1994) Scanning laser photostimulation: a new approach for analyzing brain circuits. J Neurosci Methods 54:205-218.

Mason R, Groos GA (1981) Cortico-recipient and tecto-recipient visual zones in the rat's lateral posterior (pulvinar) nucleus: an anatomical study. Neurosci Lett 25:107-112.

Morishima M, Kawaguchi Y (2006) Recurrent connection patterns of corticostriatal pyramidal cells in frontal cortex. J Neurosci 26:4394-4405.

Sawatari A, Callaway EM (1996) Convergence of magno- and parvocellular pathways in layer 4B of macaque primary visual cortex. Nature 380:442-446.

Sawatari A, Callaway EM (2000) Diversity and cell type specificity of local excitatory connections to neurons in layer 3B of monkey primary visual cortex. Neuron 25:459-471.

Yabuta NH, Callaway EM (1998a) Cytochrome-oxidase blobs and intrinsic horizontal connections of layer 2/3 pyramidal neurons in primate V1. Vis Neurosci 15:1007-1027.

Yabuta NH, Callaway EM (1998b) Functional streams and local connections of layer 4C neurons in primary visual cortex of the macaque monkey. J Neurosci 18:9489-9499.

Yoshimura Y, Callaway EM (2005) Fine-scale specificity of cortical networks depends on inhibitory cell type and connectivity. Nat Neurosci 8:1552-1559.

Yoshimura Y, Dantzker JL, Callaway EM (2005) Excitatory cortical neurons form fine-scale functional networks. Nature 433:868-873.

Zarrinpar A, Callaway EM (2006) Local connections to specific types of layer 6 neurons in the rat visual cortex. J Neurophysiol 95:1751-1761.